Università degli Studi della Basilicata

Department of Agricultural, Forestry, Food and Environmental Sciences

PhD in Agricultural, Forestry and Food Sciences

XXXVIII cycle

Scientific Disciplinary Sector:

AGRI-04/B – Agricultural Mechanics

(ex AGR/09 – Agricultural Mechanics)

PhD Thesis

The optimization of industrial refrigeration systems for the fruit and vegetable sector

Supervisor

Prof. Giovanni Carlo Di Renzo

PhD student

Orkhan Mammadov

Co-supervisor

Prof. Ing. Giuseppe Altieri

Coordinator

Prof.ssa Teresa Zotta

Academic Year 2025/2026

Abstract

The thesis focuses on refrigeration plants design criteria to define the optimal technological solutions for fruit and vegetable cold storage, aiming to improve both the system energy efficiency and the final product quality. The study has been carried out through a combination of industrial-scale test using real-time system monitoring in the cold rooms available in the UNIBAS-MAClab and in local packing house. The collected data was used to validate the simulation model developed.

In the first phase, tests were carried out in an industrial cold storage facility (in the packing house), where temperature and humidity were continuously monitored under evaporation conditions vary according to the test protocol. Results showed that, with a direct expansion system and a temperature difference (ΔT) of about 5 °K between the air and the evaporator surface, it is possible to maintain the relative humidity in the range 91–93%, which minimizes product dehydration while ensuring efficient energy use.

The second phase, initiated in the MACLAB and subsequently extended to the industrial cold room, focused on the monitoring and analysis of key refrigeration parameters — including pressures, temperatures, and power consumption — to evaluate the system's real-time performance and stability. Based on these observations, an intelligent defrost control strategy was developed and benchmarked against conventional time-based methods. The proposed approach achieved up to a 70% reduction in defrost cycles, leading to lower energy consumption and improved overall system efficiency.

A MATLAB simulation model was also developed to estimate fruit and vegetable weight loss under various thermo-hygrometric conditions, supporting predictive evaluation of storage performance.

Finally, an energy analysis was performed to evaluate the impact of inverter-driven components on system performance. The use of inverters for the compressor, condenser fans, and evaporator fans led to energy savings of up to 34%, with corresponding reductions in CO_2 emissions and operating costs.

Overall, the results demonstrate that an integrated, data-driven approach combining experimental testing, smart control strategies, and dynamic modeling can significantly enhance the efficiency, reliability, and sustainability of refrigeration systems used in the fruit and vegetable cold storage sector.

Summary

Abstract 2
Summary 3
1. Foreward 4
2. Postharvest facility's cold rooms 5
2.1. Cold Storage of Fruits and Vegetables 5
2.2. Structure of Cold Rooms 7
2.3. Thermal Load Assessment for Refrigerated Storage 9
2.4. Refrigeration Equipment to Controll Cold Room Temperature 16
2.4.1. Compressors 16
2.4.2. Condensers 18
2.4.3. Air Cooled Evaporator & Air Cooler 20
2.4.4. Thorolling Device 24
2.5. Refrigeration Cycle on the Pressure–Enthalpy Diagram 26
2.6. Cooling Systems: Overview and Classification 28
2.7. Effects of Temperature and Relative Humidity on Product Quality 30
2.8. Defrost 33
2.8.1. Frost Formation and Growth on Heat Exchangers 35
2.8.2. The defrost process 36
3. Materials and Methods 48
3.1. Cold room environmental and refrigeration data Measurement and Monitoring System 48
3.2. Chiller Employed in the Laboratory Setup 62
3.3. Cold Room Setup 63
3.4. Image Acquisition System for Frost Depositing 69
3.5. Defrost control and monitoring system 71
3.6. Experimental Configurations and Test Plan 76
3.7. Simulation Model of Weight Loss for Horticultural Products 78
4. Results 80
4.1. Comparison of Defrost Depositing Control 80
4.2. Evaluation of the Refrigeration System Efficiency 86
4.3. Data processing of ambient air temperature and humidity under various cold-room operating conditions 92
4.4. Application of the Weight-Loss Simulation Model 100
4.5. Energy Saving Assessment Through Inverter Control 102
5. Conclusions 106
References 110

1. Foreward

The economic and logistical structure of fruit and vegetable supply chains depends on the cold chain i.e. the cold storage facilities. Efficient storage of fruits and vegetables is essential to preserve their quality, safety, and longevity along the supply chain. Because fresh fruit and vegetable remain fresh without additional treatments such as blanching, freezing, or canning (Iturralde-García et al., 2022). However, their limited shelf life — in some cases less than one week — represents a major challenge. Approximately 45–55% of global fruit and vegetable production is lost or wasted along the value chain, compared with 35% for seafood, 30% for cereals, and 20% for meat (Lufu et al., 2020). Over the last forty years, extensive research and field studies have consistently shown that between 40% and 50% of fresh fruits and vegetables produce in developing nations are wasted before reaching consumers.

Controlled-temperature storage of horticultural produce has transformed markets and improved profitability by decoupling production from sales across time and space, even for highly perishable goods. Inadequate storage temperatures, by contrast, promote bacterial and fungal growth, leading to spoilage, partial or total product loss, and in the worst cases food-safety risks. Under proper conditions, refrigeration allows the market to receive products over periods that depend on species, variety, and product type with color, flavor, texture, aroma, and nutritional value as close as possible to their original state. The actual storage life, however, depends on the efficiency and quality of the equipment: efficient systems reduce waste and thus improve profitability.

An efficient plant maintains target conditions uniformly, avoiding warm spots and thermal oscillations that degrade quality. Conversely, an inefficient plant uses more energy to achieve the same result and causes temperature fluctuations in the room that accelerate deterioration, increasing postharvest rejects. Improving efficiency also lowers fixed operating costs.

The plant's overall efficiency can be framed across the following components:

- Control of the air temperature in the cold room (and therefore product temperature).
- Relative humidity control of the storage atmosphere.
- Selection and control of evaporator fans for air distribution within the room and through the product stack.
- Selection and control of mechanical and electrical components of the refrigeration system.
- Thermal insulation and airtightness of the envelope.
- Defrost control and management.

The thesis focuses on refrigeration plants design criteria to define the optimal technological solutions for fruit and vegetable cold storage, aiming to improve both the system energy efficiency and the final

product quality. The study has been carried out through a combination of industrial-scale test using real-time system monitoring in the cold rooms available in the UNIBAS-MAClab and in local packing house. The collected data was used to validate the simulation model developed.
A MATLAB simulation model was also developed to estimate fruit and vegetable weight loss under various thermo-hygrometric conditions, supporting predictive evaluation of storage performance.
Finally, an energy analysis was performed to evaluate the impact of inverter-driven components on system performance.

2. Postharvest facility's cold rooms

Cold rooms are now an integral part of postharvest facilities for fruit and vegetables, where all pre-shipment operations are carried out. The placement and layout of the cold-storage area within the facility is a strategic decision that directly affects productivity: it determines the number of pallet moves from unitization to truck loading, cycle times, and the actual travel paths of forklifts and pallet jacks—both loaded and unloaded.
Given the wide variability of operating conditions across production regions, there is no single "best" layout for horticultural cold stores. Nonetheless, adhering to a few core principles is essential to avoid design pitfalls (Bachmann & Earles, 2000). In particular, the room volume should reflect the daily and seasonal throughput of each commodity and the expected inbound/outbound flows, as well as the pre-cooling method employed. For sizing, it is also crucial to consider the type of packaging used for each product—both as received from the field and after packing—because packaging governs heat and mass transfer, airflow resistance, and the configuration of unit loads.
Engineering choices for the refrigeration plant and air coolers (evaporators) must align with: the product mix and its thermo-hygrometric requirements (temperature and RH setpoints); storage density and packaging permeability; the required air recirculation and distribution through the stacked product; and the plant architecture (direct expansion, flooded, or secondary refrigerants). These decisions determine the achievable heat-transfer performance, air-exchange patterns, and defrost strategy, and ultimately govern product quality and the overall efficiency of the system.

2.1. Cold Storage of Fruits and Vegetables

Cold rooms are engineered environments for the storage of fruits and vegetables under optimal temperature and relative humidity conditions, defined by species, cultivar, market stage, and packaging type. These conditions can be managed automatically with modern control and supervision systems (Beni et al., 2001). Designing a cold room requires proper sizing and integration of both structural and mechanical/electrical components: the refrigeration unit, aircoolers, piping, defrost

systems, electrical systems, insulated sandwich panels, doors, and the PLC and sensors for automated control.

Plant sizing is generally based on the required refrigeration capacity, derived from the refrigeration load i.e., the power (kW) needed to offset:

- Transmission losses through walls, roof, and floor;
- Air exchange/infiltration due to door openings and ventilation;
- Product respiration heat;
- Internal gains from motors, fans, lighting, and personnel. (Stoecker, 2001)

Where operation includes start/stop cycles or cold start-ups, thermal transients produce peak demands above steady-state values. Consequently, heat-exchanger surfaces (evaporators, condensers) and compressor capacity should include an appropriate oversizing margin to absorb these initial higher loads.

Finally, determining the product-related load must account for each commodity's optimal storage temperature, freezing point, and chilling-injury thresholds (see Table 1) (Thompson et al., 2001).

Product	**Storage Temperature (°C) (min;max)**	**R.H. (%)**
Garlic	-1;0	60-70
Apricot	-0,5;+1	90-95
Watermelon	+7;+10	85-90
Orange	+3;+8	90-95
Asparagus	0;+2	>95
Broccoli	0;+2	90-95
Artichoke	0;+0.5	>95
Carrot	0	98-100
Cherry	-0.5;+0.5	90-95
Onion	0	65-70
Green Bean	+5;+7.5	>95
Fig	-1;0	90-95
Strawberry	0;+0.5	90-95
Persimmon	0;+1	90-95
Kiwi	0	90-95
Lemon	+12;+14	90-95
Apple	0;+1	90-95
Pomegranate	+5;+7	90-95
Pepper	7,5	>95
Pear	-1;0	90-95
Peach	-1;0	90-95
Grapes	-1;0	90-95

Table 1 - Recommended Storage Conditions for Fruits and Vegetables 2018 RAE Handbook—Refrigeration)

2.2. Structure of Cold Rooms

Modern cold rooms are built as prefabricated systems, which reduce costs compared with traditional permanent construction in masonry or reinforced concrete—now largely obsolete (Rapin & Jacquard, 2000).

The envelope is made of sandwich panels with a rigid polyurethane (PU) foam core (typical thickness 60–250 mm) and inner/outer skins in:

- galvanized or pre-painted steel (per UNI 5753/84 to prevent corrosion),
- aluminum,
- stainless steel,
- steel coated with epoxy resin.

For rooms storing fruit and vegetables at positive temperatures, panels of 100–120 mm are recommended, with steel skins > 0.5 mm and white pre-paint to maximize internal brightness. For controlled-atmosphere (CA) rooms that will be epoxy-painted, galvanized steel skins are preferred to improve coating adhesion.

Typical PU core properties (mean values): density 38–42 kg/m³, compressive strength 1.8–2.0 kg/cm², closed-cell content 95%, thermal conductivity $\lambda = 0.024$ W/(m·K).

Panel connection can be via foamed-in joints (now less common for rooms near 0°C due to higher installation costs) or via tongue-and-groove ("male/female") joints, available in multiple variants depending on the manufacturer. These joint systems are designed to enhance structural stability and airtightness, preventing panel separation caused by thermal cycling or minor settlement. New-generation joints often include mechanical latching/locking (rivets or screws); for 120 mm panels, a double tongue-and-groove is frequently used to improve both static stability and thermal tightness (see Fig. 1).

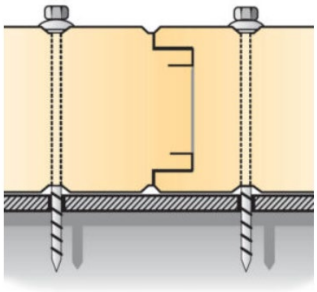

Figure 1 - Male–female interlocking joint system

The airtightness and vapor tightness of the panels are ensured by joint elements equipped with continuous gaskets. The corner nodes horizontal (wall/ceiling) and vertical (wall/wall) are hygiene-critical and should be formed with angle sections and cover trims to provide continuous, easy-to-

sanitize surfaces. Provide a flat, true bearing surface to ensure correct alignment during installation and to protect any exposed polyurethane edges. Because lifting/installation occurs on the cut edge, place a PU-specific vapor barrier (tape or membrane) between the panel and the bearing surface to prevent moisture wicking/infiltration, which would otherwise degrade the thermal insulation and risk delamination of the metal skin from the foam core. The floor must deliver thermal insulation, mechanical resistance to traffic (personnel, forklifts), and lower engagement of wall panels to ensure tightness and structural stiffness. A typical build-up for positive-temperature produce rooms includes:

- Sub-base of graded aggregate, accurately leveled and compacted with a vibratory roller, to −21 mm relative to finished floor level.
- Vapor barrier: 200-µm polyethylene sheet, turned up onto the perimeter panels (first barrier).
- Insulation: two layers of polystyrene boards, 30 mm each, laid with staggered joints.
- Vapor barrier: second 200-µm polyethylene sheet, also turned up onto the perimeter panels.
- Perimeter isolation joint: strip of expanded polyethylene (5 mm thick; height equal to the floor build-up) between the floor and all rising elements (columns, perimeter walls, curbs).
- Concrete screed: Rck 250, slump class S3, reinforced with electrowelded mesh 20×20 mm, Ø6, average thickness 150 mm. Provide slope toward the door for small rooms; for medium/large rooms (machine scrubber cleaning), set slopes per operational needs.
- Wearing layer: finish with spheroidal quartz or two-component epoxy resin in aqueous dispersion, 400–500 g/m², serving as primer/adhesion promoter and binder for broadcast quartz 0.1–0.4 mm.

Choosing the door is critical to ensure smooth loading/unloading, safe vehicle access, and—when closed—adequate thermal tightness. The most common, cost-effective solution is the horizontal sliding isothermal door, manual or motorized, with a steel frame (optionally reinforced plastic-clad). The leaf is a sandwich panel similar to the wall panels, with a perimeter frame (aluminum or steel) housing a continuous gasket that is key to limiting heat losses and ensuring airtightness. The bottom edge seals against the floor via a dedicated gasket; this is one of the most critical details because, to allow forklift and pallet-jack traffic, no floor threshold is installed. Poor adjustment at the bottom shows up as floor condensation halos, more frequent air-cooler starts and defrosts, leading to higher energy use and poorer storage conditions. For positive-temperature rooms, typical door thickness is 90–120 mm; viewports can be specified, especially for controlled-atmosphere rooms. Door size must match handling needs: larger clear openings reduce the risk of vehicles striking the frame under low-

visibility conditions. Frame/leaf protection systems are common; as a rule of thumb, a clear width ≥ 2000 mm and height ≈ 3000 mm provide a good baseline to avoid damage and improve safety. Pressure-relief valves are essential, particularly in large rooms—to balance pressure differences between inside and outside during cooling, defrost, and door operations, when air-cooler start-ups (fans and refrigerant feed) cause volume/pressure changes.

Recent developments for high-capacity applications include ceiling-mounted vertical models ("V" version); thanks to the symmetrical body, they can be installed and wired from either the inside or the outside of the room.

Proper sizing of the pressure-relief valve requires estimating the airflow needed to balance internal/external pressure:

$$Q=K\cdot V\cdot \Delta T \qquad (2.1)$$

where Q is the required air quantity ($dm^3/min \approx L/min$), K = 3.66, V is the room volume (m^3), and ΔT is the maximum temperature change inside the room over 1 minute (°C). Once Q is calculated, compare it with the manufacturer's rating tables to select the valve model that delivers the required capacity.

The room footprint should be an integer multiple of the standard pallet size, with additional allowances for perimeter protection curbs on wall panels and for air circulation between pallet rows (about 100 mm for each inter-row gap).

Room height is crucial: unused air volume increases both capital and operating costs. Multi-level storage (pallets or bins) requires suitable forklifts and increases handling times.

Based on field experience, recommended heights are:

- 5,500 mm for rooms holding palletized, ready-to-ship products with uncertain dwell time; this allows two pallet levels while keeping head space to avoid direct impingement of the air-cooler jet.
- 8,000 mm for rooms storing product in bins (6–7 levels) or, less commonly, rooms with three rack tiers for packaged, ready-to-ship goods.
- 3,500 mm for transit rooms (ready-to-ship product).

2.3. Thermal Load Assessment for Refrigerated Storage

Identifying the cold room's requirements is of fundamental importance in order to design a solution that meets their expectations. In particular, it is necessary to define the initial project data, with special attention to:

- The operating temperatures needed for the processes;
- The type of product to be handled or processed;

- The quantities and flow rates of product to be stored;
- The type of cold room required.

To proceed with the design, it is essential to calculate the thermal loads of the refrigeration system under consideration. An inaccurate evaluation may lead either to undersizing, resulting in the inability to meet cooling demands, or to oversizing, which entails unnecessarily high initial investment costs. Both situations can ultimately cause dissatisfaction for the client.

To correctly size the refrigeration system, it is necessary to calculate all the thermal loads acting on the cold room. The total refrigeration load can be expressed as:

$$Q_{total}=Q_{transmission}+Q_{respiration}+Q_{product}+Q_{infiltration}+Q_{internal}+Q_{defrost} \quad (2.2)$$

where:

- Q_{total}: the nominal refrigeration capacity required from the system; (kW)
- $Q_{transmission:}$ heat gain due to conduction through walls, floor, and ceiling from the external environment; (kW)
- $Q_{respiration}$: metabolic heat released by living microorganisms present in fresh produce (only relevant in storage of fruit and vegetables, not in freezing rooms); (kW)
- $Q_{product}$: heat to be removed from the incoming product in order to bring it from its initial temperature down to the desired storage temperature; (kW)
- $Q_{infiltration}$: heat entering the cold room during door openings and air leakage; (kW)
- $Q_{internal}$: internal heat gains from lighting, forklifts, workers, and other equipment operating inside the cold room; (kW)
- $Q_{defrost}$: heat introduced during defrost cycles to remove ice accumulated on the evaporator surfaces; (kW)

For the design of a refrigeration system, it is possible to distinguish between continuous and non-continuous heat loads:

Continuous loads

- Heat transmission through walls, floor, and ceiling ($Q_{transmission}$)
- Product respiration heat ($Q_{respiration}$)

Non-continuous loads

- Product cooling load, to bring goods from initial to storage temperature ($Q_{product}$)
- Heat gain due to door openings and air infiltration ($Q_{infiltration}$)
- Internal heat gains from motors, lighting, and people ($Q_{internal}$)
- Heat input during defrost cycles ($Q_{defrost}$)

Heat Load due to Transmission ($Q_{transmission}$)

This term represents the thermal transmission losses through the cold room envelope (walls, floor, and ceiling). It depends on the type of insulating material, its thickness, the exposure of the cold room, and the temperature difference between inside and outside.

The heat load can be calculated as:

$$Q=U\cdot A\cdot \Delta T=U\cdot A\cdot (T_{ext}-T_{int}+\Delta T_{corr}) \qquad (2.3)$$

where

- U: overall heat transfer coefficient, defined as: $U=1/\alpha_e+s/\lambda+1/\alpha_i$
- A: surface area of the wall [m^2]
- ΔT: temperature gradient between inside and outside [K], increased by the corrective factor ΔT_{corr} according to the exposure
- λ: thermal conductivity of the insulating material [W/m·K]
- s: thickness of the wall [m]
- α_i: internal heat transfer coefficient [$W/m^2\cdot K$]
- α_e: external heat transfer coefficient [$W/m^2\cdot K$]

Typical Surface Types	East Wall, K	South Wall, K	West Wall, K	Flat Roof, K
Dark-colored surfaces				
Slate roofing	5	3	5	11
Tar roofing				
Black paint				
Medium-colored surfaces				
Unpainted wood	4	3	4	9
Brick				
Red tile				
Dark cement				
Red, gray, or green paint				
Light-colored surfaces				
White stone	3	2	3	5
Light-colored cement				
White paint				

Note: Add to the normal temperature difference for heat leakage calculations to compensate for sun effect. Do not use for air-conditioning design.

Figure 2 - Temperature correction factors as a function of exposure and surface type. (Source: 2014 ASHRAE Handbook refrigeration)

Refrigeration Load due to Respiration ($Q_{respiration}$)

Each non-frozen product contains living organisms that continue to release heat as a function of the storage temperature. This phenomenon, known as respiration heat, must be considered in the design of refrigeration systems for fresh fruit and vegetable storage.

Becker *et al.* (1996) established a correlation between the amount of carbon dioxide (CO2) released by the product and the heat generated by respiration as a function of ambient temperature. The specific respiration heat can be expressed as:

$$Q_{respiration,\ specific}=10.7\cdot f\cdot 3600\cdot(9\cdot T/5+32)^{g}\ [W/kg] \qquad (2.4)$$

where:

- f and g are tabulated coefficients that depend on the specific product;
- T is the storage (ambient) temperature [°C].

Refrigeration Load for Product Cooling ($Q_{product}$)

Since this is a non-continuous load, the refrigeration requirement for product cooling is calculated in terms of the total thermal energy to be removed. This represents the energy necessary to bring the product from its initial temperature down to the desired storage temperature. It can be expressed as:

$$Q_{product}=m\cdot c_{p},\cdot(T_{initial}-T_{final}) / \Delta t \qquad (2.5)$$

where:

- m: product mass [kg];
- c_p specific heat capacity of the product above its freezing temperature [kJ/kg·K];
- $T_{initial}$: initial temperature of the product [°C];
- T_{final}: final (storage) temperature of the product [°C].

For fruits, typical values of the specific heat capacity range from 2.5 to 4 kJ/kg·K, since they are composed mainly of water.

Refrigeration Load due to Door Openings ($Q_{infiltration}$)

Whenever a cold room door is opened to the external environment, a natural air exchange occurs between the two spaces. This phenomenon results in the inflow of warm ambient air into the cold room, contributing to an additional refrigeration load.

A widely used method for estimating this air infiltration is the Gosney and Olama correlation, expressed as:

$$Ga = C_{inf} \cdot A \cdot H^{-2} \cdot ((\rho_i - \rho_o)\rho_i)^{1/2} \cdot (2/(1 + (\rho_i/\rho_o)^{1/3}))^{3/2} \cdot (\rho_i - \rho_o/2) \qquad (2.6)$$

where:

- Ga: mass flow rate of infiltrated air [m^3/s];
- C_{inf}: infiltration coefficient, typically 0.692 [$m^{1/2}/2$];
- A: door width [m^2];
- H: door height [m];
- ρ_i: density of cold room air [kg/m^3];
- ρ_o: density of warm ambient air [kg/m^3].

Once the mass flow rate of infiltrated air has been determined, the refrigeration load due to door openings can be calculated as:

$$Q_{infiltration} = G_a \cdot (h_{a,o} - h_{a,i}) \qquad (2.7)$$

where:

- G_a: mass flow rate of infiltrated air [kg/s];
- $h_{a,o}$: specific enthalpy of the outside (ambient) air [kJ/kg];
- $h_{a,i}$: specific enthalpy of the inside (cold room) air [kJ/kg].

The enthalpy difference accounts for both the sensible and latent heat introduced with the warm, humid ambient air entering the cold room.

Internal Heat Gains ($Q_{internal}$)

Internal heat loads can be calculated as:

$$Q_{internal} = Q_{lighting} + Q_{personnel} + Q_{motors+equipment} \qquad (2.8)$$

where:

- $Q_{lighting}$: heat released by lighting fixtures inside the cold room. This value depends on the activities carried out in the space and on the type of lighting technology installed.

  The thermal energy introduced by the lighting system can be calculated as:

$E_{lighting}=Q_{lamp}\cdot S\cdot \Delta t_{ist}$

where:

Q_{lamp}: specific lighting power [W/m²];

S: floor area of the cold room [m²];

Δt_{ist}: duration of lighting operation per cycle [h].

The corresponding refrigeration load is then:

$$Q_{lighting}=E_{lighting}/\Delta t \qquad (2.9)$$

where Δt is the reference period (typically 24 h)

- $Q_{personnel}$: heat released by workers inside the cold room, which includes both sensible and latent heat contributions.

  The sensible and latent heat released by a person inside the cold room depends on clothing, gender, and physical activity, as specified in the standard EN 28996 (1994). Since this is a non-continuous load, the thermal energy introduced is evaluated based on the assumed occupancy time.

  Heat released per person: Q_p, according to reference tables

  The thermal energy introduced is calculated as:

  $E_{personnel}=Q_p\cdot \Delta t_{ist}$

  The corresponding average refrigeration load is:

  $$Q_{personnel}=E_{personnel}/\Delta t \qquad (2.10)$$

  where Δt is the reference time interval (typically 24 h)

- $Q_{motors+equipment}$: heat released by powered equipment operating inside the cold room, such as forklifts or processing machinery. Since this equipment does not always operate at full load, a utilization factor in the range of 0.6–0.8 is typically applied.

  Since this is a non-continuous load, the thermal energy introduced by motors and equipment located inside the cold room is calculated based on operating assumptions. The main contributions are:

Heat released by the fan motor of the selected air cooler (value obtained from manufacturer data once the fan is chosen);

Other processing machines: in this case, it is assumed that no additional equipment is installed inside the cold room;

Forklift operation inside the cold room:

- Forklift rated power: $Q_{forklift}$
- Operating time: Δt_{ist};
- Utilization factor: fu=0.6 since the forklift runs at full power only during specific activities (e.g., lifting);
- Electrical efficiency: η_{el}

The thermal energy released is calculated as:

$$E_{(motors+equipment)}=f_u \cdot Q_{forklift} \cdot \Delta tist \cdot (1-\eta_{el}) \qquad (2.11)$$

The corresponding average refrigeration load is:

$$Q_{motors+equipment}=E_{motors+equipment} \cdot \Delta t \qquad (2.12)$$

where Δt is the reference period (typically 24 h)

Defrost Load ($Q_{defrost}$)

Since defrosting is a non-continuous load, it is calculated in terms of the thermal energy introduced during defrost operations.

To evaluate this contribution, the defrost efficiency $\eta_{defrost}$ is defined as the ratio between the energy actually required to remove frost ($E^*_{defrost}$) and the total energy supplied to the defrost system ($E_{supplied}$):

$$\eta_{defrost}= E^*_{defrost} / E_{supplied} \qquad (2.13)$$

Experimental studies (Niederer, 1976; Stoecker, 1983; ASHRAE, 1989) suggest an average efficiency of about 20%. Consequently, it is assumed that approximately 80% of the energy supplied during defrosting is released into the cold room and must be considered in the refrigeration load calculation.

The following assumptions are typically made:

- Number of defrost cycles per day: N;

- Defrost duration of one cycle: Δt_{ist};
- Defrost efficiency: $\eta_{defros}=0.20$.

The total thermal energy introduced by defrosting is then:

$$E_{defrost}=N\cdot Q_{defrost,datasheet}\cdot(1-\eta_{defrost})\cdot\Delta tist \qquad (2.14)$$

where:

- $Q_{defrost,datasheet}$: defrost power provided by the manufacturer, as specified in the equipment datasheet;

The corresponding refrigeration load can be calculated as:

$$Q_{defrost}= E_{defrost} / \Delta t \qquad (2.15)$$

where Δt represents the considered time interval (e.g., 24 h for daily load balance).

2.4. Refrigeration Equipment to Controll Cold Room Temperature

A refrigeration system for cold room applications is typically composed of four main components, each of which plays a crucial role in the refrigeration cycle:

- Compressor, which circulates the refrigerant and increases its pressure;
- Condenser, where the refrigerant releases heat to the surroundings;
- Expansion valve, which regulates the flow and reduces the pressure of the refrigerant;
- Evaporator, where the refrigerant absorbs heat from the cold room.

These components are interconnected by refrigerant piping and, together, ensure the proper removal of heat from the storage space, maintaining the desired low temperature

2.4.1. Compressors

The compressor is the heart of the refrigeration plant: it draws superheated vapor from the evaporators, raises its pressure and temperature, and discharges it to the condenser. Compressor technology has a decisive impact on efficiency, reliability, and operating cost.

The main types of compressors used in industrial refrigeration are screw, reciprocating, centrifugal, and rotary vane. In the fruit-and-vegetable cold-chain—where cold rooms are typically large and

installed capacities are substantial—the two dominant compressor types are reciprocating and screw machines

- Reciprocating (piston) compressors

  Typically preferred for capacities < 150 kW: good efficiency at medium–low loads, flexible capacity control (cylinder unloading, digital), straightforward maintenance, and lower cost.

- Screw compressors.

  Generally the standard > 400 kW: high mass-flow capability, smooth/quiet operation, excellent integration with economizer and variable-speed drives (VSD/VFD); maintenance is more structured.

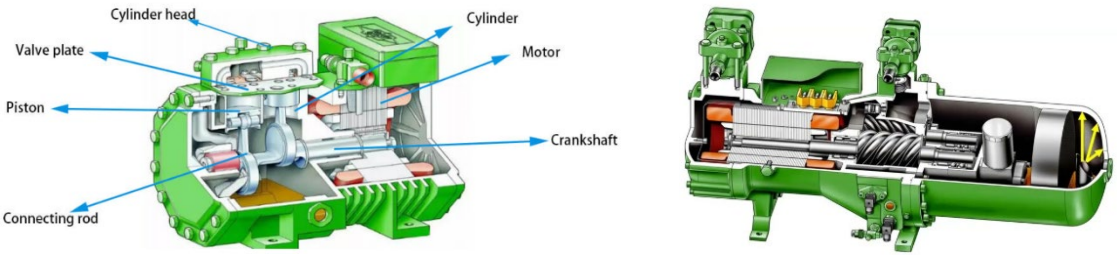

a b

Figure 3 - a) Piston Compressor b) Screw Compressor (Source: BITZER)

In multi-room produce facilities with variable loads, modularity (several compressors in parallel) is often more efficient than a single large machine.

To cut operating costs and raise availability:

- Use multiple compressors in parallel, sized in capacity steps to track the real load, reducing part-load losses and inrush at start.
- Employ a PLC for hour equalization, sequencing (start/stop), load balancing, and alarms.
- Cooling demand in produce plants is highly discontinuous (peaks during precooling/processing; lows overnight/early morning). Sustained part-load operation penalizes efficiency; mitigate it with:
- Staging: switch machines in/out to keep running compressors near their best efficiency point.
- VSD/VFD on at least one unit: modulates mass flow and improves part-load efficiency; on screws, VSD usually outperforms the slide valve at deep turndown.
- Slide valve (screw) and cylinder unloading/digital (reciprocating): useful, though typically less efficient than VSD for wide modulation.

- Floating setpoints: optimize suction pressure and condensing/evaporating temperatures to ambient and product needs (raising suction pressure within quality limits reduces compressor work).
- Economizer (screw): boosts EER/COP at medium–high compression ratios.

2.4.2. *Condensers*

After leaving the compressor, the high-pressure superheated refrigerant vapor enters the condenser. The heat-transfer process in a refrigerant condenser occurs in three stages:

- Desuperheating of the hot gas
- Condensing of the gas to liquid state and release of the latent heat
- Subcooling of the liquid refrigerant

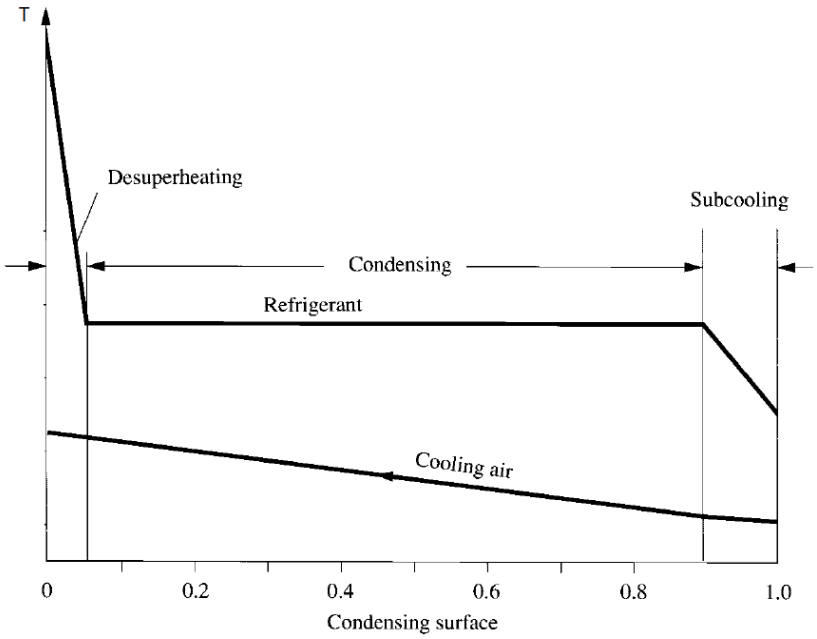

Figure 4 - Temperature curves of refrigerant and cooling air of the air-cooled condenser

Although the heat transfer coefficient on the hot gas side is relatively low during the desuperheating stage, the larger temperature difference between the superheated refrigerant vapor and the cooling medium enhances the overall heat transfer rate in this region. Subcooling, on the other hand, occupies only a small fraction of the condenser surface. For simplicity in analysis, an average heat transfer coefficient is therefore applied to the entire condenser surface, while the condensation process is assumed to take place at the constant condensing temperature.

Heat rejection to the ambient can be achieved through different technologies: air-cooled condensers, water-cooled condensers (often combined with cooling towers), or evaporative condensers (hybrid

systems using both air and water in a single unit). Common construction types include plate heat exchangers, shell-and-tube designs, and finned-tube coils.

Air-cooled condensers

- Pros: lowest CAPEX and complexity; no water use; simple maintenance. Well suited to small–medium plants (~< 100 kW).
- Cons: efficiency tracks dry-bulb temperature; as ambient rises, condensing temperature (Tcond) rises and COP falls.
- Design guideline: size for peak conditions with Tcond ≈ +45 °C.
- Optimizations: floating condensation (lower Tcond in shoulder seasons), EC/VSD fans, microchannel coils, adiabatic pre-cooling during peaks (small water use, large benefit), acoustic control.

Figure 5 - Air-Cooled Condenser (Source: ONDA)

Water-cooled with cooling tower or dry cooler

- Recirculated water cooled in a cooling tower yields lower, stable T_{cond} ~ +35 °C, largely set by wet-bulb rather than dry-bulb conditions.
- Tower process: water distributed over fill against forced air; a fraction evaporates, removing latent heat and cooling the loop. Requires make-up (evaporation + blowdown), which in hot weather can reach ~10–20% of recirculation.
- Ancillaries: basin, recirculation pumps, water treatment (anti-scale/corrosion, Legionella control), blowdown to limit cycles of concentration.
- Pros: better annual COP (lower T_{cond}), smaller compressor kW.

- Cons: higher CAPEX/OPEX (water, treatment, maintenance), greater system complexity.

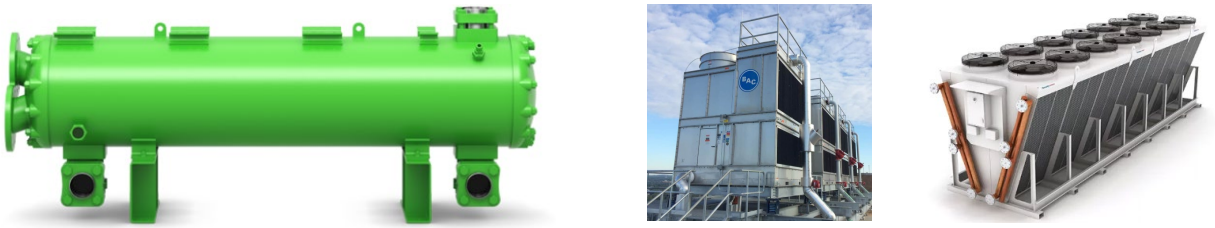

a b c

Figure 6 - a) Water-Cooled Condenser (Source: BITZER); b) Cooling Tower (Source: EVAPCO); c) Dry Cooler (Source: Themokey)

Evaporative condensers

- Combine condenser coil, recirculating spray, and fans in one unit; performance comparable to plate-and-tower pairs, often with smaller footprint.
- Typical performance: $T_{cond} \approx T_{wb}$ + 5–8 K approach → in many Mediterranean summer hours that means ~30–35 °C.
- O&M: similar to towers (make-up, treatment, blowdown, hygiene).

Heat recovery and system synergies

- Heat recovery from the desuperheater or condenser can supply domestic/process hot water and, in produce plants, defrost circuits (hot water or secondary loops).
- Return water from defrost (once filtered) can be routed back to the tower basin to shave basin temperature during peaks—benefit is modest but helps reduce Tcond and water consumption.

2.4.3. Air Cooled Evaporator & Air Cooler

Although the compressor is often referred to as the heart of the system—being the only moving component and usually the most expensive one—the stored products are unaffected by the refrigeration tonnage or by the specific type of compressor, condenser, or other auxiliary equipment. In reality, the preservation of product quality primarily depends on the performance of the evaporator, since it is the heat exchanger directly exposed to the stored commodities. When operating with direct expansion, this component is called the evaporator; in contrast, in indirect systems where a secondary fluid (typically a glycol–water mixture) circulates inside, it is more appropriately referred to as an air

cooler. In both cases, the high-pressure side of the system serves as a supporting section, providing the necessary conditions for efficient operation of the cooling unit in contact with the products.

The evaporator or the air cooler in the case of secondary fluid systems—plays a decisive role in food preservation, as it ensures air circulation within the cold room at the temperature and humidity levels required for the specific product being stored. Proper airflow distribution is equally important, as it guarantees uniform temperature throughout the storage chamber and within the product mass, preventing localized fluctuations.

The selection of the air cooler is therefore application-specific and must be tailored to the expected requirements. For instance, high-humidity storage facilities intended for products such as fruits and vegetables demand a different air cooler design compared to low-humidity storages for commodities like onions or seed grains. Furthermore, special applications such as blast freezers or precooling units call for an altogether different approach, since the cooling rate, airflow pattern, and heat transfer requirements vary substantially from those of conventional cold storage.

The removal of heat from products—whether through cooling or freezing—is essential to prevent or slow down microbial growth and chemical degradation. In the modern food supply chain, product quality is paramount for both consumer satisfaction and economic return. Regardless of whether the application involves post-harvest cooling, blast freezing, process cooling, or long-term storage, several factors ultimately determine the preserved quality of the product. Among these, temperature control and proper air distribution within refrigerated warehouses are of primary importance.

The rate at which product temperature is reduced (pull-down time) is especially critical, as it directly affects the final condition and marketable shelf life of the goods. Even small deviations, on the order of 1.1 to 1.6 K above or below the desired setpoint, can be detrimental to sensitive products. For this reason, air distribution must remain uniform throughout the storage space, avoiding stagnant zones that could compromise the preservation process

In fruit, vegetable, and other positive-temperature cold storages, the primary function of the air cooler is to reduce the product temperature from ambient to the desired level, while also maintaining the required humidity within a prescribed time frame. Its role is to ensure that the products can be stored for the expected duration without deterioration in quality or excessive weight loss. The cooling unit is not intended to enhance the quality of the incoming produce, but rather to preserve and retain the quality present at the time of loading throughout the storage period.

Figure 7 - Air-Cooled Evaporator (Source : ONDA)

Both evaporators and air coolers are generally made of copper tubes combined with copper or aluminum fins. Copper is chosen because of its excellent thermal conductivity, ease of fabrication, and good corrosion resistance, while the fins increase the surface area available for heat transfer, thereby improving efficiency.

The main difference between a direct expansion evaporator and a secondary-fluid air cooler lies in the working medium and the construction details. In a direct expansion evaporator, the refrigerant enters in a two-phase state (liquid–vapor mixture). To achieve proper distribution, a distributor is installed at the inlet: it splits the refrigerant flow into several capillary tubes, each feeding one of the parallel evaporator circuits. This configuration introduces additional pressure losses but is necessary to ensure that all circuits receive an even mixture, avoiding maldistribution and ensuring uniform heat transfer.

a b

Figure 8 - Distibutor; b) Capillary Tubes

In contrast, an air cooler designed for a secondary fluid (such as a glycol–water solution) handles the coolant in a single-phase liquid state. In this case, the inlet header alone is sufficient to divide the flow evenly among the tubes, and no distributor with capillary connections is required. This simplifies the design and reduces pressure drop, although secondary fluids generally provide lower heat transfer coefficients compared to direct expansion refrigerants.

Some of the most important factors that the air-cooler designer must carefully consider include:

- the frontal surface area of the coil;
- the number of tube rows;
- the fin spacing (fin pitch);
- the airflow rate and air velocity;
- the refrigerant mass flow rate;
- the refrigerant temperature.

One design option is to arrange the fan and coil in either a draw-through or a blow-through configuration (Fig. 9).

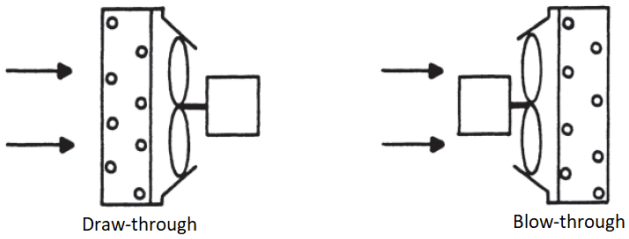

Figure 9 - Fan and coil arrangements

The blow-through type was more commonly used in the past; in this arrangement, the heat released by the fan motor is absorbed by the air before it enters the coil, slightly improving the coil's thermal effectiveness due to the higher mean air temperature. In a draw-through configuration, instead, the fan motor heat is added to the air after it has passed through the coil. The main advantage of the draw-through design is the greater air throw that can be achieved compared to blow-through. Outlet air velocities from the fan in a draw-through unit can reach up to 20 m/s, allowing throws of approximately 60 m.

Frontal area	0.5-0.6 m2 / 1 m3 of room Volume
Number of tube rows	From 4 to 8 rows
Number of fins per m	From 100 to 200 per meter
Fin pitch	4.5 mm: Storage at positive temperatures 6.0 mm: Storage at positive temperatures

	7-8 mm: Storage of fruit and vegetables at high humidity.
Air speed	0.5 m/sec should be air speed through the fruits
Fan diameter	300-600 mm
Delta T	max 2.5 C during storage period

Table 2 - Design and operational parameters of evaporator coils installed in environments for cooling horticultural products

2.4.4. *Thorolling Device*

After leaving the condenser, the liquid refrigerant flows through the throttling device, most commonly a thermostatic expansion valve (TXV) or, in more advanced systems, an electronic expansion valve (EEV). The passage through this restriction causes an abrupt pressure drop, from the condensation pressure on the high side to the evaporation pressure on the low side. This pressure reduction leads to partial vaporization of the refrigerant, creating a two-phase mixture that enters the evaporator and absorbs heat from the warmer environment.

The correct selection of the expansion valve is critical, as it determines the refrigerant flow rate to the evaporator and therefore the amount of heat that can be removed. A poorly sized or improperly applied valve inevitably causes operational issues:

- an undersized valve underfeeds the evaporator, reducing system capacity;
- an oversized valve struggles to control the refrigerant flow, increasing the risk of liquid
- refrigerant returning to the compressor suction line, which can cause severe mechanical
- damage.

Thermostatic Expansion Valves (TXV)

The TXV maintains a nearly constant level of superheat at the evaporator outlet. When the thermal load increases, the resulting higher superheat causes the valve to open, admitting more refrigerant until the preset superheat value is restored. This self-regulating action ensures efficient use of the evaporator surface, even under varying load conditions. An additional advantage of the TXV is greater flexibility during system charging, since it is less sensitive to the precise refrigerant charge compared to fixed-orifice devices.

The TXV regulates refrigerant flow mechanically, based on the balance between bulb pressure, evaporator pressure, and spring force. Its performance depends on a sufficient pressure differential across the valve, meaning that a minimum pressure ratio between the high and low side is required for stable operation. To avoid hunting and ensure reliability, TXVs typically operate with a higher

superheat setting compared to electronic expansion valves. While robust and widely used, this limits their ability to fully optimize evaporator utilization under varying operating conditions

Figure 10 - Thermostatic Expansion Valve (TXV) (Source: DANFOSS)

Electronic Expansion Valves (EEV)

The EEV offers a more sophisticated control strategy, adjusting refrigerant flow based on continuous monitoring of system parameters. In addition to maintaining superheat, EEVs can be integrated into advanced control systems to regulate evaporation temperature, optimize defrost cycles, or even control relative humidity in cold rooms. Their ability to act as tight shut-off devices also eliminates the need for a separate solenoid valve on the liquid line. Overall, EEVs provide higher precision, flexibility, and efficiency, especially in modern refrigeration systems where energy optimization and product quality are critical.

The EEV, driven by a stepper motor and controlled electronically, is far less sensitive to downstream pressure variations. This allows the system to operate at lower condensing pressures, reducing compressor work and improving overall efficiency, especially in variable ambient conditions. Moreover, EEVs can maintain a much lower and more stable superheat than TXVs, thereby improving evaporator effectiveness and increasing system capacity. Their precise modulation not only enhances energy efficiency but also extends product quality preservation in cold storage applications.

Figure 11 - Electronic Expansion Valve (EEV) (Source: CAREL)

2.5. Refrigeration Cycle on the Pressure–Enthalpy Diagram

A vapor-compression system removes heat from produce via an evaporator, rejects it in a condenser, and circulates refrigerant with a compressor and expansion valve. On the pressure–enthalpy (p–h) diagram, the four idealized steps are:

- evaporation (heat absorption at nearly constant pressure, h_4-h_1);
- compression (enthalpy rise/work input, h_2-h_1);
- condensation (heat rejection at nearly constant pressure, h_2-h_3);
- throttling/expansion (isenthalpic to the evaporator inlet, h_3=h_4).

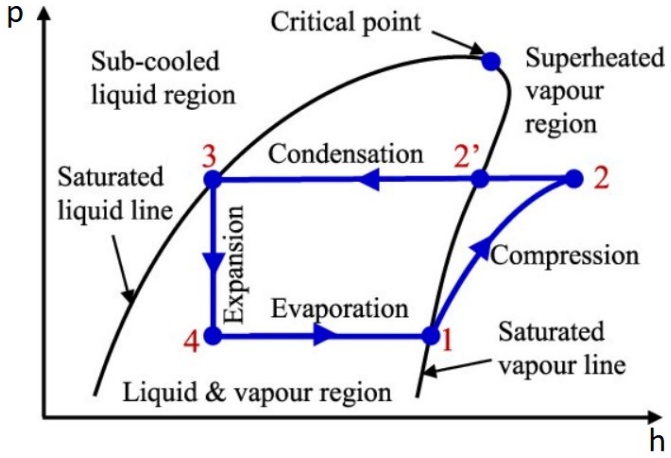

Figure 12 - p–h Diagram of the Refrigeration Cycle

On the pressure–enthalpy (p–h) diagram, the main energy interactions of the refrigeration cycle can be expressed through enthalpy differences:

- Refrigeration effect (cooling capacity):

  $Q_{ev} = h_1-h_4$, [kJ/kg] (2.16)

  This represents the useful effect of the refrigeration cycle: the heat absorbed by the refrigerant in the evaporator from the cooled environment or product.

- Compressor work:

  $P_{comp} = h_2-h_1$, [kJ/kg] (2.17)

  This is the mechanical work required to compress the refrigerant vapor from the evaporating pressure up to the condensing pressure. It represents the energy input needed to maintain the cycle.

- Condenser load (heat rejection):

  $Q_{cond} = h_2 - h_3 = Q_{ev} + P_{comp}$, [kJ/kg] (2.18)

  This is the total heat rejected to the surroundings in the condenser, which equals the sum of the absorbed refrigeration effect and the compressor work.

Coefficient of Performance (COP) is the most common indicator used to evaluate the efficiency of a refrigeration system. It is defined as the ratio between the useful refrigeration effect and the work supplied to the compressor:

$$COP = Q_{ev}/P_{comp} \quad (2.19)$$

The COP expresses how effectively a system converts input energy into useful cooling. A higher COP means that more cooling is achieved for the same amount of power consumed, leading to lower operating costs and improved energy efficiency. Conversely, a low COP indicates that the system requires more energy to perform the same refrigeration duty.

In practice, the COP is strongly influenced by operating conditions: increasing the evaporating temperature and reducing the condensing temperature both improve COP, while large temperature differences reduce it. For this reason, COP is a key parameter for comparing different refrigeration systems, optimizing their operation, and assessing their economic and environmental impact.

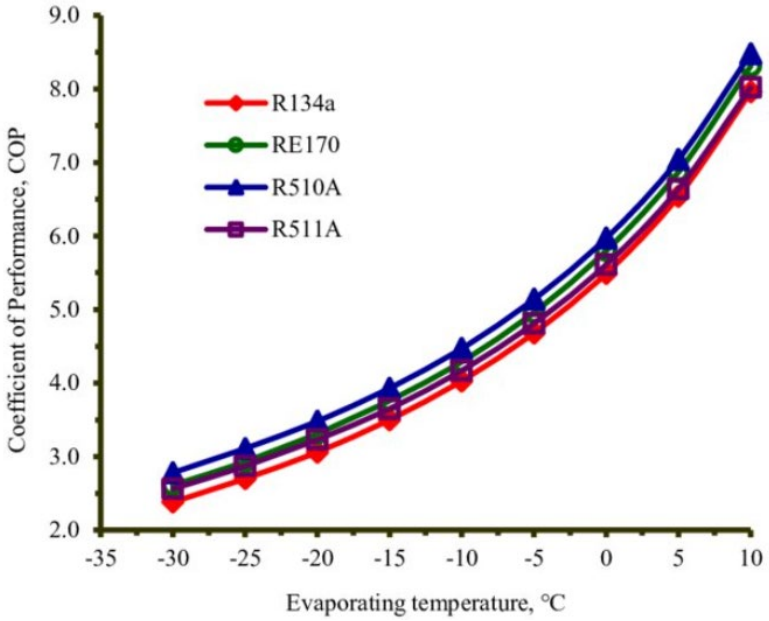

Figure 13 - Variation of COP with Evaporating and Condensing Temperatures

2.6. Cooling Systems: Overview and Classification

By Heat Exchange Architecture

From the perspective of heat exchange architecture, cooling systems for refrigerated storage are mainly divided into two categories: Direct Expansion (DX) and Indirect Systems:

Direct Expansion (DX):

In this configuration, the refrigerant evaporates directly inside the coil placed in the cold room. After passing through the expansion valve, the refrigerant boils in the evaporator tubes, absorbing heat from the surrounding air. DX systems are the most common solution in small and medium sized cold rooms because of their simplicity, compactness, and high energy efficiency. Their main challenges are the precise control of superheat and the management of defrost cycles, both necessary to guarantee safe operation and efficient heat transfer.

Indirect Systems:

In an indirect refrigeration system, the cooling effect is provided by a secondary refrigerant, i.e., a fluid cooled down by the primary refrigeration plant, which absorbs heat from the load and increases in temperature. In some cases, the secondary refrigerant can also be a phase-change medium, condensing in the primary system and evaporating at the cooling load. Historically, before the phase-out of CFCs, refrigerant R-11 was sometimes used in this role, while today carbon dioxide (CO_2) is often employed as a volatile secondary refrigerant.

Secondary refrigerants have been used for many decades, and their importance has recently increased due to trends such as reduced primary refrigerant charges, enhanced safety, and leak isolation. Despite disadvantages—mainly the additional pumping energy and the need to operate at a lower evaporating temperature to compensate for extra temperature differences introduced by the secondary loop—indirect systems are becoming more widespread.

The choice of a suitable secondary refrigerant depends on fundamental properties, including:

- viscosity,
- specific heat,
- density,
- thermal conductivity.

Traditionally, calcium chloride brines were widely used; nowadays, aqueous ethylene glycol solutions are among the most common secondary refrigerants in industrial refrigeration. Ethylene

glycol has a sufficiently low freezing point for many applications, is non-flammable under normal operating conditions, and can be used with steel, aluminum, or copper piping. Its viscosity is a key transport property, influencing both pressure drop and convective heat transfer: while lower than propylene glycol solutions, it is higher than calcium chloride brines. Ethylene glycol poses only a moderate fire hazard (flash point ~113 °C) and is less corrosive than calcium chloride brine. However, its viscosity increases sharply at very low temperatures, making applications below –40 °C impractical. Finally, ethylene glycol is slightly toxic, and therefore it must not come into direct contact with food products.

Indirect Systems for the Fruit and Vegetable Sector

In the storage and preservation of fruit and vegetables, indirect cooling systems are often the preferred option despite their higher initial investment. On average, indirect refrigeration systems are about 20% more expensive than direct expansion systems, yet their advantages in terms of product quality preservation and operational reliability often justify the additional cost. The main reasons are related to product quality, operational safety, and system reliability.

By circulating a secondary fluid, the risk of refrigerant leakage into the storage chamber is minimized, thereby ensuring that the stored products are not exposed to direct contact with primary refrigerants. This aspect is particularly important for the fruit and vegetable sector, where food safety and compliance with strict hygienic standards are crucial.

Another fundamental aspect in fruit and vegetable cold rooms is the requirement for high relative humidity. Maintaining high humidity levels helps prevent product dehydration and weight loss during storage. To achieve this, the temperature difference (ΔT) between the cooling medium and the cold room air should be kept as small as possible.

In direct expansion systems, this ΔT cannot typically be reduced below 5–6 K. This limitation arises from the need to maintain a minimum superheat at the evaporator outlet, ensuring both the safe operation of the compressor and the proper functioning of the expansion valve. If ΔT were reduced further, liquid refrigerant carryover and unstable valve control could occur.

In contrast, indirect systems are not subject to this constraint. Since the cooling is provided by a secondary fluid (e.g., glycol solution) that remains in a single-phase liquid state as it circulates through the air cooler, no superheating requirement exists. The fluid simply increases in temperature as it absorbs heat, without the risk of liquid return to the compressor. For this reason, ΔT can theoretically be reduced to as little as 1 K, allowing much gentler cooling. This allows the air to be

cooled more gently, minimizing condensation and thereby preserving humidity levels and reducing product dehydration

Moreover, indirect systems allow a centralized refrigeration plant to be located outside the storage area, simplifying maintenance and reducing the probability of contamination or accidental leaks in direct contact with the commodities. Another advantage is the greater stability of air cooler operation, since the secondary fluid provides a more uniform temperature distribution and reduces risks of local maldistribution, a factor that helps maintain the freshness and shelf-life of perishable products.

Although indirect systems involve higher capital and operating costs—due to pumping power requirements and an additional temperature lift—the benefits in terms of product quality, safety, and regulatory compliance often outweigh the drawbacks, making them a more suitable solution for the fruit and vegetable supply chain.

2.7. Effects of Temperature and Relative Humidity on Product Quality

Even after harvest, fruits and vegetables remain living organisms, continuing their metabolic activity. The most critical processes are respiration and transpiration. During this process, ambient air oxygen reacts with the reserve sugar or starch of the harvested products, breaking it down into carbon dioxide (CO2), water, and releasing heat energy (2667 kJ) as a result. (Eq. 2.20). The rate of this process strongly depends on temperature:

$$C_6H_{12}O_6 + 6O_2 \rightarrow 6CO_2 + 6H_2O + respiration\ heat \qquad (2.20)$$

Transpiration, on the other hand, refers to moisture loss, which is influenced by relative humidity. Fruits and vegetables generally become unmarketable after losing 5–10% of their initial weight through water loss, as this causes wilting and shrivelling (Lufu et al., 2020).

The structural integrity of the product plays a key role in its postharvest stability. Whole fruits are naturally protected by their skin tissues and cuticle, which act as barriers against pathogens, insects, and excessive water loss (Velderrain-Rodríguez et al., 2015).

Fresh-cut produce, however, is highly perishable. Operations such as peeling, slicing, or cutting remove or damage protective tissues, exposing the flesh to microbial contamination, enzymatic browning, and accelerated deterioration (Shen et al., 2019).

From a commercial perspective, postharvest management must reconcile biological needs with market demands. Consumers expect fruits and vegetables to be available throughout the year, easy to handle, resistant to browning and disease, and to retain desirable quality attributes—flavor, aroma, color, appearance, firmness, and juiciness—for as long as possible. Yet, biological limitations impose strict timeframes between harvest and consumption. Fruits such as strawberries and peaches, which

reach optimal quality at or just after harvest, can only be stored for a few days or weeks, after which any change reduces quality (e.g., softening or overripening). In contrast, pome fruits such as apples and pears can be stored for extended periods, provided that cold conditions are applied immediately after harvest to support proper ripening and aroma development.

Cold storage represents the primary technology for delaying ripening in most fruits. Complementary strategies include controlled atmosphere (CA) storage, with reduced oxygen and elevated carbon dioxide levels, and modified atmosphere (MA) storage. In some cases, chemical, biological, or natural agents are also applied to slow deterioration. However, consumer acceptance of chemical treatments is limited, as they are often perceived as artificial interventions or even potential health risks. By contrast, refrigeration, CA, MA storage, and the use of natural compounds or antagonistic microorganisms are generally well received, as they are seen as safer and more natural preservation methods

Transpiration rates, or the loss of water from fresh-cut, are influenced by the moisture content of the surrounding air, typically indicated as relative humidity (RH). At a consistent temperature, even slight fluctuations in relative humidity can have a notable impact on the rate of water loss in fresh produce (Lufu et al., 2020). When the relative humidity is too low, transpiration rates for fresh produce increase, leading to shriveling, weight loss, diminished crispness, and a deterioration in appearance. Conversely, excessively high relative humidity levels can foster mold and rot development, along with issues like water condensation on surfaces and a reduction in the strength of paper-based packaging of the fresh-cuts. Moreover, storing green vegetables under conditions that induce shriveling can accelerate the decline in vitamin C content (Lee & Kader, 2000).

The rate of moisture loss from fruits and vegetables is usually expressed by an equation of the following form (ASHRAE Transactions 1985, Vol. 91, Part 1):

$$\dot{m}=K\cdot A\cdot(p_s-p_a) \qquad (2.21)$$

where:

$\dot{m}$ = rate of moisture loss, (mg/s)

K = mass transfer coefficient, (mg/s·m^2·kPa);

A = surface area of product, (m^2);

p_s = water vapor pressure of evaporating surface, (kPa);

p_a = water vapor pressure of surrounding air, (kPa);

Optimal relative humidities for the preservation of most fruits and vegetables typically fall within the range of 90–95%. However, some fruits, including apples, pears, and berries, thrive better at the

higher end of this humidity spectrum. Certain vegetables also benefit from higher humidity levels, even approaching 100%. Leafy vegetables like lettuce, cabbage, and celery, as well as sweet corn, radishes, melons, and various others, are among those that are better preserved under such conditions.

Relative humidity (RH) is always subject to change, influenced by numerous factors within the microclimate. Altering nearly any aspect of the microclimate can impact RH. Consequently, maintaining RH within a narrow range at high levels in large storage rooms presents practical challenges. For instance, to illustrate the difficulty, in order to sustain 95% RH at a temperature of 0°C, the average temperature difference between the air and the evaporator must be approximately 0,5°C (Paull, 1999)

.The primary mechanisms contributing to an increase in relative humidity (RH)in the cold storage:	*The primary mechanisms contributing to a decrease in relative humidity (RH) in the cold storage:*
• evaporative moisture loss from the product; • infiltration of warm, moist ambient air through doors; • evaporation of free water from internal surfaces; • sublimation of coil frost during defrost; • desorption of water from paper-based packaging materials; • active humidification.	• dehumidification via condensation or frosting by the air cooling coils; • sorption of water by paper-based packaging materials • condensation of water on internal surfaces.

Relative humidity (RH) is affected by several factors, such as the surface area of the refrigeration air cooler in the storage room, the temperature difference between the coil and the air, air exchange rates, temperature distribution within the room, and the type of commodity and packing material used. In facilities operating near 0°C, RH significantly influences the rate of frost formation on air-cooling coils, which in turn affects the need for defrosting. Defrost cycles result in temperature and RH fluctuations that may hasten the degradation of product quality.

The main mechanisms that can be used to keep the relative humidity high in the cold rooms for fresh-cuts are (Sujau et al., n.d.):

- Reducing the sensible heat.

This involves design strategies such as increasing insulation levels, minimizing lighting and fan power, and operational practices like adjusting fan speed during low heat loads and turning off unnecessary lighting.

- Increasing the heat exchange surface of the refrigeration coil (i.e minimise air to refrigerant temperature difference).

Design considerations focus on optimizing the size of the refrigeration coil and the method of refrigerant supply, such as using flooded coils or secondary refrigerants rather than direct expansion coils. Operational practices, like setting the superheat for direct expansion coils, are also crucial to minimize the air-to-refrigerant temperature difference.

- Selecting Air Temperature Control Systems

Utilizing systems that ensure the cooling coil remains fully wetted is essential for maintaining high RH. This may involve modulating refrigerant temperature instead of using on/off control for refrigerant supply.

- Packaging Material Selection and Equilibration:

The choice of packaging materials and their equilibration with the environment before entering the cold store is vital. For instance, paper-based packaging can influence cold store RH, with lower RH in the packaging area leading to moisture adsorption, potentially lowering cold store RH, and vice versa.

- Smart defrosting control

Implementing intelligent defrosting control systems can help minimize disruptions to RH caused by defrost cycles

Without auxiliary humidification, the design relative humidity of 95% is very difficult to be maintained, because the rate of moisture removal at the coil is higher than that entering with the infiltration air.

2.8. Defrost

When the surfaces of air coolers, which are the coldest surfaces in the cold room, operate at temperatures below 0°C and also below the dewpoint temperature of the air, frost formation on the coil is inevitable. In certain scenarios, icing may occur, where moisture from the air condenses into liquid water before freezing into ice. However, the more prevalent occurrence is when water vapor undergoes direct transformation into a solid state, resulting in frost buildup on the coil (W. Stoecker, 1998). Typically, the rate of frost growth is relatively slow when the relative humidity (RH) remains

below 40%. However, in the fresh-cut sector where the relative humidity in the cold rooms is very high, the growth rate will inevitably increase. This phenomenon is linked to the mass and energy exchange process that occurs between humid air and a cold surface whose temperature is below the dew temperature of humid air and below a few degrees of 0°C. The primary factor influencing the growth of frost on the surface of heat exchangers is the air speed, characterized by the Reynolds number. Alongside air speed, other crucial parameters include surface temperature, the extent of the heat exchanger's surface area, and relative humidity. When air speed surpasses a critical threshold, or Reynolds number, its impact on the growth phenomenon appears to be minimal. Conversely, below this critical value, the dependence on air speed becomes more pronounced, significantly influencing the frost growth process (O'Neal D.L., et. al "Measurement of Frost Growth and Density in a Parallel Plate Geometry" ASHRAE Transactions; Vol 90, pt.2).

Although light frost accumulation slightly improves heat transfer of the coil (ASHRAE Refrigeration handbook 2010 page 14.4). If the continuous accumulation of this frost is not removed, the performance of the evaporator deteriorates since the frost acts as resistance to heat flow as also increases the air side resistance reducing the air flow. Because frost has a low effective thermal conductivity (<0.6 W/(m·K)), contrasting with the high thermal conductivity of typical heat exchanger materials (>100 W/(m·K)), it diminishes the thermal efficiency of the system (Mohammad et al., 2024). Even a thin ice layer of 1.5 to 2 mm can decrease heat transfer by 5-15% (with fin spacing of 7mm). The compromised airflow further impacts cooling capacity, reducing it anywhere from 20 to 100%. So of these two penalties, restricting the air-flow rate is the most serious. As a result, the refrigeration system loses efficiency, and the temperature and humidity of the air can deviate significantly from the required values. In the case of a completely frosted coil, it is possible that the air will no longer be able to pass through it, making the work done by the refrigeration unit useless with a considerable energy waste. Reduced heat-transfer efficiency means more energy is needed to achieve the same amount of cooling. Consequently, the coefficient of performance (COP) or the capacity of the refrigeration system will degrade appreciably and sometimes may even lead to system shutdown. (Hakkaki-Fard et al. 2014)

Defrosting is imperative to uphold system efficiency. Yet, the timing and duration of defrost cycles are pivotal factors influencing system performance. Premature or delayed defrosting can lead to energy wastage. However, inefficient management of defrost cycles often results in excessive energy consumption for cooling purposes.

2.8.1. *Frost Formation and Growth on Heat Exchangers*

The formation and growth of frost on heat exchanger surfaces has long been a subject of experimental and theoretical investigation. Studies have been conducted on simple geometries such as plain cylinders, flat plates, and parallel plates, in order to better understand the mechanisms of frost deposition under different operating conditions.

Among the key factors influencing frost accumulation are: surface temperature, air velocity (often expressed through the Reynolds number), and ambient relative humidity. In general, a lower surface temperature or higher humidity leads to a faster increase in frost thickness. However, the influence of air velocity is more complex. Some authors (e.g., Schneider) suggested a weak dependence, whereas others (e.g., O'Neal, Hosoda, Yamakawa) demonstrated that above a certain critical Reynolds number, the growth rate of frost changes significantly. For example, O'Neal identified a threshold of about Re = 15,900 for parallel plate heat exchangers: below this limit frost growth is strongly affected by air velocity, while above it the influence becomes marginal. Similar results were reported by Yamakawa, who observed that increasing Reynolds number up to ~13,000 increased frost thickness by ~15% over 2.5 hours, but further increases in velocity produced only minor changes.

Another important aspect concerns the distribution of frost across the heat exchanger surface. Frost often forms more quickly in the upstream regions directly exposed to cold, humid air, and more slowly in the downstream sections. This effect is particularly evident in finned-tube coils, where the front rows accumulate more frost and thus contribute disproportionately to pressure drop. Experiments by Niederer confirmed that frost growth is more pronounced on the frontal area of the coil, whereas Schneider reported less variation depending on the section studied.

To predict frost growth, several analytical and numerical models have been developed. Classical approaches couple the governing equations of heat and mass transfer, considering conduction through the frost layer, convective heat exchange with air, and mass diffusion of water vapor. The frost layer is typically modeled as a porous medium, whose density and thermal conductivity evolve over time. While such models can be accurate, they are mathematically complex and often solvable only numerically.

From a heat transfer perspective, frost has a dual effect. On the one hand, the rough surface of frost enhances the local air–frost convective coefficient compared to a clean, smooth surface. On the other hand, the increasing thickness and low conductivity of the frost layer introduce significant thermal resistance, reducing the global heat transfer coefficient of the coil. In practice, the overall effect is a

progressive decline in heat exchanger performance, usually stabilizing after about 60–90 minutes of operation under frosting conditions.

More recent studies (e.g., Yan and colleagues) have focused on finned-tube heat exchangers with different fin geometries, aiming to quantify how design parameters such as fin spacing, thickness, and arrangement influence both frost deposition and air-side pressure drop. These works highlight that the proper design of air coolers must balance thermodynamic efficiency, frost tolerance, and defrosting strategy.

2.8.2. The defrost process

The defrosting process typically comprises three stages:

- The defrost method (i.e. the means used to heat the battery and melt the ice)
- The defrost frequency (i.e. the calculation of when it is appropriate to start defrosting)
- The defrost duration (i.e. the calculation of when it is appropriate to end the defrost)

The defrosting method must adapt to the amount of ice that forms during normal operation and the state of the air present around the coil. Ideally the defrost frequency should adapt to the amount of ice present on the coil requiring a reliable method of measuring ice thickness. It would be ideal to find a hypothetical compromise between a high frequency (coil always efficient but a lot of energy spent on defrosting) and a reduced one (reduced defrost consumption but poor coil efficiency). The defrost duration varies based on the layer of ice formed. Since it cannot be measured exactly, two methods are mainly adopted, one based on the physical principle of phase change at constant temperature (0 C) and the other on the dynamic principle linked to the working pressures. No matter what kind of defrost methods are applied, the defrost controls should be implemented based on demand. It is important to accurately detect the presence and growth of the frost. However, the frost formation and growth is a transient process with dynamic heat and mass transfer. It depends on six primary parameters, the air temperature, the air relative humidity, the air velocity, the air cleanliness, the temperature and wettability of the heat exchanger surface. To monitor all those parameters simultaneously is a hard work for the practical refrigeration facility (W. Wang et al. 2011)

Several methods are available in refrigeration practice, each with specific advantages, limitations, and fields of application.

The defrost method

The most widely adopted are:

- Compressor shutdown (off-cycle) defrost;

- Electric resistance defrost;
- Hot-gas defrost;
- Water (spray) defrost.

Compressor Shutdown (Off-Cycle) Defrost

The simplest and most widely used defrosting technique is the off-cycle defrost, also known as compressor shutdown defrost. In this method, the refrigerant flow to the evaporator is interrupted by stopping the compressor, while the evaporator fans continue to circulate air across the coil. The relatively warmer room or ambient air then melts the frost accumulated on the finned surfaces.

This approach is only effective when the surrounding air temperature remains above approximately 1 °C, since sufficient sensible heat must be available to raise the coil surface temperature above the freezing point. If the ambient temperature is too low, frost removal becomes incomplete or requires excessively long cycles.

Experimental studies, such as those by Shang (2009), have demonstrated that fan operation during the off-cycle improves defrosting performance, particularly in air-source heat pump (ASHP) units. The main advantages of this method are its simplicity, low initial cost, and minimal control requirements. For this reason, it is commonly adopted in medium- and high-temperature cold rooms.

However, the process also has limitations. Since the energy required for melting frost comes solely from the ambient or room air, defrosting tends to be relatively slow. Prolonged cycles may also lead to fluctuations in room temperature and humidity, which can negatively impact product storage conditions. Consequently, compressor shutdown defrost is best suited for applications with moderate frost accumulation and where tight humidity control is not critical.

Typical defrost duration: 45–90 minutes

Typical Defrost Sequence (Off-Cycle):

1. The compressor stops, interrupting refrigerant supply to the evaporator.
2. The evaporator fans remain in operation, circulating relatively warm room air across the frosted coil.
3. The frost gradually melts due to the sensible heat of the air.
4. Meltwater is collected in the drain pan and discharged.

5. After a preset time (or when a termination thermostat signals sufficient defrost), the compressor restarts and the refrigeration cycle resumes.

Electric Heating Defrost

Figure 14 - Defrost Heater Element

Electric defrost relies on electrical heating elements installed either adjacent to, or integrated within, the evaporator coil. During a defrost cycle, the refrigerant supply to the evaporator is stopped and the heaters are energized. Heat transfer takes place through a combination of radiation, convection, and conduction between the heaters, the coil surfaces, and the surrounding air, causing the accumulated frost to melt.

In practice, the heater is often positioned beneath the evaporator, with heat rising by natural convection to warm the coil and the frost. Most of the heat transfer occurs by convection and radiation, with only a small fraction by conduction.

Since this method introduces external heat into the refrigerated space, only part of the generated energy is effectively used to melt frost. A significant portion is transferred to the surrounding air and to the stored products, temporarily raising their temperature. This excess heat must be removed when the refrigeration system resumes normal operation. As a result, electric defrost is relatively energy intensive, with typical defrost efficiencies ranging from 30% to 50%.

Despite these drawbacks, electric defrost offers some clear advantages:

- It is reliable, simple to control, and relatively inexpensive to install;
- It provides fast frost removal compared to off-cycle defrost;
- It can be applied in low-temperature applications where other defrost methods are ineffective.

On the other hand, its operating cost is high because of the additional power consumption, and excessive heating can negatively affect product quality if temperature fluctuations are not properly managed.

Several studies have investigated ways to improve the efficiency of electric defrost. Bansal et al. (2010) developed a thermal model to analyze energy flows from defrost heaters in household refrigerators, concluding that radiant heaters tend to reach unnecessarily high temperatures for the sole purpose of frost melting. Melo et al. (2013) compared different types of electric heaters (distributed, calrod, and glass tube) and different power control strategies (integral power, power steps, and pulsating power). Their results showed that while all heaters performed similarly, the highest efficiency approximately 48%—was achieved using a glass tube heater operated in stepped power mode.

In cases where frost accumulation on the evaporator is limited, under such conditions, the evaporator may become “clean” in a short time, i.e., before the defrost cycle—controlled by a simple timer—has been completed. Once all the frost has melted, the heat produced by the defrost heaters is no longer absorbed by the phase change of ice, and the evaporator temperature rapidly rises above 0 °C.

This phenomenon leads to two critical consequences:

1. Excessive increase of the cold room air temperature, with negative effects on product preservation.
2. Overheating of the defrost heaters, which are no longer cooled by melting frost. If the power supply is not promptly interrupted, the heaters may reach incandescent temperatures and suffer irreversible damage.

Often, such failures are not immediately detected. Over time, however, the lack of effective defrosting results in the accumulation of a thick frost layer on the evaporator, seriously compromising system performance.

It is therefore essential that, in the event of rapid frost melting, the defrost cycle is automatically terminated to prevent both excessive room temperature rise and heater damage. For this purpose, two safety devices are typically installed:

- a defrost termination thermostat, which interrupts the cycle when the evaporator temperature exceeds a preset value (commonly around 5-10 °C);

It must be positioned where frost persists the longest, in order to ensure proper cycle termination. Since heating elements are usually placed at the bottom of the evaporator—where the greatest ice accumulation occurs—the sensor should be mounted in the middle-upper section of the coil, typically between the first two rows of tubes and inserted between the fins. It is essential that the sensor is located away from the direct influence of the heaters (electric rods or hot-gas tubes), otherwise it would detect artificially high temperatures and terminate the defrost cycle prematurely.

- a safety thermostat, which cuts the heater power supply in case of excessive overheating or abnormal current draw.

Typical defrost duration: 20–45 minutes

Typical Defrost Sequence (Electric Resistance):

1. Pump-down phase: the liquid line solenoid closes and the compressor continues running until the low-pressure switch stops it, ensuring the evaporator is emptied of liquid refrigerant.
2. The compressor remains off, interrupting refrigerant flow to the evaporator.
3. The evaporator fans are stopped to avoid distributing warm air into the cold room.
4. The electric heaters are energized, transferring heat to the coil and melting the frost.
5. Drain phase: heaters switch off once the defrost termination thermostat reaches the set temperature (e.g., 5-10 °C); meltwater continues to drain naturally from the evaporator.
6. Post-drip phase: fans remain off for an additional period, allowing residual droplets to fall and preventing water from being blown into the cold room.
7. The compressor and fans restart, resuming normal refrigeration.

In summary, electric defrost remains one of the most widely used techniques in commercial and industrial refrigeration due to its effectiveness and simplicity, though at the expense of higher energy consumption.

Hot gas Defrost

Hot gas defrost (HGD) is one of the most effective defrosting techniques, widely applied in commercial and industrial refrigeration systems. In this method, the superheated refrigerant vapor discharged from the compressor is diverted directly into the evaporator (or outdoor coil), bypassing the condenser and expansion device. The hot, high-pressure refrigerant condenses inside the frosted

coil, releasing its latent heat, raising the coil temperature above 0 °C, and melting the accumulated frost. Since the evaporator is heated internally by condensation, less excess heat is released into the cold room compared to electric resistance defrost.

System configuration requires the installation of:

- a dedicated hot gas line, normally closed by a solenoid valve,
- an expansion device (capillary, calibrated orifice, or electronic expansion valve) that regulates flow and pressure of the hot gas into the evaporator.

During defrost:

- the compressor must remain in operation, supplying hot discharge gas;
- the expansion valve continues feeding refrigerant, though at reduced capacity, since part of the discharge gas is diverted for defrosting;
- the solenoid valve for hot gas opens, allowing hot discharge vapor to enter the evaporator and raise its temperature above 0 °C;
- control can be optimized by modulating the hot gas valve (continuous or pulsed operation), achieving smoother defrost and avoiding overheating.

Advantages of hot gas defrost:

- Faster and more efficient frost removal compared to electric and off-cycle defrost;
- Lower heat load introduced into the cold room;
- Possibility to maintain partial cooling capacity during defrost;
- Reduced energy penalty compared to electric heaters.

Limitations and drawbacks:

- Increased mechanical stress on the compressor, which must operate continuously under high discharge conditions, leading to accelerated wear and potentially shorter service life;
- he high-temperature refrigerant vapor is introduced into a low-temperature evaporator and its nearby piping. The resulting steep thermal gradients can cause thermal shock, and repeated cycles may lead to stress cracking and refrigerant leaks around the evaporator.

- More complex piping and control requirements (dedicated hot gas line, valves, and safety devices);
- Initial investment cost is higher than electric defrost;
- Risk of liquid slugging if hot gas injection is not well controlled.

Defrost duration is highly variable and depends on frost accumulation, coil design, and control strategy. With well-designed regulation (e.g., electronic expansion valves modulating based on evaporator pressure or temperature), defrost can be optimized to minimize energy use and reduce thermal stress on the stored products.

Typical defrost duration: 5–15 minutes

Typical Defrost Sequence (Hot Gas Defrost)

1. Pump-down phase:
    - The liquid line solenoid closes and the compressor continues running until the low-pressure control stops it, ensuring the evaporator is emptied of liquid refrigerant.
    - This prevents liquid hammering and ensures safe introduction of hot discharge gas.
2. Compressor restarts and continues operating:
    - The compressor supplies hot, high-pressure refrigerant vapor at the discharge.
    - Unlike electric or off-cycle defrost, the compressor remains active throughout the process.
3. Fans OFF:
    - The evaporator fans are stopped to avoid blowing warm, humid air into the refrigerated room.
    - This reduces heat transfer to the stored products.
4. Hot gas solenoid opens:
    - A dedicated solenoid valve on the hot gas bypass line opens, allowing hot discharge vapor to flow directly into the evaporator inlet.

- Flow is regulated either by a calibrated orifice/capillary tube or by an electronic expansion valve (EEV), which modulates based on evaporator pressure or temperature.

5. Defrosting phase:
   - The hot gas condenses inside the evaporator tubes, releasing latent heat and raising the coil surface temperature above 0 °C, melting the frost.
6. Drain phase:
   - When the frost is melted, heaters are not needed; meltwater continues to drain naturally from the evaporator.
   - The hot gas valve closes once the defrost termination thermostat reaches the setpoint temperature (e.g., 5-10 °C) or maximum time expires.
7. Post-drip phase:
   - A short waiting period follows with fans still off, allowing residual water to drain completely and preventing droplets from being blown into the cold room.
8. Restart of normal operation:
   - The hot gas valve closes completely.
   - The compressor and evaporator fans resume normal cooling operation.

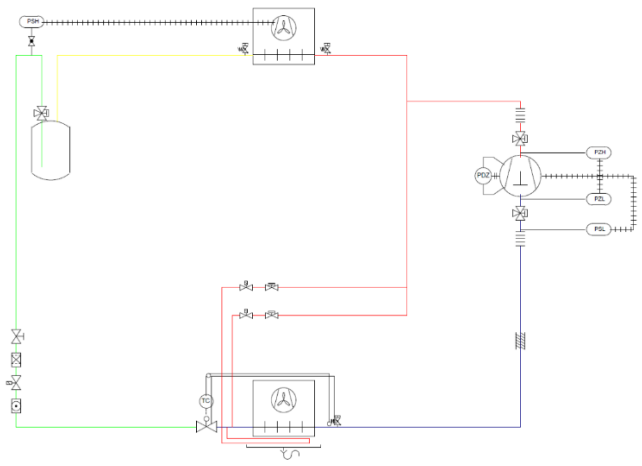

Figure 15 - Schematic of Single-Flow Hot Gas Defrost

Water Defrost

Water defrost relies on spraying water over the coil to melt the accumulated frost. The system consists of distribution ramps positioned above the coil, from which water is sprayed onto the finned surfaces. The ice partly melts and partly detaches as flakes, which are collected in the drain pan and discharged from the cold room.

From a product quality perspective, this method is particularly advantageous in fruit and vegetable storage, since it restores the cooler performance without excessively heating the air in the cold room. The absence of significant temperature fluctuations helps maintain high humidity levels, thereby reducing product dehydration. For this reason, water defrost is often considered the best solution in post-harvest and fresh produce applications.

However, the method presents some drawbacks:

- The colder the water, the more volume is required; therefore, slightly warm water—often recovered from the condenser outlet—is typically used.
- Water consumption is relatively high, around 8–10 liters per kilogram of frost removed.
- Detached ice flakes may obstruct the drain line, causing overflow into the cold room. Proper drainage and heating of the drain pan are essential to prevent re-freezing.
- Automatic operation is more difficult to implement compared to other defrost methods, and heating devices are usually required to ensure complete melting of detached ice.
- During the initial spraying, water may freeze on the coil until the surface reaches 0 °C, which can temporarily increase ice mass, especially in low-temperature applications if refrigerant is not pumped out beforehand.
- Unlike hot gas defrost, the energy supplied in water defrost is not recovered in the refrigeration cycle but lost to the system balance.

Despite these limitations, for horticultural cold rooms water defrost remains the most product-friendly technique, as it minimizes drying effects and maintains optimal air humidity.

Typical Defrost Sequence (Water Defrost – Air Cooler with Secondary Loop)

1. Defrost initiation: control system starts the defrost cycle.
2. Isolate the coil from the secondary circuit: close the control valve on the air cooler or switch a 3-way valve to bypass; the pump continues circulating through the bypass line.

3. Fans OFF: evaporator fans are stopped to avoid water droplets being blown into the cold room.
4. Water spray ON: the solenoid valve opens and slightly warm water (e.g., condenser outlet water) is evenly distributed over the coil surface through spray nozzles or ramps.
5. Defrosting phase: frost melts or detaches as ice flakes; monitoring is by time and/or by a defrost termination sensor placed between fins in the critical section.
6. Water OFF (termination): the water spray stops when the coil temperature reaches a setpoint (e.g., ~5 °C) or when the maximum defrost time is reached.
7. Drain phase: with fans still off, residual water and ice flakes are allowed to drain completely through the heated drain pan and piping.
8. Post-drip phase: a short additional waiting period ensures that no residual droplets remain before fans restart.
9. Re-coupling the coil: reopen the control valve of the secondary loop (or reset the 3-way valve) gradually, to avoid thermal shocks.
10. Fans ON and cooling resume: fans restart and the system returns to normal operation.

The defrost frequency

- *Time initiated*

  The time-initiated defrost is the most common and widely applied strategy in industrial refrigeration systems. Its popularity comes from its simplicity and ease of implementation, since it does not require any specific sensors to detect frost accumulation on the evaporator surface.

  In this control method, both the initiation and termination of the defrost cycle are governed by a predefined timer, regardless of the actual amount of frost present on the evaporator. The system is typically programmed to perform a fixed number of defrost cycles per day (for example, two, three, or four), each with a preset duration determined during system setup.

  However, this simplicity also introduces several functional limitations. Because the defrost operation is not based on real frost accumulation or operating conditions, it is possible that:

  - the defrost cycle is excessive, occurring when the evaporator has little or no frost, which results in unnecessary energy consumption and undesirable temperature and humidity fluctuations in the cold room;

- the defrost cycle is insufficient, when the interval between two cycles is too long, allowing frost buildup to degrade heat transfer and airflow through the coil.

Throughout the year, the temperature and humidity of the air entering the cold room may vary significantly due to seasonal changes and door openings. For instance, during summer — when ambient air is warmer and more humid — the frost formation rate is higher, often requiring three to four defrost cycles per day. In contrast, during winter, when the air is cooler and drier, one defrost per day may be sufficient.

These observations highlight that, although the time-initiated defrost strategy is robust and reliable, it does not ensure optimal performance in terms of energy efficiency and temperature stability inside the cold room. For this reason, in modern refrigeration systems, time-based defrost is increasingly being replaced or supplemented by demand-based defrost control strategies, which adapt the frequency and duration of the defrost cycles to the actual operating conditions and frost accumulation on the evaporator.

- *Comparing the heat transfer rate on the air and refrigerant side of the evaporator*

The comparison between the heat transfer rate on the air side and that on the refrigerant side of the evaporator is a complex task, both in laboratory and in real operating conditions. Accurately determining the heat transfer parameters requires precise measurements of air flow rate, temperature, and humidity, as well as refrigerant mass flow rate, pressure, and enthalpy at the inlet and outlet of the evaporator. Even small measurement uncertainties can lead to significant errors in the calculated heat transfer rates. In controlled laboratory environments, it is sometimes possible to obtain reasonably accurate data through detailed instrumentation and calibration procedures. However, in field applications, such measurements are far more difficult due to variable operating conditions, limited sensor placement, and external disturbances such as fluctuations in ambient temperature, door openings, or variations in air distribution. As a consequence, the comparison between the air-side and refrigerant-side heat transfer rates cannot always be used as a reliable reference for real-time control strategies, such as defrost management. Inaccurate or delayed measurements could lead to incorrect estimation of frost accumulation, compromising both the energy efficiency and the temperature stability of the refrigeration system.

- *Capacitive defrost*

The capacitive defrost sensor operates based on the principle of capacitance measurement, where the capacitance changes according to the presence of ice between the evaporator fins. In this system, an insulated stainless-steel wire serves as one electrode, while the evaporator fins act as the second electrode. The space between them forms a dielectric region whose properties

vary depending on whether it is filled with air, water, or ice. As frost accumulates on the evaporator, the air between the fins is gradually displaced by ice, which has a higher dielectric constant than air. This causes the measured capacitance (expressed in picofarads, pF) to increase proportionally to the ice thickness. During defrosting, the sensor continuously monitors this capacitance value: when defrost starts, the melting ice becomes wet, leading to a temporary increase in the pF signal due to the higher permittivity of water; as the ice completely melts and water drains away, the capacitance decreases to its baseline level, signaling that the evaporator is clean and defrosting can be terminated. The sensor output can be provided as a 4–20 mA analog signal and/or as a digital output transmitted to the main control unit (e.g., PLC or supervisory controller). This allows the system to initiate and stop defrost cycles automatically based on the actual frost condition rather than on a fixed time schedule. Compared to traditional time- or temperature-based defrost strategies, the capacitive method offers significant advantages in terms of accuracy and energy efficiency, as it ensures that defrosting occurs only when necessary and terminates exactly when complete.

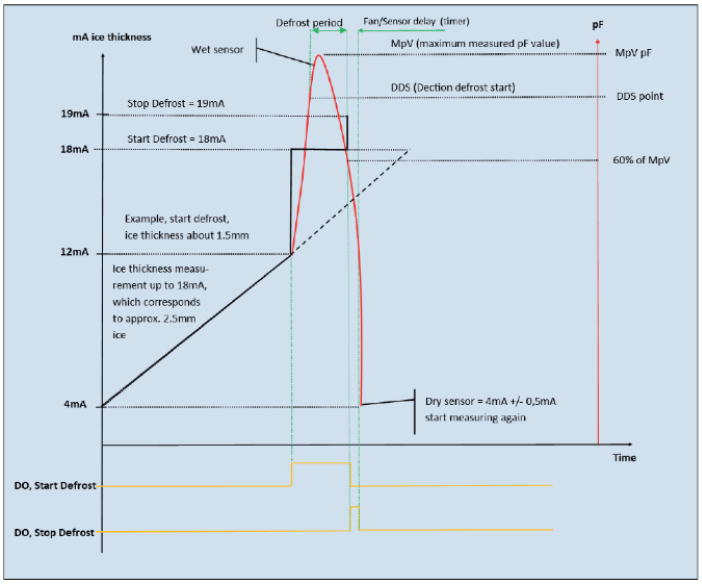

Figure 16 - Output Signal Configuration of the Capacitive Measurement System (Source: HB)

3. Materials and Methods

3.1. Cold room environmental and refrigeration data Measurement and Monitoring System

3.1.1. System Description

The monitoring system is a performance analysis tool developed for the diagnostics and optimization of refrigeration and air conditioning systems. Its methodology is based on direct measurements taken on the refrigeration circuit, without the need for permanent installation of invasive measuring instruments. This feature allows for rapid installation, immediate access to detailed data, and a comprehensive assessment of the unit's performance under various operating conditions.

The main elements are:

- PT1000 temperature probes

Figure 17 - PT1000 Temperature Sensor

The temperature sensors used in the system are Pt1000 DIN class A, characterized by high precision and stability. These are resistance temperature detectors (RTDs) that exploit the variation in platinum resistivity with temperature: as the temperature increases, the electrical resistance of the sensing wire increases linearly.

Construction features

- Surface mount: Designed to be mounted on pipes or surfaces, they provide reliable measurement without the need for direct insertion into the refrigerant.

- Mechanical robustness: Built to withstand the impacts and stresses typical of machine rooms or field installations.
- Connection cable: High-quality 5 m silicone cable with teleplug, featuring good flexibility and high temperature resistance.Punta sensore: lunghezza di 40 mm con scanalatura per garantire il corretto contatto con la superficie e migliorare la trasmissione termica.
- Degree of protection: The probe is sealed and submersible, eliminating the risk of condensation and allowing use in humid environments.
- Temperature range: Approved for operation between -50°C and +150°C, making it suitable for applications on both very cold suction lines and hot discharge lines.

Metrological performance

- Accuracy class: DIN class A, with maximum deviation equal to

$$\pm(0.15+0.002\cdot|t|)\ °C$$

where t is the temperature in °C

- Cable resistance: for the standard 5 m version, the overall resistance is 1.32 Ω, corresponding to an error of approximately +0.34 °C to be considered during calibration.
- Tempo di risposta: tipicamente dell'ordine di pochi secondi in condizioni di buon contatto termico, garantendo una lettura dinamica durante variazioni di regime.

Other technical aspects

- Linearity: Pt1000 sensors exhibit more linear behavior than other types of RTDs (e.g. Pt100), making it easier to convert from resistance to temperature.
- Reliability over time: platinum is chemically stable and resistant to oxidation, ensuring a long service life and very low drift.
- Compatibility: The resistive signal is standardized, allowing integration with most measuring instruments and control systems.

- Pressure transducers

Figure 18 - Pressure transducer

Pressure transducers are piezoresistive, designed for refrigeration circuit applications. These sensors convert refrigerant pressure into a proportional electrical signal, allowing real-time determination of the fluid's thermodynamic states, mass flow, and cycle efficiencies.

Construction features

- Piezoresistive technology: The heart of the sensor is a silicon chip, isolated by a layer of oil and coupled to a stainless steel membrane. The deformation of the membrane under pressure generates a change in resistance, which is converted into an electrical signal.
- Advanced manufacturing: The transducers are manufactured using an automatic brazing line, enabling mass production with high repeatability and quality.
- No internal gaskets: The construction without cavities, O-rings, or internal seals eliminates the weak points typical of traditional transducers, reducing the risk of leaks and improving long-term reliability.
- Materials: All parts in contact with the refrigerant are made of stainless steel, ensuring corrosion resistance and compatibility with most refrigerant gases and oils.
- Pressure connection: Standard ¼" flare (7/16"-20 UNF) connection with Schrader depressor valve and Teflon seal, allowing assembly and disassembly without refrigerant leaks.

Electrical characteristics

- Output signal:
  - Standard: 1–5 VDC
  - Optional: 4–20 mA for compatibility with industrial systems.
- Power supply: 8–28 VDC, suitable for various types of controllers and acquisition systems.

- Connector: Packard Plug type, industrial standard, which ensures quick and robust connection.

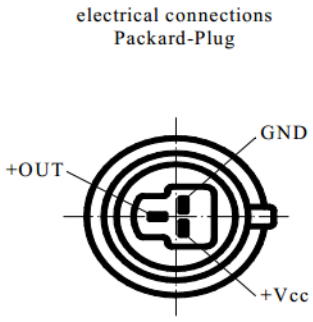

Figure 19 - Top view of the sensor

Performance and technical specifications

- Measuring range: For the application considered, transducers with a range of 1…12 bar (suction line) and 0…32 bar (discharge line) were used, suitable for covering the typical evaporation and condensation pressures in refrigeration systems.
- Accuracy: <1% FS (Full Scale), including linearity, hysteresis, and repeatability.
- Operating temperature: -20 to +100°C, suitable for use in suction and discharge lines.
- Temperature compensation: guaranteed between -10 and +70°C, to minimize drift due to temperature variations.
- Weight and dimensions: approximately 70 g in weight and 60 mm in height (without connector), making them compact and easily integrated into small spaces.

Main advantages

- High mechanical and electrical robustness, suitable for harsh environments such as engine rooms.
- Sealless design → greater reliability and durability.
- Easy installation and removal thanks to the Schrader depressor.
- Universal compatibility with HFC, HFO, CO_2 refrigerants (up to certain pressure levels), and common industry blends.

- Current clamps

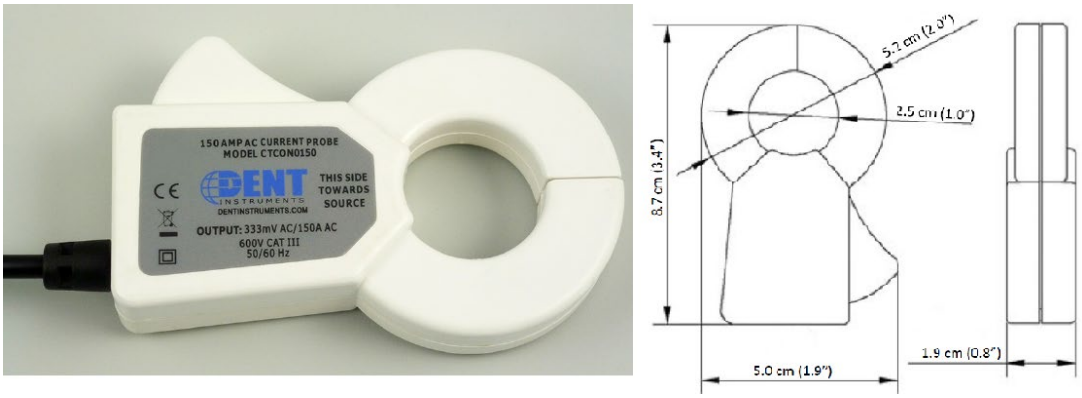

Figure 20 - Current clamps

The current clamp used is a high-performance clamp-on current transformer, model 150A EZ Clamp from DENT Instruments. It is a compact and easy-to-handle instrument, designed for both temporary and long-term energy monitoring applications. Its clamp-on design allows for one-handed installation even in tight spaces, clamping around insulated cables or conductors without interrupting the circuit.

Main features

- Measuring range: 0.5–300 A AC
- Output: 333 mV @ 150 A AC (2,22 mV/A AC), with a maximum output of 666 mV @ 300 A AC
- Window: 1" (25 mm) internal diameter, suitable for most electrical wiring in refrigeration and HVAC applications
- Accuracy: <1% error over the entire measuring range (0.5–300 A AC)
- Phase shift: <1° for currents 5–25 A, 1° from 25–150 A, <1.5° from 150–300 A
- Operating frequency: 50–400 Hz

Electrical characteristics

- Polarity of the conductors:
    - Red = high, positive (+)
    - Black = low, negative (–)
- Orientation: the label on the clamp must face the source to ensure the correct measurement phase.

Mechanical characteristics

- Material: White ABS body, self-extinguishing, UL 94 V-0 rating
- Cables: 2,4 m long, 22 AWG cross-section, 600 V insulation
- Operating temperature: –25°C to +70°C

Safety and certifications

- Maximum operating voltage: 600 VAC, Category III
- Dielectric strength: 5200 VAC, 50/60 Hz for one minute
- Certifications: Complies with UL STD 61010-1 and certified to CAN/CSA STD C22.2 No. 61010-1

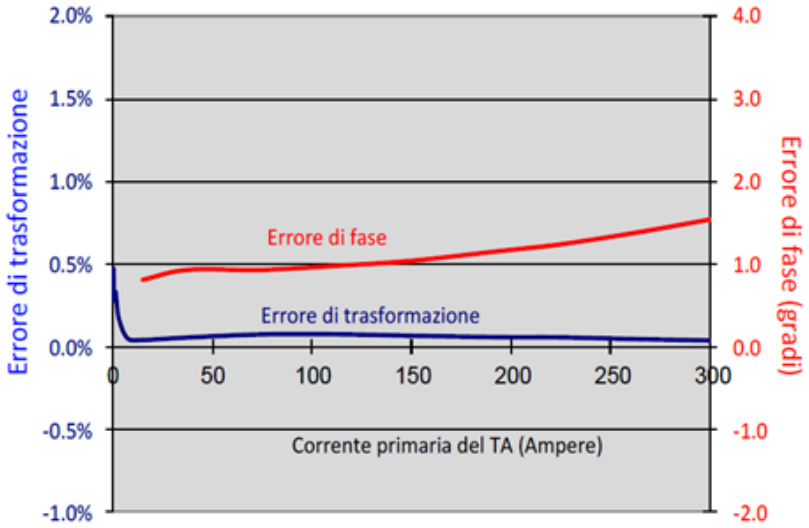

Figure 21 - Clamp meter accuracy curves

- Magnetic cables for voltage measurement

Figure 22 - Magnetic cables for voltage measurement

Magnetic cables are designed for safe and reliable voltage measurement in electrical circuits. These accessories allow for quick connection to conductors, without the need for clamps or pin probes, while ensuring high operational safety.

Main features

- Rated voltage: Tested and certified for use up to 300 V (equivalent to 520 V phase-to-phase), in compliance with the CAT III measurement category, suitable for electrical panels and power equipment.
- Compatibility: Suitable for instruments with high input impedance, such as monitoring and data acquisition systems.
- Labeling: Each conductor is color-coded in compliance with market standards, facilitating correct connection to the different phases and reducing the risk of errors.
- Magnetic connection: The terminals are equipped with magnetic tips that allow for stable and secure attachment to conductive surfaces, reducing installation time and increasing operator safety.

Mechanical characteristics

- Insulation: High-strength cable, designed to ensure reliability even in the harsh environments typical of refrigeration and air conditioning systems.
- Flexibility: The cables are easy to handle and durable, suitable for frequent or temporary connections during testing and monitoring.
- Color coding: Standardized to ensure compatibility with single-phase and three-phase systems.

Operational benefits

- Quick and secure connection without the need for additional tools.
- Reduced risk of accidental short circuits thanks to the stable magnetic attachment.
- Measurement reliability, ensured by use with instruments with high internal resistance.
- Regulatory compliance and certifications to ensure safe use in industrial environments.

- Powermeter:

Figure 23 - Power Meter

The power and electrical energy meter designed to record all relevant electrical quantities in a refrigeration system.

It allows you to analyze fundamental parameters such as:

- active power,
- current,
- voltage,
- power factor,
- energy consumed.

It can be used in any electrical system, from single-phase with neutral to three-phase with or without neutral, and represents an essential component of the monitoring system.

Communication and data acquisition

Data is collected via Modbus/RS485 protocol, which allows transmission over long distances and, if necessary, also via wireless modem.

The EP Scout has been developed to be compatible with both:

- Rogowski coils (standard range 5–4000 A), ideal for high-power systems;
- clamp meters (CT) with 333 mV output, characterized by high accuracy on small and medium-sized systems (0.5–150 A).

Technical specifications

- Service type: Single-phase with neutral, three-phase with/without neutral
- Voltage channels: 80–346 V AC (LN), 600 V (LL), CAT III category

- Current channels: 0.525 V AC max, CT with 333 mV output, measurement up to 4000 A with Rogowski coils
- Mains frequency: 50/60 Hz
- Waveform sampling: 12 kHz
- Accuracy: Class 0.2 ANSI C12.20-2010 (±0.2%, typical <0.1%)
- Communication: Modbus RS485
- Operating temperature: –7 to +60 °C
- Humidity: 5–95% non-condensing
- Power supply: Direct from L1 and L2
- Housing: ABS plastic, flammability rating UL 94-V0

Operational benefits

- Wide range of applications: from small systems (150 A clamp) to large systems (4000 A Rogowski coil).
- High measurement accuracy even with distorted waveforms, thanks to high-frequency sampling (12 kHz).
- Standardized and reliable communication via Modbus/RS485.

- Central unit

Figure 24 - Central unit of the monitoring system

The central unit processes data from a series of sensors installed at key points of the system:

- PT1000 temperature probes, used to calculate superheat, subcooling, air-side heat balances, and secondary-side performance.
- Compressor suction and discharge pressure transducers, which allow determination of thermodynamic state points, refrigerant mass flow rate, and overall cycle efficiency.

- Clamp meters for measuring absorbed current.
- Magnetic cables for voltage measurement.

The integration of these quantities allows us to obtain the electrical power absorbed by the compressor and, consequently, the COP (Coefficient of Performance) and other performance parameters.

Data acquisition and processing

The collected data are sent to a PC platform, which uses the thermodynamic correlations of refrigerants contained in the RefProp database (NIST, USA).

Thanks to pre-configured analysis templates, data is processed automatically and can be exported for further processing.

This approach allows a complete characterization of the system in terms of:

- cooling capacity,
- COP,
- efficiency of individual components,
- rapid identification of anomalies or inefficiencies.

Performance indicators

The commonly used performance indices (COP, EER, kW/RT) are highly dependent on the operating conditions and often do not faithfully represent real operation, since the systems rarely operate at the design point.

To overcome this limitation, the System Efficiency Index (SEI) is used, which expresses the real efficiency of the system compared to the ideal Carnot cycle under the same operating conditions.

- The SEI, expressed as a percentage, shows how close the actual system is to the theoretical maximum limit, allowing for an objective comparison between different units or the same system under varying operating conditions.
- In addition to the overall SEI, the system calculates the sub-efficiencies
    - Cycle efficiency: Deviation from the ideal Carnot process.
    - Compressor efficiency: Includes mechanical and electrical losses (isentropic efficiency).

- Condenser efficiency: Comparison with an ideal condenser with infinite surface area.
- Evaporator efficiency: Comparison with an ideal evaporator with infinite surface area.

These parameters are largely independent of external conditions and are a useful tool for benchmarking, fault detection and performance optimization.

Internal method and energy balance

The calculation principle adopted is the so-called internal method, based on the first law of thermodynamics and the thermophysical properties of the refrigerant, without requiring specific manufacturer data.

At the heart of the method is the compressor's energy balance, from which the refrigerant mass flow rate is derived and, consequently, all the main performance indicators:

- COP,
- cooling/heating capacity,
- isentropic compressor efficiency.

The approach ensures reliable and repeatable measurements, with typical uncertainties in the order of ±5–7%, widely acceptable for both continuous monitoring applications and diagnostic and optimization activities.

3.1.2. Application of the system

Installing temperature sensors

Class A Pt1000 temperature probes were installed at key points in the refrigeration circuit.
Some analysis methods allow surface mounting of the probes directly on the pipes, due to their low sensitivity to measurement errors.
However, to ensure maximum accuracy, rigorous procedures must be followed:

- The probes were positioned 15 cm away from the compressor, flanges, valves, or other components that could alter the surface temperature of the pipe;
- Before installation, paint and oxidation were removed;

- Thermally conductive paste was applied and the probe was secured with aluminum tape; it was then covered with closed-diffusion insulation to prevent condensation or ice formation;

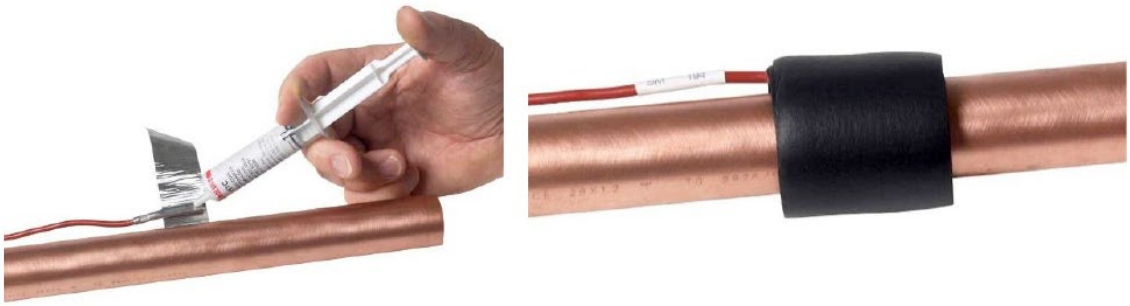

Figure 25 - Sensors installation using heat transfer paste, aluminum tape, and thermal insulation

- for copper pipes, a tight insulation of 60 mm × 8 mm was used

The installed probes allow monitoring of the following parameters:

- Compressor suction line → compressor superheat calculation.
- Compressor discharge line → discharge temperature calculation and compressor operating conditions check.
- Evaporator (glycol side, inlet and outlet)→ to calculate the temperature difference across the heat exchanger and thus evaluate its heat transfer efficiency.
- Condenser air inlet and outlet → air-side heat exchange efficiency calculation.
- Condenser outlet → subcooling determination and refrigerant charge check.
- Throttle valve inlet → total subcooling measurement.

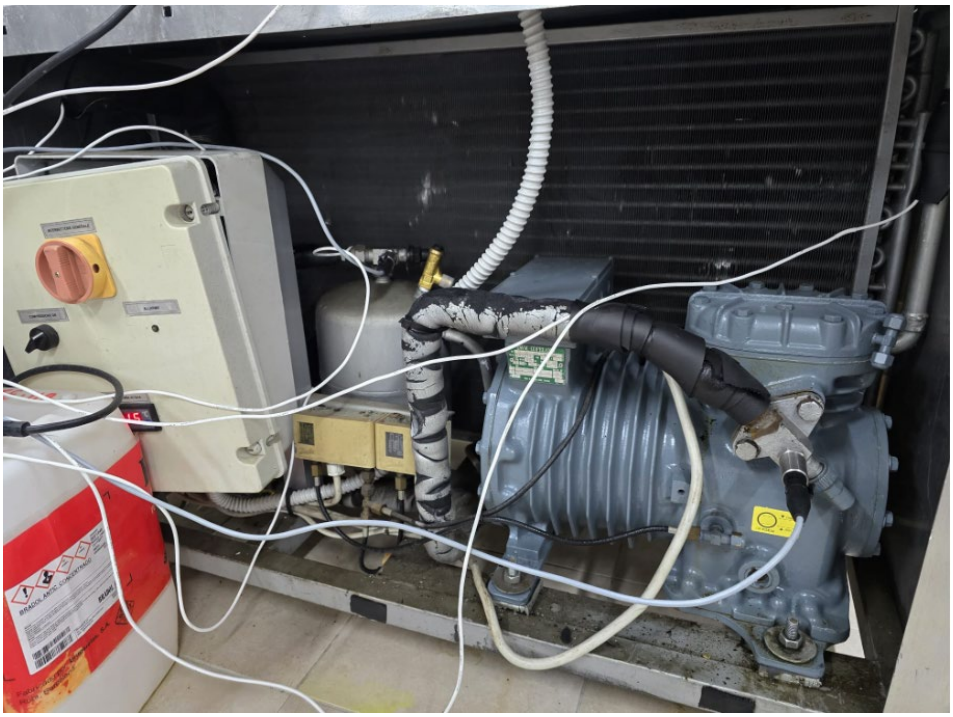

Figure 26 - Temperature sensors installation

Installing pressure transducers

Piezoresistive transducers are installed near the compressor inlet (suction) and at the liquid receiver connected to the compressor discharge line. The latter location was chosen for convenience of installation. Since the pressure drop between the compressor outlet and the receiver, including the condenser, is negligible under the operating conditions, this pressure difference was disregarded in the analysis.

- High-pressure transducer: range 0–35 bar, output 0–10 V.
- Low-pressure transducer: range 0–10 bar, output 0–10 V.

These measurements allow us to define the thermodynamic points of the cycle and, together with the temperatures, calculate the refrigerant mass flow rate, efficiency, and cooling capacity.

Installing the power meter

The power meter was connected to the central unit via RS485 Modbus protocol. Power is supplied directly from L1 and L2.

The following were used:

- 333 mV clamp meters (range 0,5–150 A) for low/medium currents,
- magnetic voltage leads for measuring the voltage channels.

This configuration allows for the determination of current, voltage, active power, power factor, and energy absorbed by the compressor.

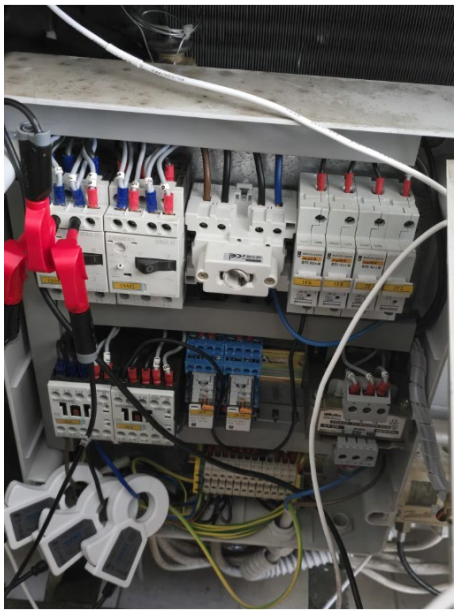

Figure 27 - Installation of magnetic voltage probes and current clamps on the compressor switch for electrical power measurements

Verification and calibration procedures

Before starting the analyses, all sensors were verified to be functioning correctly:

- Pressure: Checked against atmospheric pressure (~101 kPa) to validate the offset.
- Temperature: Simultaneous comparison of all probes in agitated water (uniformity test), with a typical tolerance of ±0.15 K.
- Electrical power: Check that the transducers signal zero with the clamps disconnected and compare the measured values with the compressor's nameplate data.

Defrosting strategies analyzed

The system allowed us to compare three different operating modes:

- Timed defrost → cycles at fixed intervals, independent of the actual evaporator status.
- Capacitive defrost → start-up based on the ice thickness detected by the dielectric sensor.
- Fan absorption-based defrost → activation when a certain electrical power
- consumption threshold is exceeded.

3.2. Chiller Employed in the Laboratory Setup

The refrigeration unit (chiller) is designed to produce chilled ethylene glycol–water solution (40% by weight), which is then circulated to the air cooler installed in the cold room.

The system consists of a semi-hermetic reciprocating compressor (Copeland DLL-401), operating with R407F as refrigerant. At the outlet of the liquid receiver, the refrigerant passes through a thermostatic expansion valve (Danfoss), where its pressure and temperature are reduced before entering the plate heat evaporator (Onda S62). Inside the evaporator, the refrigerant evaporates by absorbing heat from the glycol solution, cooling it from –7 °C (inlet) to –12 °C (outlet). The vaporized refrigerant is then returned to the compressor to complete the cycle.

On the condensation side, heat rejection takes place in an air-cooled condenser (Thermokey CHD 22450) with a nominal capacity of 12 kW. The condenser is equipped with two fans, 450 mm diameter each, ensuring an airflow of approximately 10000 m³/h.

The compressor has a nominal cooling capacity of 5.69 kW (at Te = –20 °C, Tc = 45 °C) with a power consumption of 3.13 kW.

The chiller incorporates two pumping circuits:

- Primary circuit (refrigerant–glycol exchange): circulation is provided by a centrifugal pump Ebara CDA/A 150M, with a flow range of 20–100 L/min, a maximum head of 52 m, and operating speed of 2850 rpm.
- Secondary circuit (glycol distribution to air cooler): circulation is ensured by a Rover Pompe unit, with a flow rate of 28 L/min, a maximum head of 22 m, and a nominal speed of 2850 rpm.

This configuration allows the chiller to operate as an intermediate stage between the refrigeration cycle and the air coolers, ensuring stable glycol temperature levels and reliable operation of the indirect cooling system.

Figure 28 - Air-Cooled Chiller in the Laboratory Setup

3.3. Cold Room Setup

The experimental tests were carried out in the laboratory of the University, inside a cold room with internal dimensions of 2.7 × 2.4 × 2.4 m.

Inside the chamber, an Onda air cooler was installed, with overall dimensions of 1.64 × 0.63 × 0.49 m. The heat exchanger is composed of a finned pack with galvanized steel frame, 16 mm copper tubes, and aluminum fins with pyramidal corrugation, designed to reduce dirt accumulation. The fin spacing is 7 mm, resulting in a total heat transfer surface of 26.2 m^2. The coil includes two circuits with 1" connections on the same side and an internal volume of 9 dm^3. The copper tubes are mechanically expanded into an aluminum counter-plate to avoid direct contact with the galvanized steel, thereby minimizing corrosion risks under prolonged vibration.

The air cooler is equipped with two axial fans (Weiguang, model YWF4E-350S), each with a 350 mm blade diameter, absorbed power of 102 W, and current of 0.66 A, for a total of 204 W and 1.4 A overall. The fans operate at 230 V – 1Ph – 50 Hz, with a nominal speed of 1420 rpm. According to the manufacturer's data, the sound power level is 75 dB(A) and the sound pressure level is 49 dB(A) at a distance of 3 m. Each fan is driven by an external rotor motor (protection class IP54, insulation class F) and equipped with a high-efficiency shroud featuring an enlarged collar, designed to ensure maximum airflow (4900 m^3/h) while maintaining low noise levels.

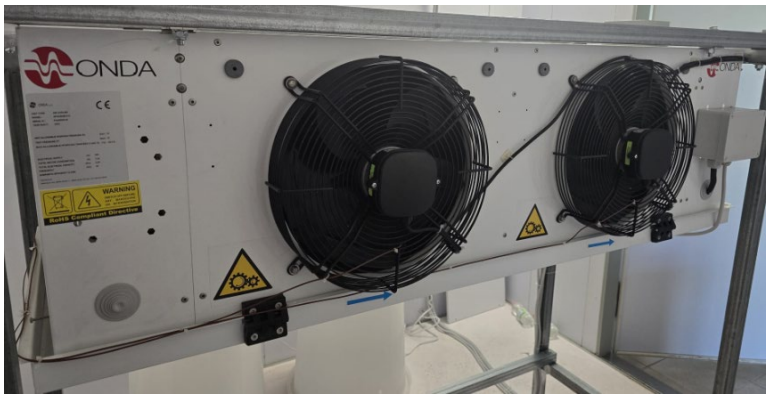

Figure 29 - Air-Cooler

For defrost, an electric defrost system was installed, consisting of six heating elements with a total power of 4 kW. The evaporator is supplied by a 40% ethylene glycol–water solution.

Property	Unit	Value (40% Ethylene Glycol)
Concentration	% by weight	40%
Freezing point	°C	–23
Density (at 20 °C)	kg/m³	~1.065
Specific heat (cp at 0 °C)	kJ/kg·K	~3.3
Thermal conductivity	W/m·K	~0.40
Dynamic viscosity (at 0 °C)	mPa·s	~6

Table 3 - Thermophysical properties of 40% ethylene glycol–water solution

The theoretical design conditions of the air cooler, as specified by the manufacturer, are reported below.

Cooling capacity	3.10 kW
Air flow rate	4900 m³/h
Inlet air temperature	0°C
Inlet relative humidity	89%
Outlet air temperature	-1.3°C
Outlet relative humidity	92.8%
Inlet fluid temperature	-8°C
Outlet fluid temperature	-3.8°C
Fluid volumetric flow rate	0.72 m³/h
Fluid mass flow rate	760 kg/h
Pressure drop	18 kPa
Fluid velocity inside the tubes	0.52 m/s

Table 4 - Nominal operating conditions of the air cooler (manufacturer data)

Capacity	2858	W
Sensible Capacity	2134	W
Latent Capacity	724	W
Sensible/Total Capacity Ratio	0.7468	
Quantity of Produced Water	1.04	kg/h
Exchange Surface	26.2	m2
Global Exchange Coefficient	13	W kg/(m² kJ)
Fin Thickness	0,15	mm
Coil Internal Volume	9	l
Tubes External Diameter	16	mm
Tubes Internal Diameter	15.3	mm
AIR SIDE		
Volumetric Air Flow	4900	m3/h
Mass Air Flow	6319	kg/h
Face Velocity on the Coil	2,25	m/s
Inlet Air Density	1,29	kg/m3
Inlet Air Temperature	0	°C
Inlet Air Relative Humidity	89.00 %	%
Inlet Air Specific Humidity	3.4	g/kg
Inlet Air Enthalpy	8.4	kJ / kg
Outlet Air Temperature	-1,2	°C
Outlet Air Relative Humidity	94.00 %	%
Outlet Air Specific Humidity	3.2	g/kg
Outlet Air Enthalpy	6.77	kJ / kg
Pressure Drop	33	Pa
Dry Fin Efficiency	0.6732	
Wet Fin Efficiency	0.5674	
Fin Medium Temperature	-2	°C
FLUID SIDE		
Fluid	ETHYLENE GLYCOL / WATER 40% (1 bar A)	
Volumetric Fluid Flow	0.7	m³/h
Mass Fluid Flow	760	kg/h
Fluid Velocity	0.5	m/s
Inlet Fluid Temperature	-8	°C
Outlet Fluid Temperature	-3.8	°C
Total Pressure Drop Fluid Side	18.92	kPa

Table 5 - Calculated cooling capacity of the air cooler

To verify the actual thermal performance of the air cooler and to assess the reliability of the manufacturer's data, a thermal balance calculation was carried out based on the measured operating conditions of the glycol–air heat exchanger.

The analysis considered the air-side and fluid-side heat transfer processes, assuming steady-state conditions, uniform air velocity across the coil surface, and negligible heat losses to the surroundings.

The glycol–water mixture properties were evaluated for a 40% ethylene glycol concentration, and the air properties were calculated at the average temperature and humidity measured during the tests.

The results of the performance estimation are summarized in Table 5, which compares the nominal cooling capacity declared by the manufacturer with the calculated value obtained from experimental data and heat transfer equations.

As can be observed, the calculated cooling capacity (2.8 kW) is slightly lower than the manufacturer's nominal value (3.1 kW), with a deviation of approximately 10%.

This difference can be attributed to several factors. Firstly, the manufacturer's rating is typically based on standardized test conditions (e.g., specific air inlet temperature, humidity, and flow rate) that may differ from the actual laboratory conditions.

Secondly, certain geometric or surface characteristics—such as fin corrugation profile, tube expansion ratio, or internal surface roughness—are not explicitly provided by the manufacturer and therefore could not be accurately included in the thermal model. Additionally, minor measurement uncertainties in airflow rate, glycol flow, or temperature sensors may also contribute to this discrepancy.

Nevertheless, the calculated value is in good agreement with the nominal data, confirming the correct sizing and expected performance of the heat exchanger under the tested operating conditions.

To maintain proper humidity conditions during the tests, two ultrasonic humidifiers were also installed inside the cold room. Each unit operates at 220 V with a power consumption of 25 W, a tank capacity of 5 L and a maximum mist output of 350 mL/h. The devices are suitable for coverage areas up to 30 m², ensuring uniform humidity distribution throughout the chamber during experimental operation.

Before performing the thermal performance evaluation, the system was operated under steady-state conditions for at least 30 minutes to ensure stable airflow and coolant temperature. The following initial operating conditions were measured:

- Air inlet temperature: 0.0 ± 0.3 °C
- Air inlet relative humidity: 89–92%
- Glycol inlet temperature: –7.0 ± 0.2 °C
- Glycol outlet temperature: –12.0 ± 0.2 °C

- Glycol volumetric flow rate: 28 L/min
- Airflow rate through the coil: 4900 m³/h (nominal)
- Coil surface condition: clean coil, no visible frost

All measurements were taken under stable loading conditions inside the cold room, ensuring reliable comparison between calculated and nominal performance.

Figure 30 - Ultrasonic humidifier

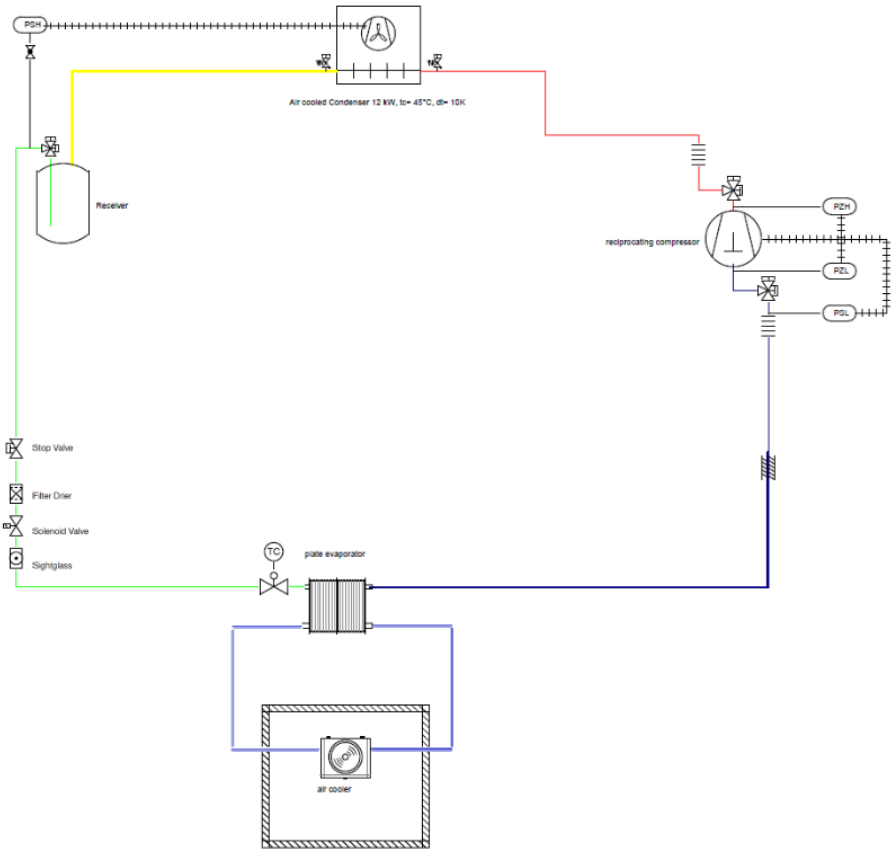

Figure 31 - Single Flow Diagram

Cooling Load Calculation:

Temperature Outside Air:	35 °C
Relative Humidity Outside Air:	65 %
Temperature Inside Air:	0 °C
Relative Humidity Inside Air:	97 %
Daily balance	
Runing time per day:	18 h
Entries:	8 /Day
Air Exchange:	0.5 /h
Condensed water Air Exchange:	0.168 kg/h
Occupants:	1 h/Day
el. Capacity:	3 W/m²
Refrigeration Capacity:	2.412 kW
Share Cooling goods:	1.321 kW [54.77 %]
Share el. Capacity:	0.025 kW [1.07 %]
Share Air Exchange:	0.272 kW [11.31 %]
- Air Exchange Latent:	0.16 kW [6.64 %]
- Air Exchange Sensible:	0.112 kW [4.66 %]
Share Transmission Walls:	0.465 kW [19.3 %]
Share Occupants:	0.016 kW [0.67 %]
Share Ventilator Evaporator:	0.3 kW [12.43 %]
Share Defrost Evaporator:	0.01 kW [0.42 %]

	Area [m²]	Transmission Heat transmission [W/m²K]	Temperature Outside Air [°C]	Capacity Transmission [W]
Wall 1	5.76	0.18	35	36.2
Wall 2	6.48	0.18	35	40.8
Wall 3	6.48	0.18	35	40.8
Wall 4	5.76	0.18	35	36.2
Ground	6.48	0.68	35	154.2
Ceiling	6.48	0.18	35	40.8

Quantity [/Day]	Temperature Cooling goods [°C]	Heat capacity before Solidification /[kJ/kg K]	Heat capacity after Solidification /[kJ/kg K]	Solidification eat /[kJ/kg]	Share Cooling goods [W]
1000 kg Apple	25	3.64	1.88	281	1321.6

Quantity [/Day]	Capacity Solidification /[W]	before	Capacity Solidification eat /[W]	Share Respiration heat [W]	Share Cooling goods [W]
1000 kg Apple	1291.9		0	29.6	1321.6

3.4. Image Acquisition System for Frost Depositing

To visually monitor the growth and distribution of frost on the aircooler surface, a video acquisition system was installed inside the cold room. This setup allowed continuous visual observation of the evaporator during operation and made it possible to correlate frost accumulation with operating parameters such as temperature, humidity, and defrost cycles, providing valuable support for experimental validation.

PoE Switch – Cudy FS1006P

A Power over Ethernet (PoE) switch, model *Cudy FS1006P*, was used to supply both power and data connection to the network devices through a single Ethernet cable (RJ45).
The main technical specifications are as follows:

- 6 × 10/100 Mbps Ethernet ports, including 4 PoE ports;
- Total PoE power budget: 60 W (maximum 30 W per port);
- Compliant with IEEE 802.3af/at PoE standards;
- Power supply voltage: 48–57 V DC;
- Automatic detection and surge protection functions;
- Operating temperature range: –10 to +55 °C.

This device ensured stable power delivery to the IP camera and network connectivity to the video recorder.

Network Video Recorder (NVR) – Dahua DHI-NVR-2104-S3

Video recording and management were handled by a Dahua Network Video Recorder (NVR), model *DHI-NVR-2104-S3*.
Its main features include:

- Support for up to 4 IP channels, up to 6 MP resolution;
- Incoming bandwidth: 80 Mbps;
- Video compression: H.265/H.264;
- 10/100 Mbps Ethernet interface;

- HDMI and VGA video outputs;
- Support for 1 × SATA HDD up to 6 TB;
- Remote access via Dahua SmartPSS or web interface.

The NVR was installed outside the cold room, connected to the PoE switch, and configured for continuous digital recording and data storage.

IP Camera – Dahua DH-IPC-HFW2441S-S

Inside the cold room, a Dahua IP camera, model *DH-IPC-HFW2441S-S*, was installed to capture real-time images of the evaporator under low-temperature and high-humidity conditions. The main technical characteristics are:

- 1/2.9” 4 MP CMOS sensor (2688 × 1520 px);
- Fixed 2.8 mm lens, horizontal field of view ≈ 103°;
- Integrated IR illuminator with up to 30 m range, enabling monitoring during defrost or low-light periods;
- Video compression: H.265/H.264;
- PoE power supply (IEEE 802.3af);
- IP67 protection rating, suitable for humid and cold environments;
- Operating temperature range: –30 to +60 °C.

The camera was positioned to provide a frontal view of the aircooler coil, allowing visual assessment of frost buildup and removal during each defrost cycle. Captured images were stored by the NVR for later analysis of frost formation dynamics.

Figure 32 - Camera

3.5. Defrost control and monitoring system

In this phase of the research, experimental tests were carried out to study the frost formation process on the surface of an air cooler under various operating conditions.

The study was organized in two main stages. In the first stage, the cooling system and the monitoring equipment were fine-tuned, and preliminary measurements were performed to verify the accuracy and reliability of the data acquisition setup. In the second stage, based on these preliminary results, tests were conducted under controlled variations of air temperature, relative humidity, and glycol temperature, in order to analyze frost accumulation, melting behavior, and the thermal performance of the system during cooling and defrosting cycles.

The experiments were performed inside a cold room with internal dimensions of 2.7 × 2.4 × 2.4 m, equipped with an Onda air cooler measuring 1.64 × 0.63 × 0.49 m. The air cooler was supplied with a 40% ethylene glycol–water solution, circulating at a volumetric flow rate of 28 L/min. The chilled glycol was provided by a refrigeration unit using refrigerant R407F.

Before each experimental session, the system was operated until the cold-room temperature and humidity reached the following initial conditions:

- Room temperature setpoint: 0.0 ± 0.5 °C
- Room relative humidity: 95–97%
- Glycol inlet temperature: –7.0 ± 0.3 °C
- Glycol volumetric flow rate: 28 L/min
- Coil initial state: fully defrosted, with no residual frost
- Fans operating at nominal speed (≈ 4900 m³/h airflow)

These conditions allowed repeatability between tests and ensured that frost growth was monitored starting from a reproducible reference state.

Several sensors were installed to evaluate and manage the defrost cycles, with the aim of continuously monitoring the operating conditions of the evaporator and optimizing the duration of each cycle.

In particular:

- Air temperature probes: installed at both the inlet and outlet of the air cooler, on each of the two fan sections (suction and discharge sides). This configuration allows for a more accurate and representative measurement of the air temperature difference across the entire heat exchanger, enabling continuous monitoring of the heat exchange efficiency under different operating conditions, including the frost accumulation phase.

Figure 33 - Air-Cooler view from the air suction side

- Fluid temperature probes: installed on the inlet and outlet glycol lines of the air cooler. By measuring the temperature difference of the glycol solution and knowing its flow rate, it was possible to determine the heat transfer rate across the heat exchanger and evaluate its thermal performance under various operating conditions.
- Defrost termination probe: a temperature sensor was installed on the air inlet side of the air cooler, corresponding to the suction section of the fans. This is the coldest zone of the coil, where frost melts last, since the incoming warm and humid air first encounters the cold glycol entering the tubes. The probe was used to automatically terminate the defrost cycle once the coil temperature reached the predefined threshold, ensuring complete frost removal without overheating the coil or extending the defrost duration unnecessarily.

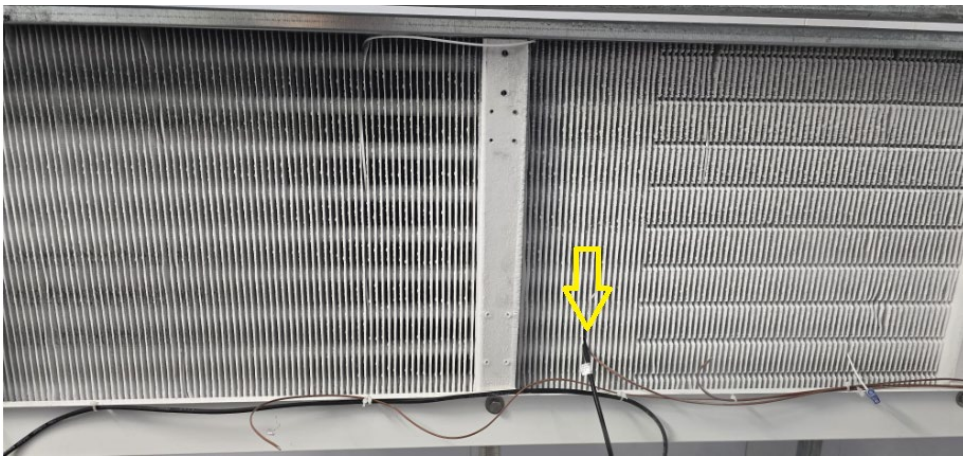

Figure 34 - Position of the defrost termination temperature probe on the air inlet (suction) side of the air cooler.

- Room air temperature probes: two temperature sensors were installed on the ceiling, positioned away from the air cooler. This configuration allows monitoring of possible temperature stratification and assessing the uniformity of air distribution inside the cold room during both cooling and defrost phases. The use of two probes enables detection of spatial gradients and improves the accuracy of the overall thermal characterization of the chamber.
- Relative humidity probes: two humidity sensors were mounted near the ceiling, in locations corresponding to the air temperature probes. Monitoring humidity at two distinct points provides a representative profile of moisture distribution within the room, allowing the evaluation of humidity stability and its variation during cooling and defrost cycles.
- Capacitive frost sensor: an insulated steel cable was installed between the evaporator fins, on the air inlet side (warm air side), where frost formation is most likely to occur.
    - An active length of 10 m was used, with vertical windings spaced 200 mm apart, to ensure uniform coverage of the air cooler surface.
    - Only the vertical active portion of the wire was considered for calibration purposes.
    - The cable end was routed outside the evaporator and connected via a terminal connector, avoiding any electrical contact with the fins.
    - The insulating coating was kept intact to preserve sensor functionality and prevent interference or short circuits.
    - During defrost, the sensor measures the dielectric variation of the medium (capacitance value in pF), which increases when the ice is wet and decreases once the

evaporator is clean. The analog 4–20 mA output was used by the controller to automatically start and stop the defrost cycle based on the detected frost thickness.

Figure 35 - Capacitive frost sensor

- Fan power consumption meters: devices were installed to continuously monitor the electrical
- power absorbed by the air cooler fans. As frost accumulates on the fins, the aerodynamic
- resistance to airflow increases, leading to higher fan power demand. Tracking this parameter
- provided an additional indirect indicator of frost formation and allowed the defrost cycle to
- be triggered once a predefined power threshold was exceeded.

All parameters were continuously monitored using LabVIEW® software, through the development of a virtual instrument capable of recording and displaying in real time the evolution of the parameters of interest throughout the research.

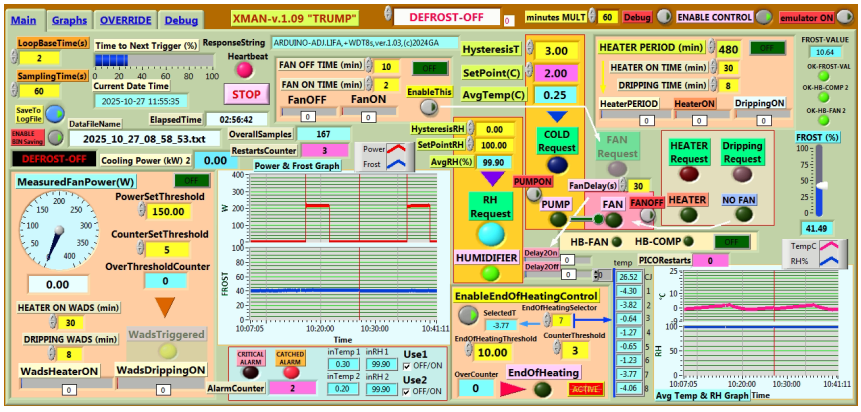

Figure 36 - Graphical interface of the virtual instrument developed with LabVIEW software for acquiring the parameters related to the experimental tests.

Figure 37 - General view of the experimental setup and monitoring instruments in the laboratory

Figure 38 - General view of the experimental setup and monitoring instruments in the laboratory

3.6. Experimental Configurations and Test Plan

To assess the influence of different defrost control strategies on frost accumulation and system performance, three operating configurations were tested. For each configuration, the objective of the experiment, the controlled parameters, and the initial operating conditions were clearly defined, as described below.

Configuration A — Timed Defrost (Baseline Mode)

Objective:

To establish a reference performance during cooling and defrost cycles activated solely based on time.

Controlled parameters:

- Fixed defrost interval (e.g., every 6 hours)
- Constant setpoint of air temperature in the cold room
- Constant glycol inlet temperature from chiller

Initial conditions:

- Room temperature: 0 ± 0.3 °C
- Relative humidity: 95–97%
- Glycol flow rate: 28 L/min
- Initial coil free of frost

This configuration represents current common industrial practice, used as baseline for comparisons.

Configuration B — Capacitive Frost Sensor Defrost

Objective:

To evaluate the benefit of adapting the defrost activation to the actual ice thickness on the evaporator surface.

Controlled parameters:

- Defrost triggered by capacitance threshold corresponding to frost thickness increase
- Defrost termination based on coil inlet temperature probe
- Room air conditions kept constant

Initial conditions:

- Same as Configuration A for fair comparison
- Sensor zeroed before each test to ensure consistent baseline capacitance

This strategy aims to reduce unnecessary defrosts and energy consumption by properly capturing frost growth dynamics.

Configuration C — Fan Power Consumption-Based Defrost

Objective:

To analyze an airflow-based defrost control, exploiting electrical fan power as an indicator of frost-induced pressure losses.

Controlled parameters:

- Automatic defrost activation when fan electrical power exceeds defined threshold
- Same termination logic as in Configuration B
- Humidity and glycol operating conditions maintained constant

Initial conditions:

- Same as previous tests
- Fan power reference (clean coil condition) measured before each experimental sequence

This method seeks to detect frost formation through aerodynamic degradation, with potential robustness against local frost non-uniformity.

Comparative Evaluation

For each configuration, the following parameters were recorded and analyzed:

- Cooling capacity of the air cooler
- COP and compressor power consumption
- Duration and frequency of defrost cycles
- Frost accumulation rate (image analysis + sensor data)
- Temperature and humidity stability in the cold room

All tests were conducted for a minimum duration of 24 h to allow full frost–defrost cycles and ensure statistical reliability.

3.7. Simulation Model of Weight Loss for Horticultural Products

To predict product weight loss during refrigerated storage, a simulation model was developed in MATLAB to estimate the mass loss of horticultural products stored in a cold room over a 24-hour period, as a function of the thermo-hygrometric conditions (air temperature and relative humidity).

In the developed model, several parameters must be specified for both the cold room and the stored commodity, including fruit density, geometric shape, room dimensions, bulk density of the stored product, fin spacing of the heat exchanger, and the air temperature and relative humidity inside the chamber.

The model computes the difference in water vapor pressure between the product surface and the surrounding air and, based on this driving force, evaluates the percentage weight loss of the product over time. In addition, the model estimates the required defrosting frequency needed to maintain effective heat transfer performance, given the operating conditions and product properties.

The driving force for transpiration is the difference in water vapor pressure between the product surface and the surrounding air. The basic formulation of the transpiration model is expressed as:

$$m' = k_t(p_s - p_a) \qquad (3.1)$$

where:

- m' is the transpiration rate, expressed as the mass of moisture lost per unit area of commodity surface and per unit time;
- k_t is the transpiration coefficient, i.e. the mass of moisture transpired per unit area of commodity, per unit water vapor pressure difference, and per unit time;
- $(p_s - p_a)$ is the water vapor pressure difference between the product surface and the surrounding air.

The water vapor pressure at the product surface, p_s, is assumed to be equal to the saturation vapor pressure at the commodity surface temperature. The surrounding air vapor pressure, p_a, is determined from the measured air temperature and relative humidity.

To estimate the transpiration coefficient k_t, the approach proposed by Fockens and Meffert (1972) was adopted. In this formulation, the overall mass transfer coefficient is expressed as:

$$k_t = \frac{1}{\frac{1}{k_a}+\frac{1}{k_s}} \qquad (3.2)$$

where:

- k_a is the mass transfer coefficient of the air film, describing the convective transfer on the product surface and depending on the airflow conditions;
- k_s is the mass transfer coefficient of the peel, representing the diffusive resistance to moisture transport through the fruit skin.

The values of the peel mass transfer coefficient $k_s$were taken from the ASHRAE Handbook (2018), which provides experimentally derived data for several fruit and vegetable species.

The air-film mass transfer coefficient $k_a$was estimated using Sherwood–Reynolds–Schmidt type correlations (Becker et al., 1996b), in the form:

$$Sh = \frac{k'_a d}{\beta} \qquad (3.3)$$

where Sh is the Sherwood number, k'_a is the air-film mass transfer coefficient, $d$is the characteristic diameter of the commodity and $\beta$is the diffusion coefficient of water vapor in air.

The model was implemented in MATLAB using a time-stepping procedure with a 24-hour simulation horizon. For each time step, the thermo-hygrometric conditions in the cold room, the product temperature, and the vapor pressure difference were updated, and the cumulative weight loss of the stored product was computed.

4. Results

4.1. Comparison of Defrost Depositing Control

During the experimental tests, three different control strategies for initiating the electric defrost cycle were analyzed:

1. the time-based method;
2. the fan power absorption method;
3. the capacitive method (based on the direct measurement of frost thickness).

In the case of the timed method, defrosting occurs every six hours, regardless of the actual presence of frost on the evaporator.

Before the defrost cycle started, the compressor operated regularly within its normal refrigeration cycle. During the defrost phase, the electric heaters, with a total power of approximately 4 kW, remained active for an average duration of 25 minutes per cycle. Consequently, the energy consumption associated with a single defrost operation is about 1.7 kWh, corresponding to 6.8 kWh per day if the cycle is performed four times within 24 hours.

Moreover, each defrost cycle caused a decrease in the relative humidity inside the cold room, which during the tests dropped from 98% to 89%, corresponding to a relative reduction of about 9%.

The second approach, based on fan power absorption, proved to be particularly interesting, as it allows the detection of frost formation in an indirect yet reliable way. With a clean evaporator, the power consumption of the fans was around 207 W, while the corresponding heat exchange capacity was approximately 3 kW.

Figure 39 - Clean aircooler (0% frost)

To determine the maximum fan power absorption, the aricooler was deliberately allowed to reach a fully frosted condition (100% frost coverage). Under these circumstances, the highest measured power consumption reached 4 kW.

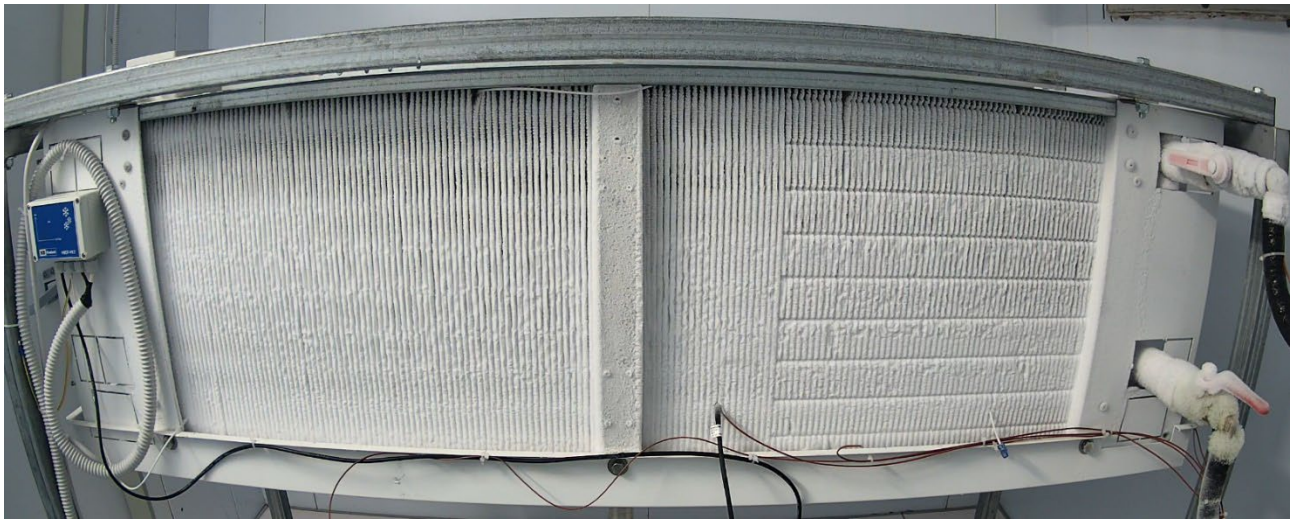

Figure 40 - Fully frosted aircooler (100% frost coverage)

While the refrigeration capacity progressively declined to 0.5 kW. This corresponds to an approximately 80% overall capacity loss relative to the initial 3 kW, as shown in Figure 41. This worst-case characterization was then used as a reference to define the defrost intervention threshold.

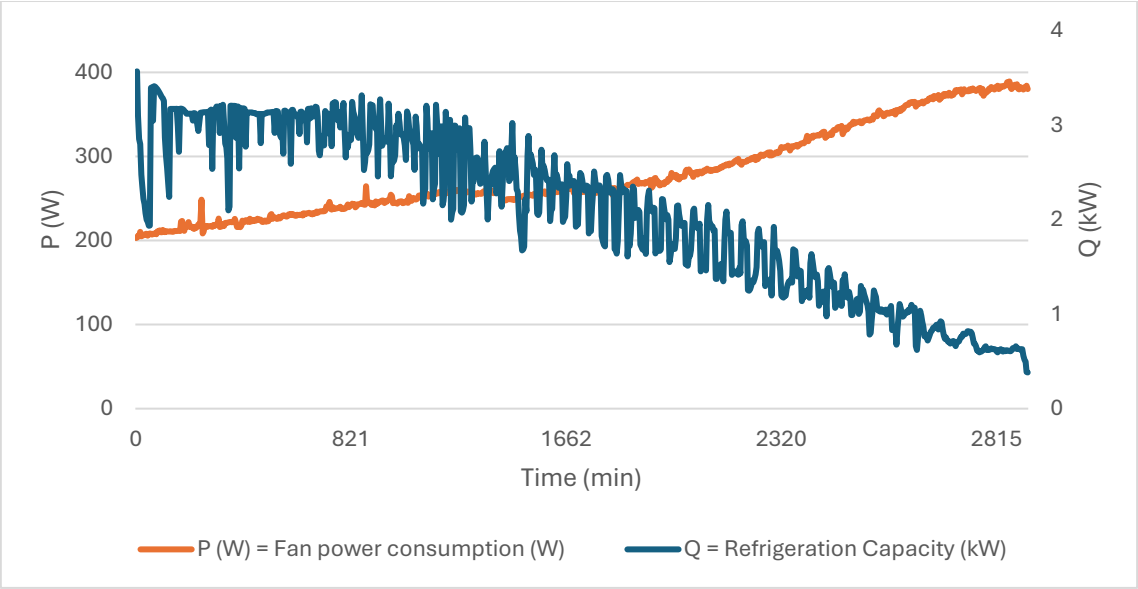

Figure 41 - Time evolution of cooling capacity and fan power consumption

By analyzing the correlation between the fan power consumption and the heat transfer capacity, an optimal threshold was identified at 250 W of fan power input, corresponding to a heat transfer rate of approximately 2.4 kW, that is, about 80% of the maximum capacity.

Figure 42 - Condition for defrost start (fan power consumption 250 W)

Assuming 400W as the maximum fan power consumption, the 250 W threshold corresponds to about 60 % of the maximum value and represents roughly a 25 % increase compared to the clean-coil condition. At this point, frost formation starts to noticeably reduce the heat exchanger's efficiency, although the overall system performance is not yet severely affected. Triggering the defrost cycle at this stage enables a preventive action, avoiding both the excessive energy demand caused by too-

frequent defrosts and the sharp drop in cooling capacity that occurs when frost buildup is allowed to progress further. Around this operating point, the cooling capacity curve (≈ 2.2 kW) begins to decline more steeply, marking the onset of significant performance degradation.

An important aspect observed during the tests is that the fan power threshold method automatically skips unnecessary defrost cycles under low-load conditions. For instance, during the evening period—when the cold room was closed and non new product was introduced—the fan power consumption never exceeded 250 W, remaining below the defrost activation threshold set at 250 W. Under these conditions, the system did not trigger any defrost cycles, whereas with the time-based method, a cycle would have been started every six hours.

This behavior resulted in an immediate energy saving of approximately 1.7 kWh for each avoided defrost, considering an electric heater power of 4 kW and an average defrost duration of about 25 minutes, while also better preserving the room's humidity.

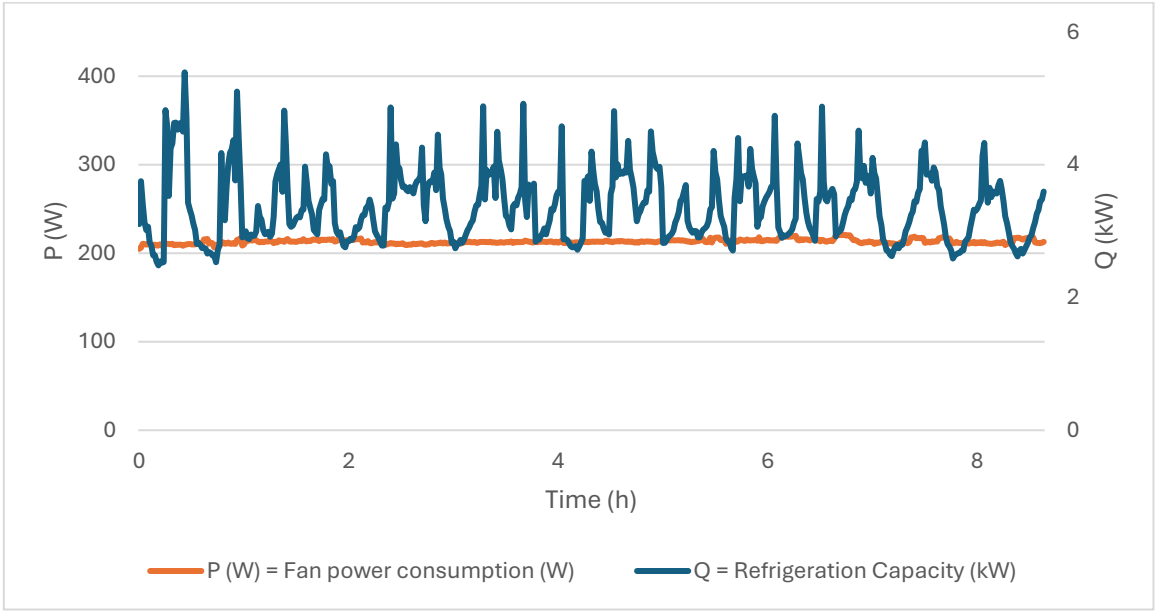

Figure 43 - Variation of cooling power and fan consumption during evening low-load operation (no defrost activation)

In summary, the results show that the fan power threshold method represents an effective compromise between energy efficiency and system performance. Compared to the time-based approach, it avoids unnecessary defrost cycles and, more importantly, prevents severe capacity degradation (up to −80 %) by anticipating the intervention at 250 W.

To further optimize system management, it is advisable to define a maximum time interval between two consecutive defrost cycles (e.g., 8–10 hours) as a safety backup, ensuring that the evaporator never operates under excessively inefficient conditions.

However, it must be considered that the variation in pressure drop (Δp) across the finned coil is not exclusively due to frost formation: it may also be increased by dust or dirt blockage on the coil or filters, bent fins, foreign objects, or abnormal airflow conditions. In such cases, fan power consumption may rise for reasons unrelated to frosting, generating false positives if fan power alone is used as a defrost trigger.
For this reason, it is recommended to combine the 250 W threshold with proper measurements and good operational practices, such as:

- regular cleaning and inspection of the coil and filters, with baseline recalibration after maintenance;
- possible measurement of Δp across the coil (or estimation of airflow rate) to distinguish between frost and dust blockage;
- cross-validation between indicators (fan power, exchanged heat, temperature/humidity) using hysteresis and validation windows to avoid rapid on/off switching;
- seasonal adjustment of the threshold and minimum/maximum limits on the interval between defrost cycles.

By doing so, the threshold-based criterion remains effective in anticipating defrost when it is truly needed, while remaining robust against increases in fan power caused by other non-frost-related factors.
Moving on to the third method tested — the capacitive approach — frost formation is measured directly by a sensor, and the defrost command is triggered when a predefined frost percentage threshold is reached.

The graph clearly shows that as the frost level measured by the capacitive system increases, the heat exchange capacity of the evaporator decreases significantly: it drops from 3 kW at 0% frost to approximately 0.5 kW when the frost level reaches 100%.

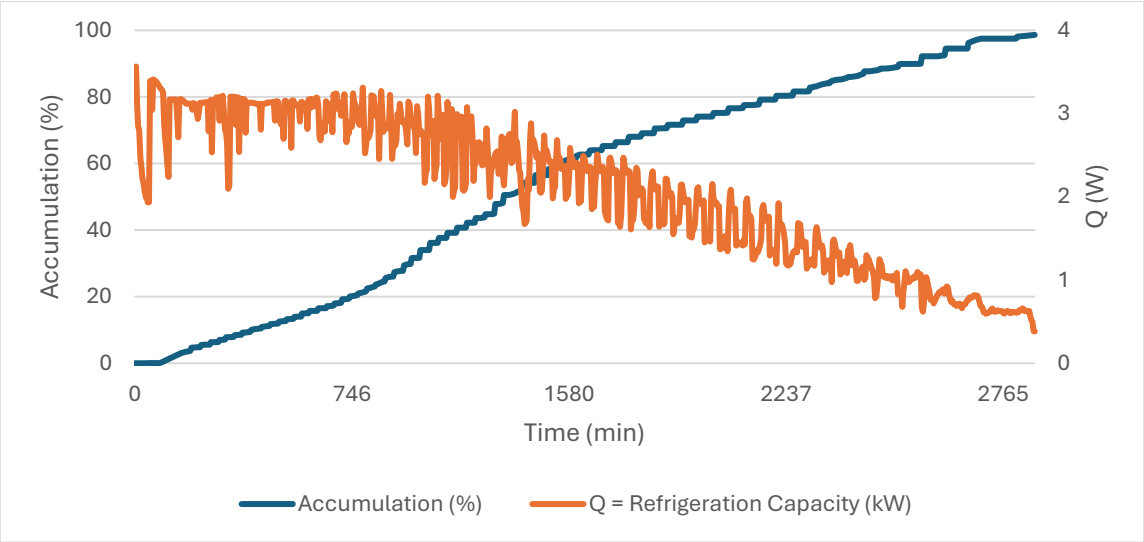

Figure 44 - Evolution of air cooler blockage (ice accoumulation) and cooling capacity with time

This behavior confirms the high sensitivity of the capacitive sensor to the actual condition of the finned coil: the signal provides a direct measurement of frost accumulation, with excellent repeatability and operational accuracy.

Depending on the application, it is possible to select the frost threshold that triggers defrosting. For example, setting the activation point at around 60% frost coverage—corresponding to an exchanged cooling power of about 2.5 kW—allows intervention before performance degradation becomes excessive, keeping the evaporator within a favorable efficiency range.

As with the fan power–based method, this approach also avoids unnecessary or random defrosts: the cycle starts only when it is truly needed and remains inactive when frost accumulation is not significant.

From a system control perspective, the capacitive logic can be further strengthened with a few measures: introducing hysteresis on the threshold (to prevent frequent reactivations), defining a minimum interval between two consecutive defrosts, and setting a maximum safety interval (e.g., 8–10 hours) to cover atypical conditions. It is also advisable to recalibrate the baseline after cleaning or maintenance operations and to perform a consistency check with other indicators (e.g., cooling power trend and thermo-hygrometric conditions).

Considering real operating conditions, these two “smart” methods — fan power threshold and frost-level (capacitive) threshold — outperform the time-based approach in terms of both energy efficiency and product quality, as they minimize disturbances to the cold-room microclimate (temperature and humidity) by activating defrost only when necessary. During the day, with product loading/unloading and air infiltration, and at night, with the room closed and low latent loads, operating conditions vary significantly; the same occurs between winter and summer seasons, when ambient humidity and air

temperature change. The time-based control does not “see” these variations and tends to run fixed, often unnecessary cycles, whereas the two threshold-based methods adapt to real conditions, reducing superfluous cycles and thermal stress.

In conclusion, integrating the two logics — for instance, triggering defrost when frost ≥ 60% *or* fan power ≥ 250 W, combined with hysteresis and time constraints — allows the evaporator to operate under stable and efficient conditions, reducing energy consumption and preserving product quality through smaller temperature and humidity fluctuations inside the cold room.

4.2. Evaluation of the Refrigeration System Efficiency

The monitoring of the dry-expansion refrigeration system confirmed that it consists of a single circuit with a nominal cooling capacity of 4 kW. The analysis of the collected data shows that the system operates correctly overall, maintaining stable performance during most of the monitored periods.

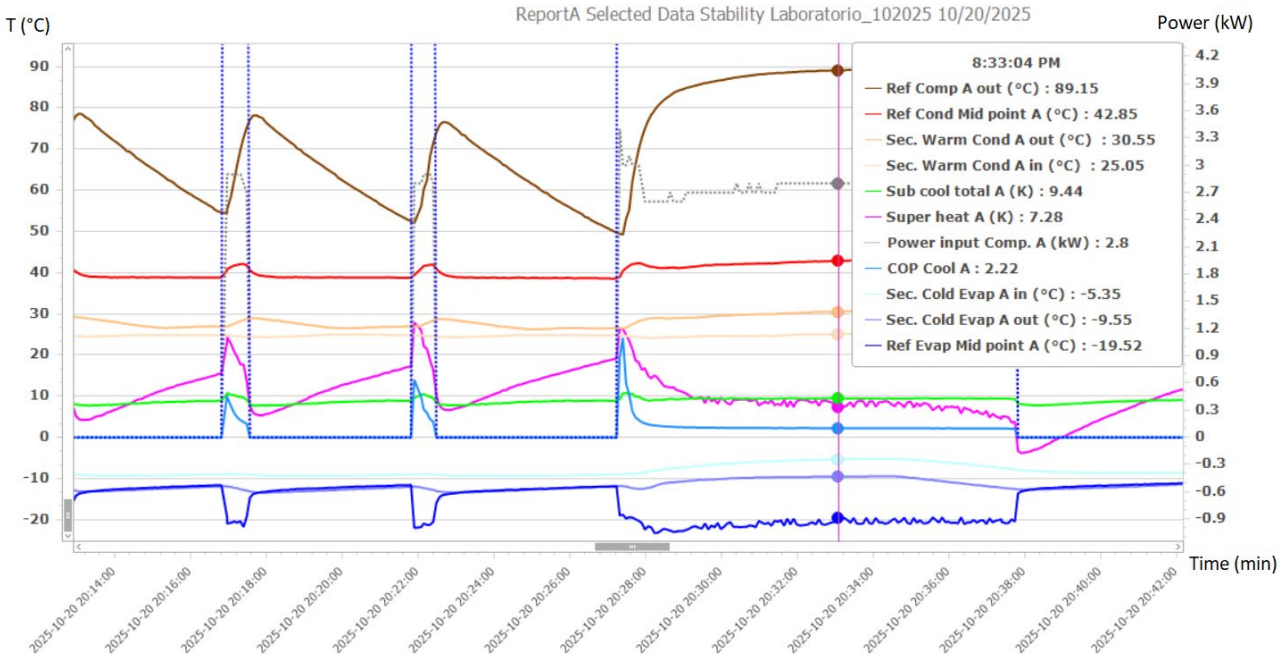

Figure 45 - Measured and calculated circuit data – representative operating excerpt

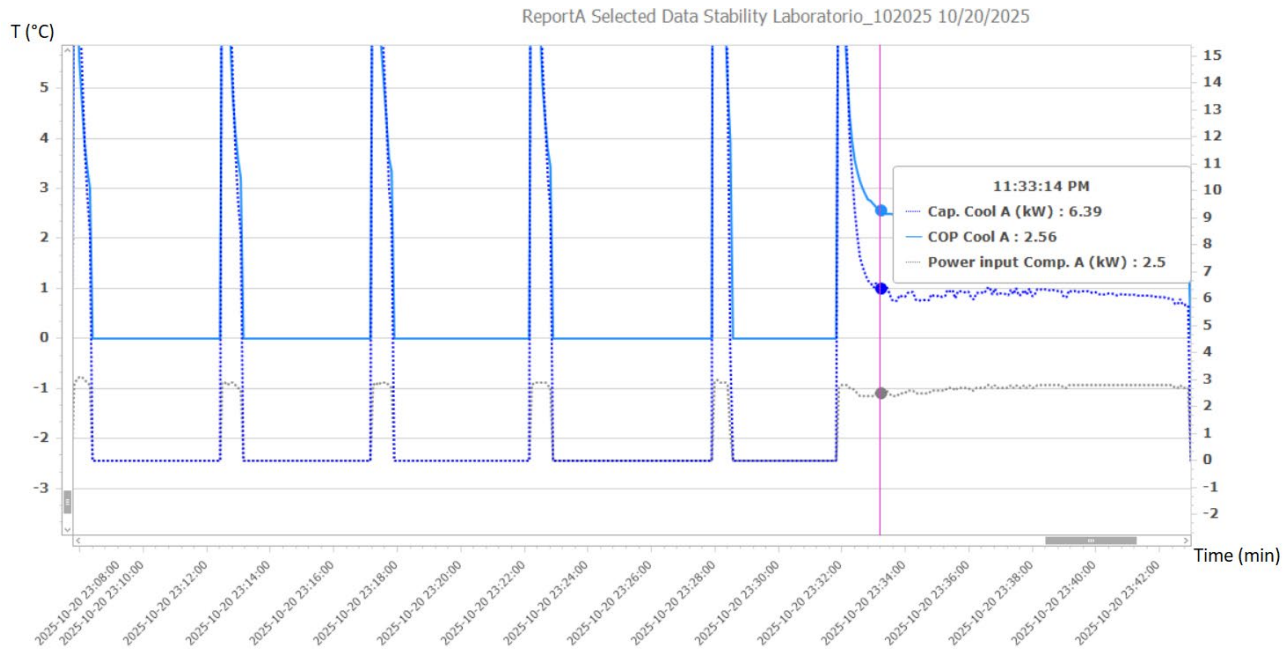

Figure 46 - Measured and calculated circuit data – representative operating excerpt

The graph also shows that the compressor does not undergo frequent on–off cycling; its operation is smooth and stable, avoiding both excessively short start intervals and overly long running periods—conditions that help extend its service life.

Air-cooled refrigeration unit performance – System Efficiency Index (SEI)

The refrigeration unit is operating under conditions close to the design specifications. In Circuit, shown in the dashboard below, operation occurs with an ambient temperature of 28 °C and a condensation temperature of 37 °C. This result indicates good condenser efficiency, as the ΔT is below 10 K, consistent with best practices for this type of system. The observed behavior shows that the system maintains a low condensation temperature, which leads to improved overall efficiency and reduced energy consumption, ensuring stable and reliable performance.

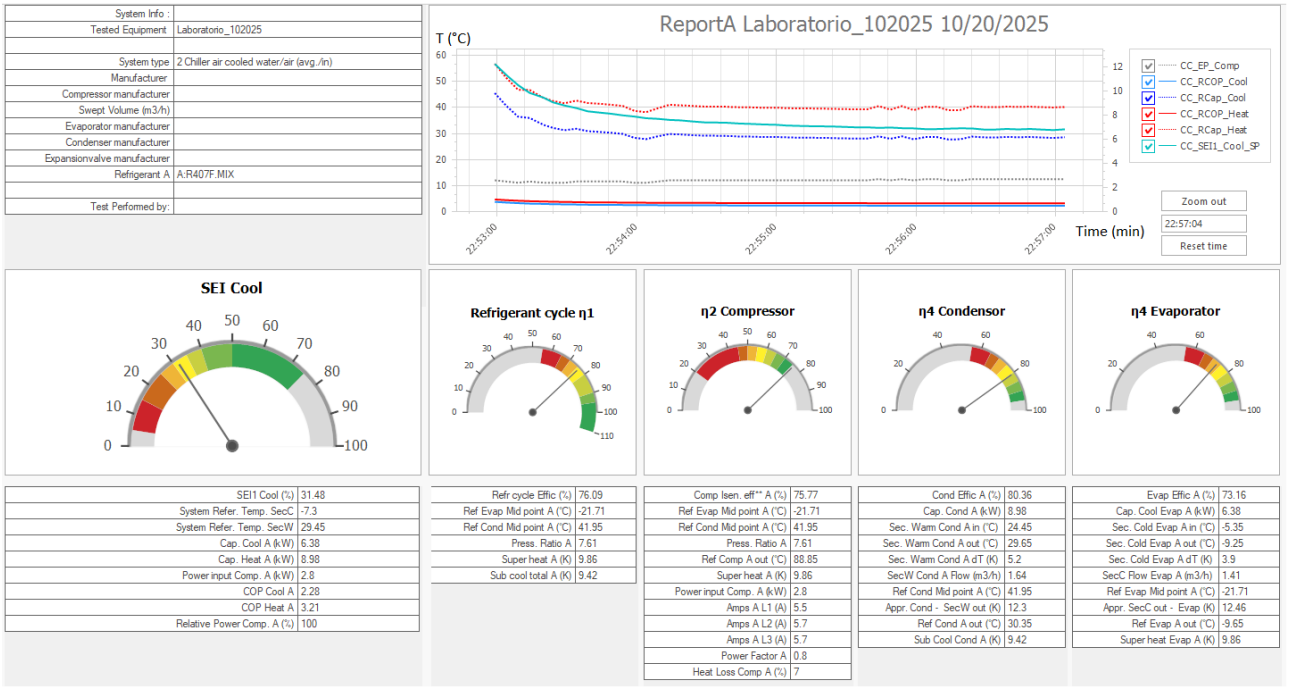

System Info :	
Tested Equipment	Laboratorio_102025
System type	2 Chiller air cooled water/air (avg./in)
Manufacturer	
Compressor manufacturer	
Swept Volume (m3/h)	
Evaporator manufacturer	
Condenser manufacturer	
Expansionvalve manufacturer	
Refrigerant A	A:R407F.MIX
Test Performed by:	

SEI1 Cool (%)	31.48
System Refer. Temp. SecC	-7.3
System Refer. Temp. SecW	29.45
Cap. Cool A (kW)	6.38
Cap. Heat A (kW)	8.98
Power input Comp. A (kW)	2.8
COP Cool A	2.28
COP Heat A	3.21
Relative Power Comp. A (%)	100

Refr cycle Effic (%)	76.09
Ref Evap Mid point A (°C)	-21.71
Ref Cond Mid point A (°C)	41.95
Press. Ratio A	7.61
Super heat A (K)	9.86
Sub cool total A (K)	9.42

Comp Isen. eff** A (%)	75.77
Ref Evap Mid point A (°C)	-21.71
Ref Cond Mid point A (°C)	41.95
Press. Ratio A	7.61
Ref Comp A out (°C)	88.85
Super heat A (K)	9.86
Power input Comp. A (kW)	2.8
Amps A L1 (A)	5.5
Amps A L2 (A)	5.7
Amps A L3 (A)	5.7
Power Factor A	0.8
Heat Loss Comp A (%)	7

Cond Effic A (%)	80.36
Cap. Cond A (kW)	8.98
Sec. Warm Cond A in (°C)	24.45
Sec. Warm Cond A out (°C)	29.65
Sec. Warm Cond A dT (K)	5.2
SecW Cond A Flow (m3/h)	1.64
Ref Cond Mid point A (°C)	41.95
Appr. Cond - SecW out (K)	12.3
Ref Cond A out (°C)	30.35
Sub Cool Cond A (K)	9.42

Evap Effic A (%)	73.16
Cap. Cool Evap A (kW)	6.38
Sec. Cold Evap A in (°C)	-5.35
Sec. Cold Evap A out (°C)	-9.25
Sec. Cold Evap A dT (K)	3.9
SecC Flow Evap A (m3/h)	1.41
Ref Evap Mid point A (°C)	-21.71
Appr. SecC out - Evap (K)	12.46
Ref Evap A out (°C)	-9.65
Super heat Evap A (K)	9.86

Figure 47 - perating dashboard at 28 °C ambient temperature – illustrative period

For compressors, a minimum compression ratio limit is specified, below which operation is not permitted. In the case of the analyzed refrigeration unit, the operating conditions remain well above this limit, while maintaining a relatively low condensation temperature compared to typical systems of the same type. This results in good energy efficiency and stable performance, fully consistent with the manufacturer's specifications.

For an optimal system, the System Efficiency Index (SEI) typically ranges between 55% and 60%. The analyzed system shows a value of 40%, which can still be considered very good. To approach the optimal level, only minor adjustments would be required—specifically, an increase in the evaporation temperature and a reduction of the suction superheat at the compressor inlet.

Comparison Between Measured and Design Performance

Based on the design data and the technical documentation of the refrigeration unit, the reference values under nominal design conditions were determined, specifically:

- Nominal COP of the system, calculated under standard operating conditions;
- Cooling capacity of the evaporator;
- Heat rejection capacity of the condenser (heat released to the environment);
- Electrical power input of the compressor;

- Reference operating conditions (evaporation and condensation temperatures, ambient temperature, and secondary fluid flow rate).

Compressor

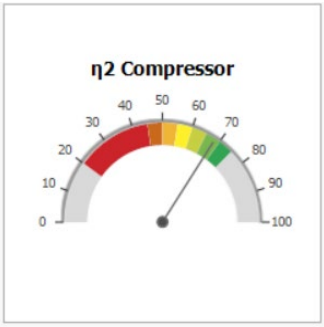

Comp Isen. eff** A (%)	68.33
Ref Evap Mid point A (°C)	-10.7
Ref Cond Mid point A (°C)	39.09
Press. Ratio A	4.55
Ref Comp A out (°C)	76.75
Super heat A (K)	11.24
Power input Comp. A (kW)	4.1
Amps A L1 (A)	21.7
Amps A L2 (A)	22.2
Amps A L3 (A)	21.8
Power Factor A	0.3
Heat Loss Comp A (%)	7

The compressor operates with an average efficiency of approximately 70%, a value considered very good and consistent with expectations for high-quality units. The measured performance indicates that the compressors are operating under stable conditions, with no signs of degradation. By comparing the measured data with the manufacturer's specifications, both the exchanged cooling capacity and the absorbed power of the compressor were found to be in very good agreement with the calculated and measured values. This consistency confirms the correct operation of the component and its alignment with the design specifications.

Condenser

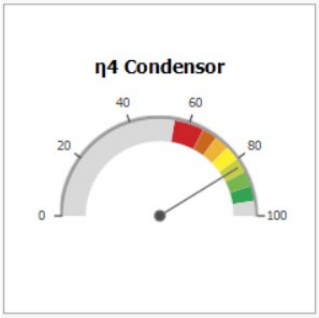

Cond Effic A (%)	82.61
Cap. Cond A (kW)	8.3
Sec. Warm Cond A in (°C)	24.05
Sec. Warm Cond A out (°C)	28.25
Sec. Warm Cond A dT (K)	4.2
SecW Cond A Flow (m3/h)	1.88
Ref Cond Mid point A (°C)	40.21
Appr. Cond - SecW out (K)	11.96
Ref Cond A out (°C)	28.85
Sub Cool Cond A (K)	9.15

The condenser shows an average efficiency of 82%, indicating good operating performance. The average temperature difference (ΔT) between the inlet air temperature and the condensation temperature is about 10 K, which is considered optimal and consistent with proper heat exchange on the air side. At the condenser outlet, a subcooling of 9 K was recorded, also in line with the expected values to ensure operational stability and proper feeding of the expansion valve.
Overall, the data confirms that the condenser operates under efficient conditions, with no evidence of fouling or heat exchange anomalies. The performance can be considered fully satisfactory and consistent with the state of the art for this type of system.

Evaporator

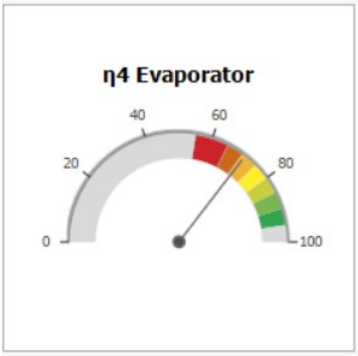

Evap Effic A (%)	70.96
Cap. Cool Evap A (kW)	6.07
Sec. Cold Evap A in (°C)	-6.75
Sec. Cold Evap A out (°C)	-9.65
Sec. Cold Evap A dT (K)	2.9
SecC Flow Evap A (m3/h)	1.8
Ref Evap Mid point A (°C)	-23.95
Appr. SecC out - Evap (K)	14.3
Ref Evap A out (°C)	-8.65
Super heat Evap A (K)	13.08

The evaporator efficiency ranges between 68% and 70%, a value considered good and consistent with the measured operating conditions. The average superheat was approximately 10 K, close to the minimum required to ensure proper operation of the electronic expansion valve, confirming that the evaporator is adequately fed.

Despite these good performances, there is room for improvement: increasing the evaporation pressure—thus reducing the ΔT between the evaporation temperature and the outlet glycol water temperature—would allow the heat exchanger efficiency to rise to values close to 90–100%. This would result in a higher overall refrigeration cycle efficiency and lower energy consumption.

Each degree of reduction in evaporation temperature leads to an estimated increase in energy consumption of 3–5%. This effect corresponds to an overall increase in circuit energy use of approximately 15–20%, even without considering the possible presence of flash gas through the expansion valve.

From the graph in Fig. 48, it can be observed that the glycol mixture temperature and the cold-room air temperature follow a similar trend over time, with nearly synchronous variations. The increase or decrease in air temperature inside the room is directly influenced by the behavior of the evaporator: when T_{ev} rises, T_{room} also tends to increase with a slight delay, whereas when T_{ev} decreases, Troom gradually drops until thermal equilibrium is restored.

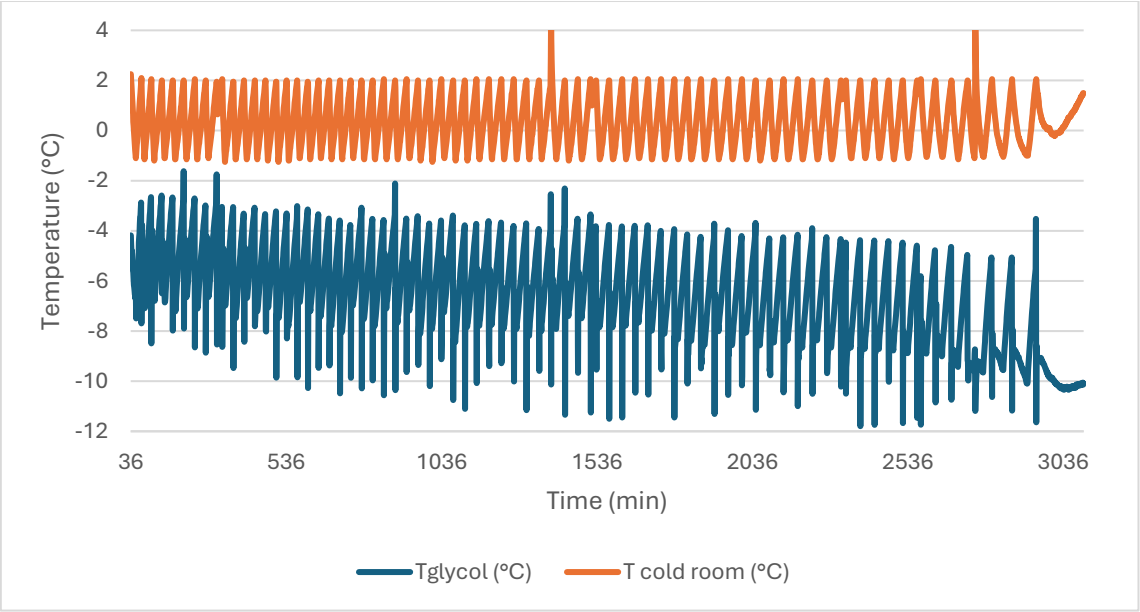

Figure 48 –Example trend of cold-room air temperature and glycol mixture temperature

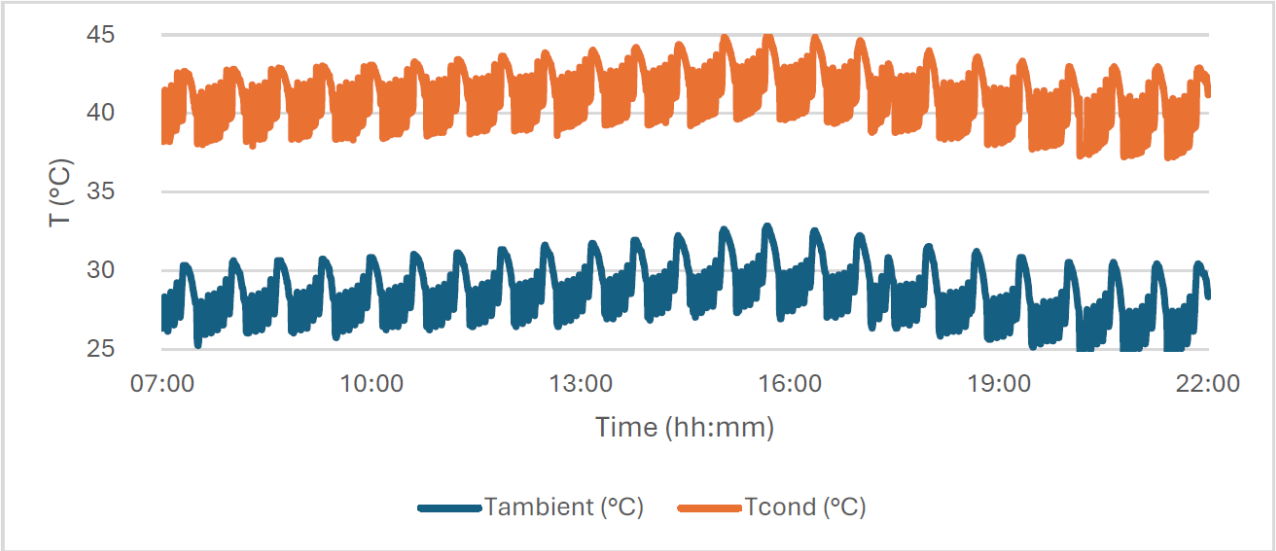

Figure 49 - Example trend of condensation temperature and outdoor air temperature over time

From the graph shown in Fig. 50, it can be observed that the Coefficient of Performance (COP) decreases almost linearly with increasing pressure ratio between condensation and evaporation (P_{cond}/P_{ev}).

This behavior is consistent with refrigeration cycle theory: as the condensation pressure (or equivalently, the condensation temperature) increases, the compression work rises more rapidly than the useful cooling capacity, resulting in an overall decrease in system efficiency.

In other words, a high pressure ratio implies greater energy consumption per unit of cooling produced, which is why it is preferable to maintain low condensation temperatures and high evaporation temperatures, insofar as product storage requirements allow.

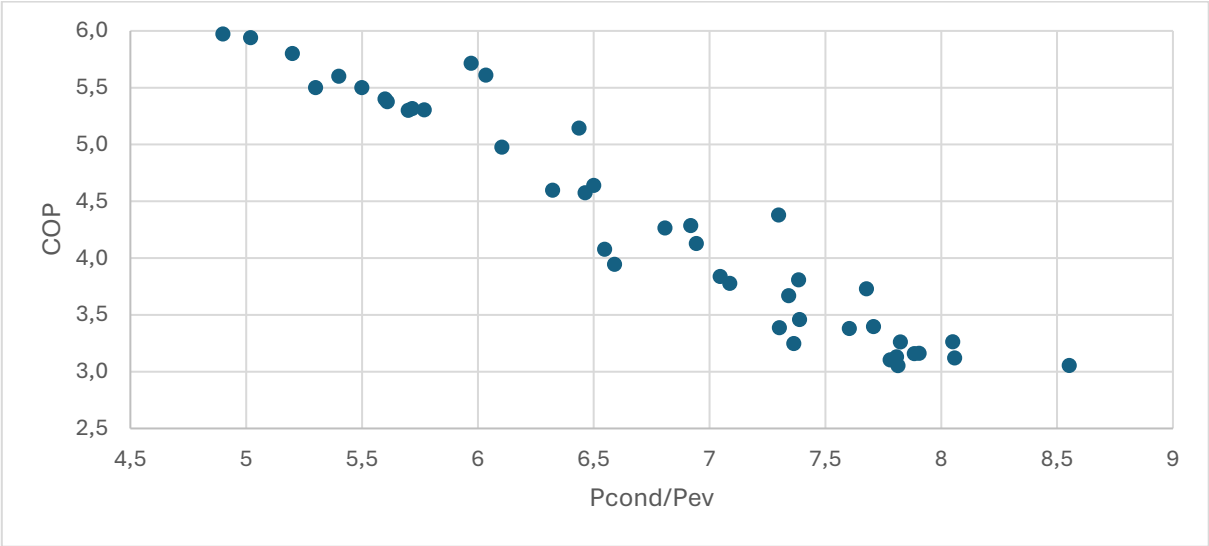

Figure 50 - COP as a function of the pressure ratio (P_cond / P_evap)

4.3. Data processing of ambient air temperature and humidity under various cold-room operating conditions.

This chapter analyzes the experimental data collected during the operation of the cold room under different operating conditions. The aim of the analysis is to evaluate the temporal evolution of air temperature and relative humidity, and to compare the system's behavior across various operating regimes characterized by different ΔT values between air temperature and evaporation temperature. The tests with ΔT = 5 K, 8 K, and 10 K were carried out in a real cold-storage facility used for fruit and vegetable preservation, while the ΔT = 2 K test was performed under controlled laboratory conditions. For each operating regime, the time profiles of air temperature and humidity inside the cold room were recorded and plotted, whereas for the ΔT = 2 K condition a single representative graph is reported.

ΔT = 5 K

With the direct expansion refrigeration system, the minimum achievable ΔT between the cold-room air and the evaporating surface under stable conditions is approximately 5 K. Below this threshold, the expansion valve can no longer properly modulate the refrigerant flow—even in the case of electronic valves—and the superheating of the vapor at the evaporator outlet may become excessively low.

Low superheating implies the possible presence of liquid refrigerant entering the compressor suction line, with the consequent risk of liquid carryover. This phenomenon can cause mechanical impacts or dilution of the lubricating oil, compromising the compressor's reliability.

Therefore, the ΔT = 5 K regime represents an optimal condition for a cold room intended for fruit and vegetable storage when using direct expansion systems.

This configuration allows maintaining a high relative humidity level inside the room, thus reducing product dehydration. As shown in Figures 51–53, the relative humidity remains at an average value of about 92% during operation, with the air temperature inside the cold room at approximately 4°C.

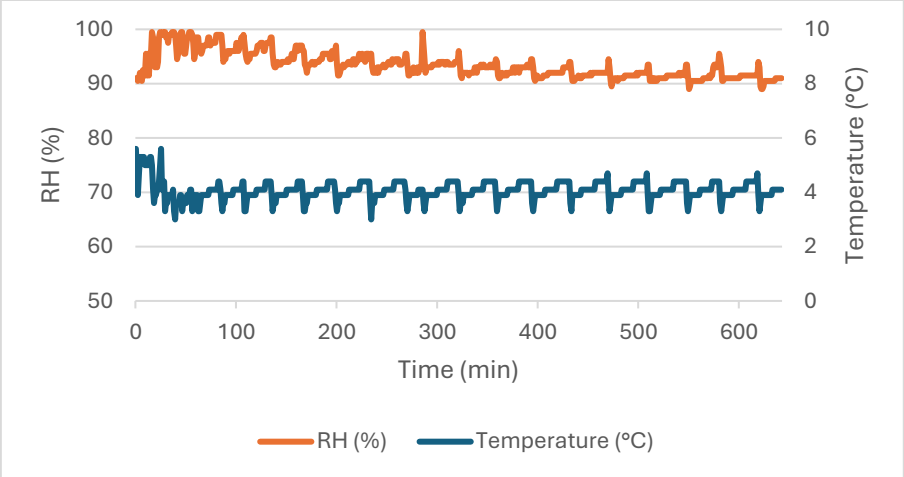

Figure 51 - Temperature and relative humidity trends in the cold room – ΔT = 5 K (Test 1)

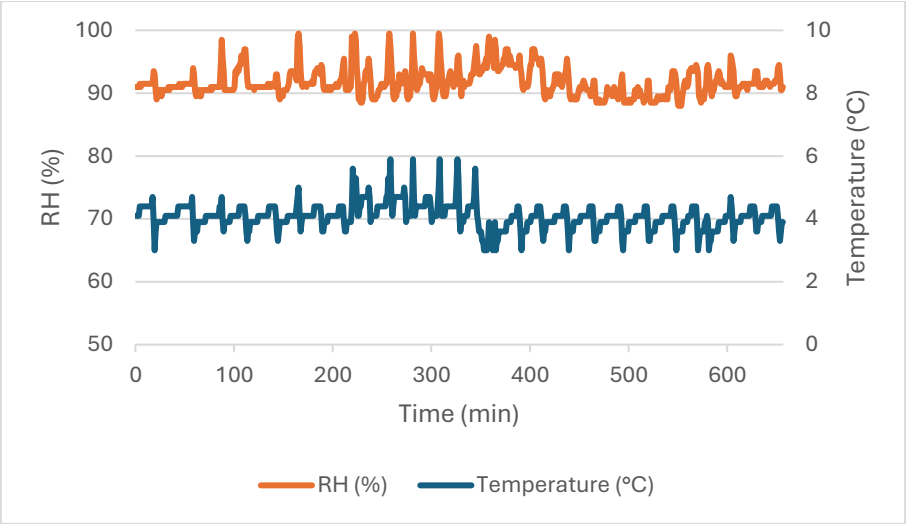

Figure 52 - Temperature and relative humidity trends in the cold room – ΔT = 5 K (Test 2)

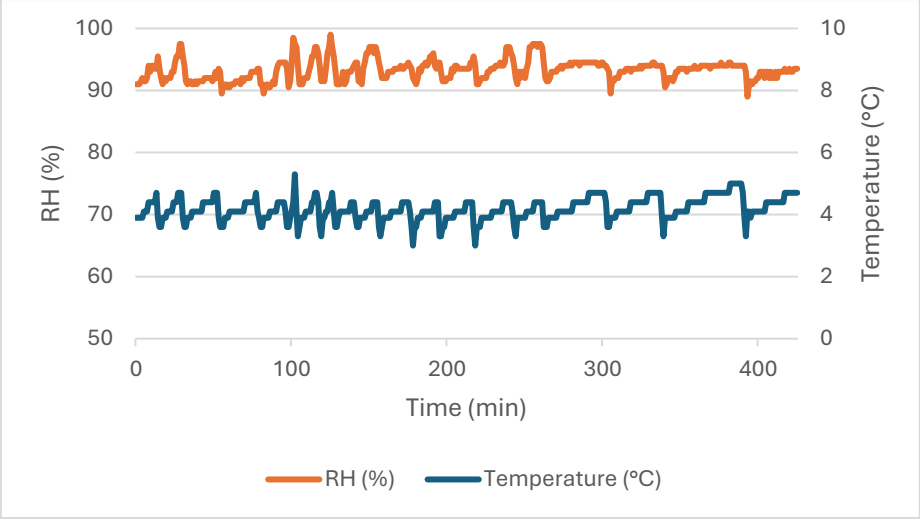

Figure 53 - Temperature and relative humidity trends in the cold room – ΔT = 5 K (Test 3)

ΔT = 8 K

In these tests, the ΔT between the cell air and the evaporation surface was increased to 8 K.

Under these conditions, as shown in graphs Fig. 54-Fig. 56, the air temperature stabilized at around 1.5 °C, while the relative humidity averaged approximately 85%.

Compared to the ΔT = 5 K regime, a decrease in relative humidity was observed due to the greater degree of air drying: by increasing the temperature difference between the air and the evaporator, the heat flow is more intense and the evaporation temperature is lower, favoring the condensation of water vapor on the evaporator.

This results in a greater specific refrigeration capacity, but at the expense of the preservation of products sensitive to moisture loss.

This regime therefore represents an operational compromise that achieves good heat exchange efficiency and a faster dynamic response of the system, but with a drier internal climate than the optimal condition for fruit and vegetables observed with $\Delta T = 5$ K.

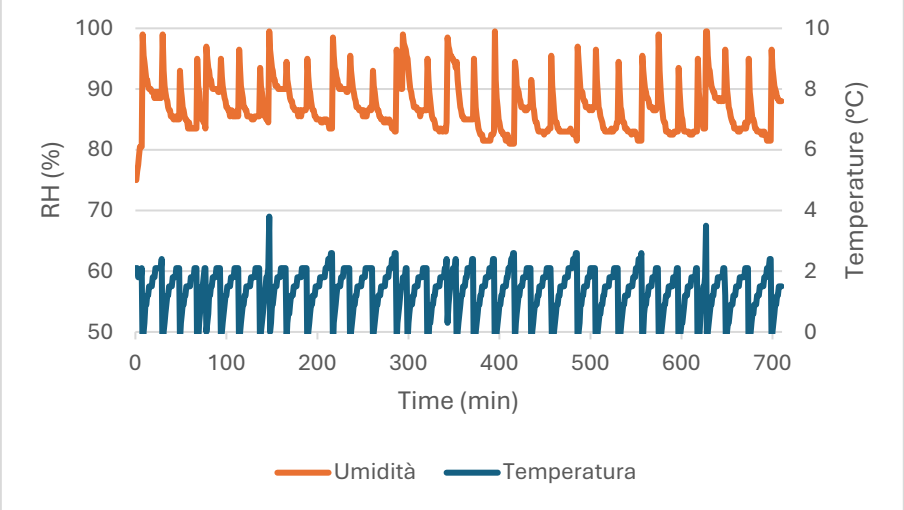

Figure 54 - Temperature and relative humidity trends in the cold room – $\Delta T = 8$ K (Test 1)

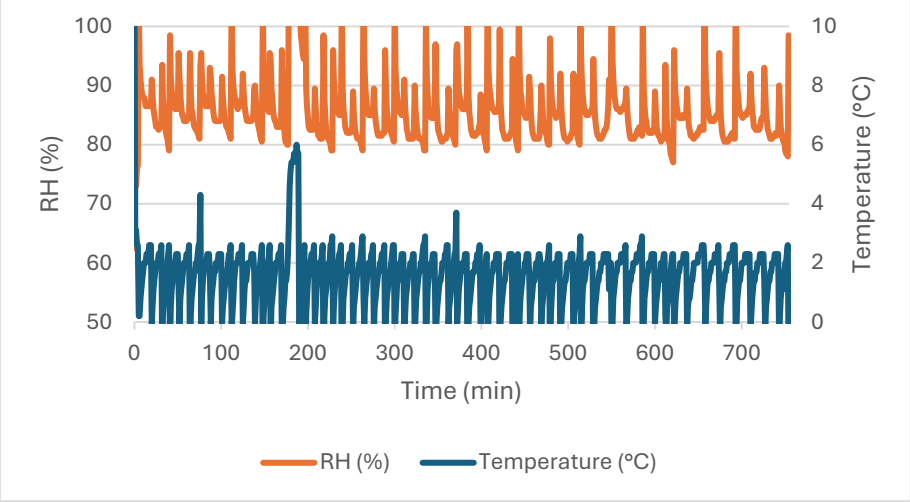

Figure 55 - Temperature and relative humidity trends in the cold room – $\Delta T = 8$ K (Test 2)

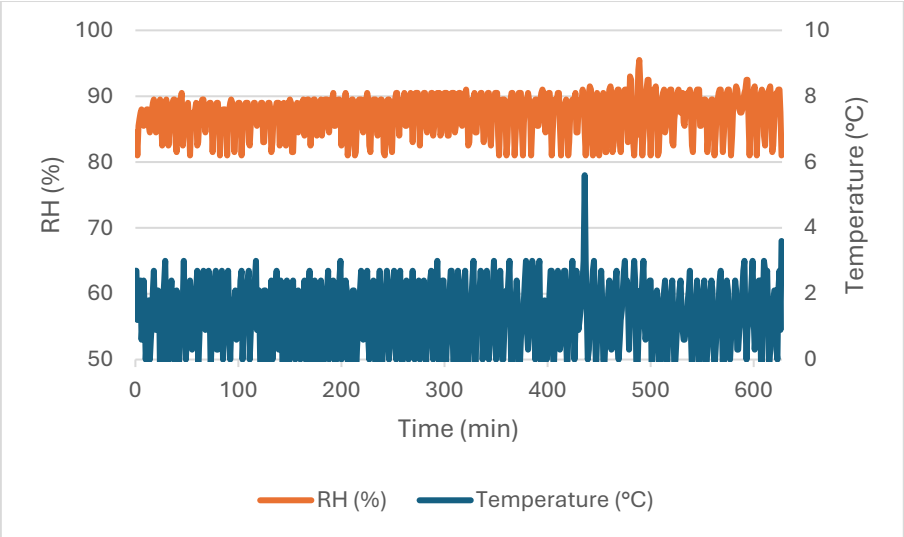

Figure 56 - Temperature and relative humidity trends in the cold room – ΔT = 8 K (Test 3)

ΔT = 10 K

In this series of tests, the ΔT between the cell air and the evaporation surface was brought to 10 K, a value that determines a more vigorous operation of the refrigeration circuit. With this configuration, the air temperature in the cell remained around 0.8 °C, while the relative humidity dropped to an average of approximately 78%, as shown in graphs Fig. 57-Fig. 59.

The greater temperature difference compared to previous regimes results in more rapid cooling of the air, but also in more intense condensation of water vapor on the evaporator, with a consequent reduction in relative humidity inside the cell. Consequently, while slightly improving instantaneous cooling capacity and the speed of temperature reduction, this regime is less suitable for the prolonged preservation of fruit and vegetables, as the drier air can promote surface dehydration of the products.

The comparison with the lower ΔT regimes (5 K and 8 K) therefore highlights how the increase in ΔT improves the thermal performance of the system but reduces the quality of the internal microclimate, making it necessary to identify an optimal compromise between energy efficiency and storage conditions.

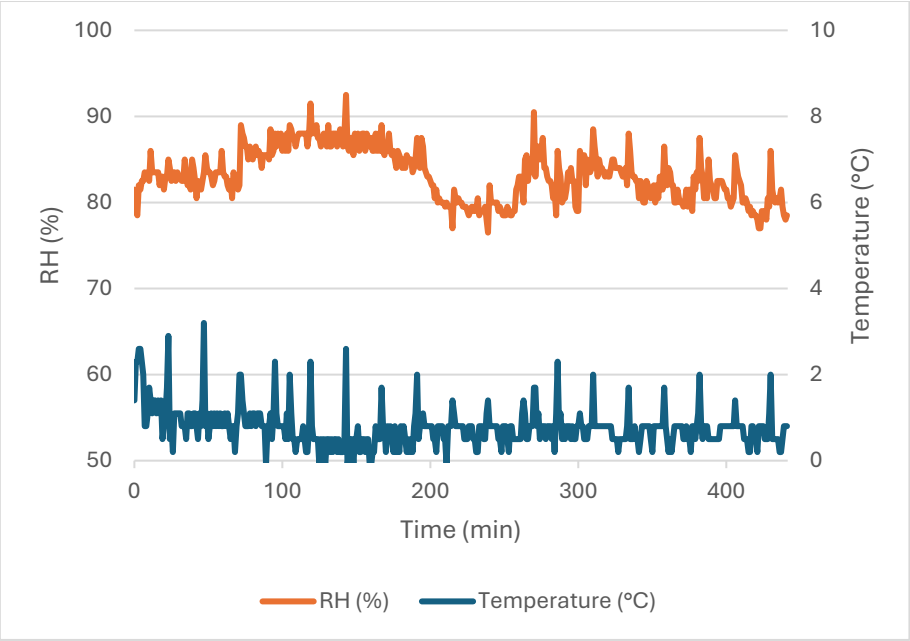

Figure 57 - Temperature and relative humidity trends in the cold room – ΔT = 10 K (Test 1)

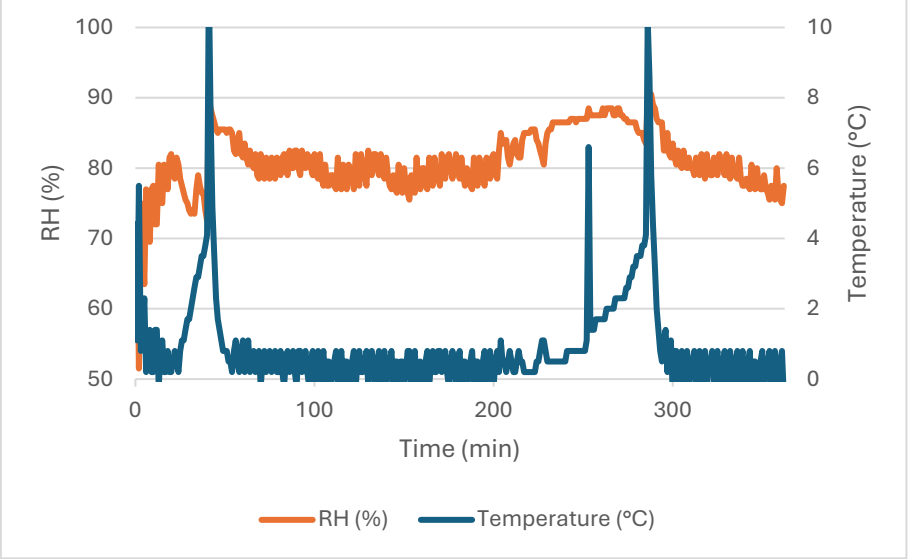

Figure 58 - Temperature and relative humidity trends in the cold room – ΔT = 10 K (Test 2)

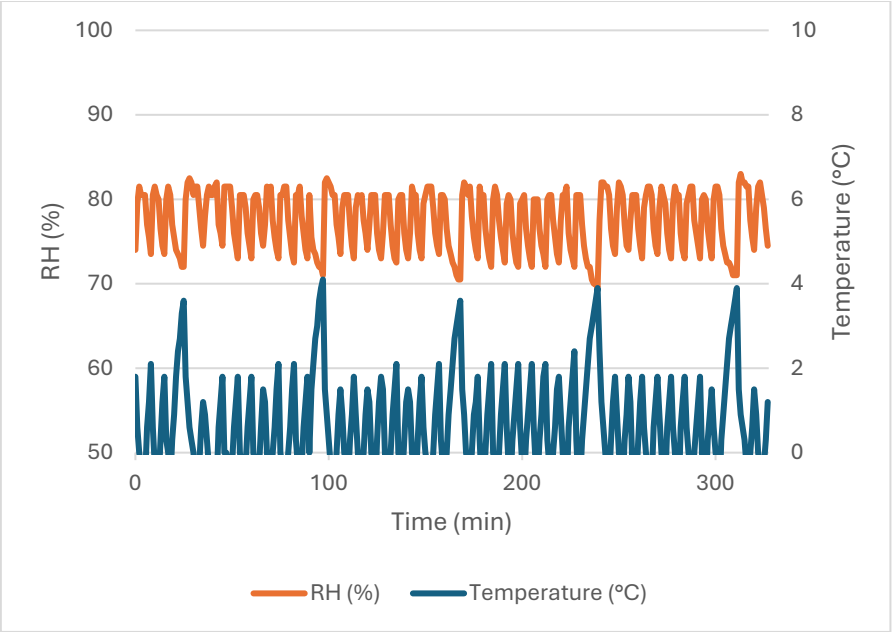

Figure 59 - Temperature and relative humidity trends in the cold room – ΔT = 10 K (Test 3)

As can be seen from the time graphs, and particularly clearly in Figure 59, simultaneous peaks in air temperature and relative humidity are observed when the cell door is opened. The entry of warmer, more humid air from the outside causes a sudden increase in internal temperature and a temporary saturation of the water vapor content, which manifests itself as a rapid increase in relative humidity. After the door is closed, the refrigeration system gradually re-establishes equilibrium conditions, returning the temperature and humidity to the nominal values of the regime under consideration.

ΔT = 2 K

The ΔT = 2 K test was conducted in the laboratory using an indirect refrigeration system, in which the air in the cell is cooled by an air cooler fed with ethylene glycol solution. In this configuration, the secondary fluid allows for more stable and modulated temperature control, reducing the thermal oscillations typical of direct expansion systems.

As can be seen from the graphs, the low ΔT between the cell air and the exchange surface allows for high relative humidity, with values close to 96%, and an average cell air temperature of approximately 1°C. This behavior confirms that, by working with small temperature differences and smoother exchanges, it is possible to ensure a very humid and stable internal microclimate, ideal for storing fruit and vegetables sensitive to dehydration.

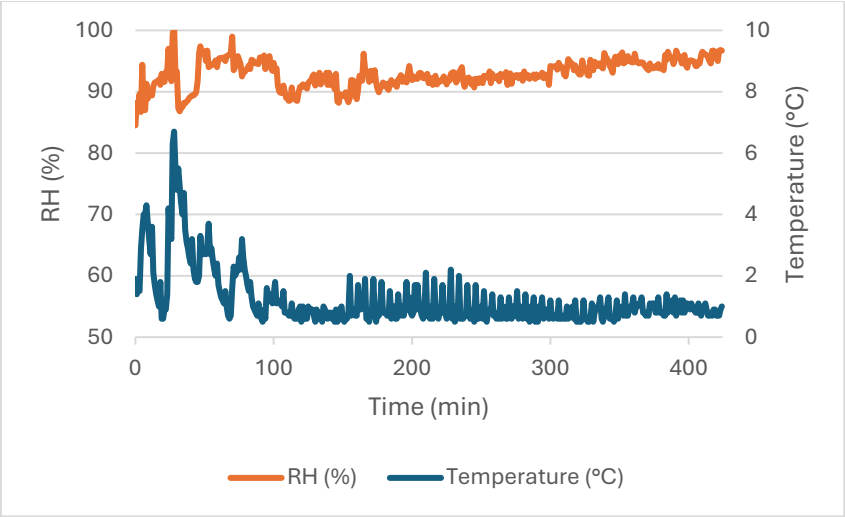

Figure 60 - Temperature and relative humidity trends in the cold room – ΔT = 2 K

In light of the results obtained, which are summarized in the graph in Fig. 61, it is evident that the prototype sizing and the design choices adopted allow, without problems under steady-state conditions (closed cell and no product movement), a humidity level of 91-93% within the cold room. When there is a change in steady-state conditions (opening the door or entry of hot product), the humidity level decreases, creating the conditions for greater moisture loss from the product. Therefore, with the chosen system solution, it is possible to create a system efficient in terms of performance and energy consumption, with a cost approximately 30% lower than a system that allows maintaining a RH level ≈ 95% but requires indirect refrigeration technology.

RH levels > 95% can only be achieved with the use of mist humidifiers.

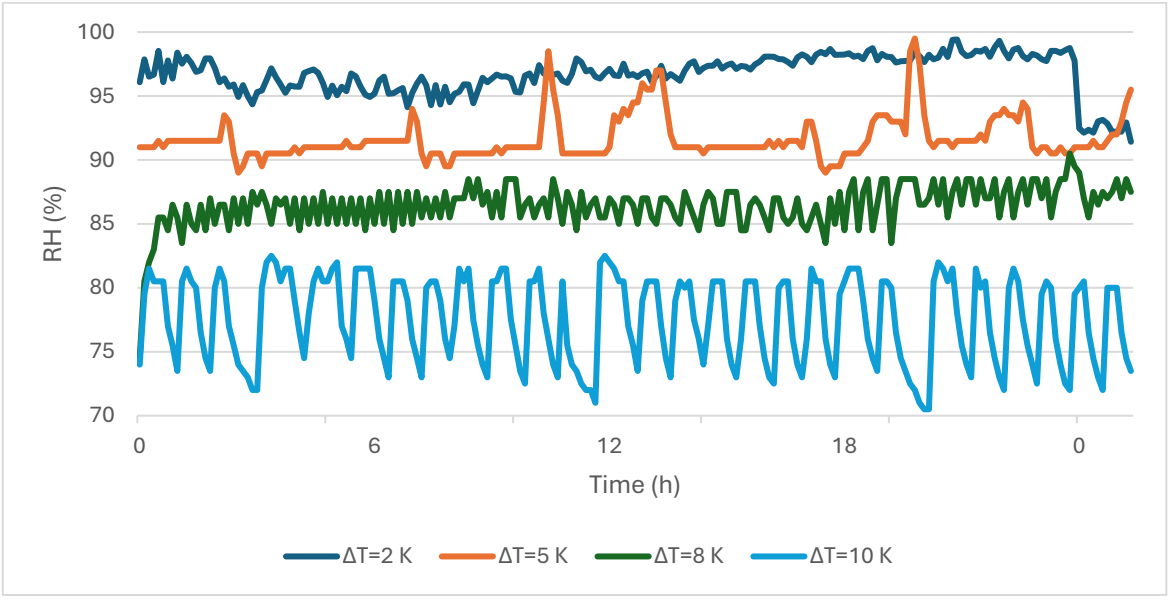

Figure 61 - Trend of relative humidity over time for different ΔT between the air in the cold room and the heat exchange surface

4.4. Application of the Weight-Loss Simulation Model

The simulation model described in Section 3.6 was applied to a representative storage scenario for horticultural products in a refrigerated room. As a case study, 150 tons of apples stored under long-term conservation conditions were considered, and the model was used to quantify the influence of room temperature and relative humidity on product weight loss over a 24-hour period.

Figure 62 shows the predicted percentage weight loss as a function of air temperature and relative humidity in the cold room. As expected, higher temperatures and lower relative humidity levels lead to a marked increase in water loss from the product.

A representative operating point is highlighted in Figure 62, corresponding to a room T_{room} = 3°C and RH = 82.5%.

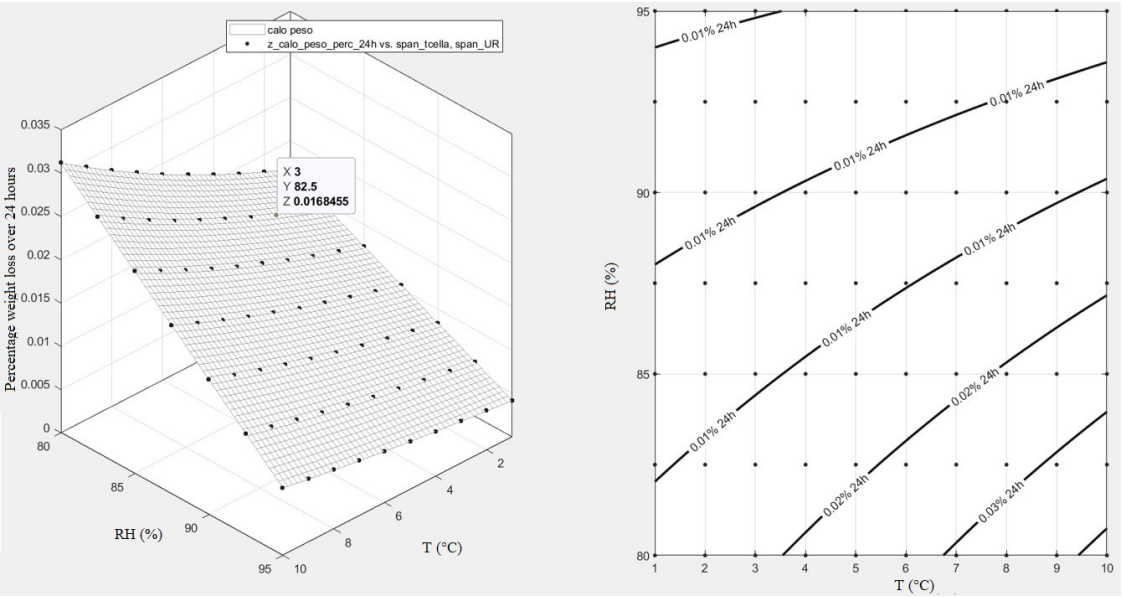

Figure 62 - Percentage weight loss over 24 hours of 150 tons of apples as a function of cold-room temperature and relative humidity

Under these conditions, the model predicts a weight loss of approximately 1.7% over 24 hours. This example clearly illustrates how a moderate decrease in relative humidity, at constant temperature, can significantly increase product dehydration.

Figure 63 reports the estimated defrosting frequency required to maintain acceptable heat transfer performance at the evaporator. As relative humidity decreases, the frost load on the coil tends to grow more rapidly, leading to more frequent defrosts, whereas at higher humidity levels the required defrost frequency is reduced for the same temperature setpoint.

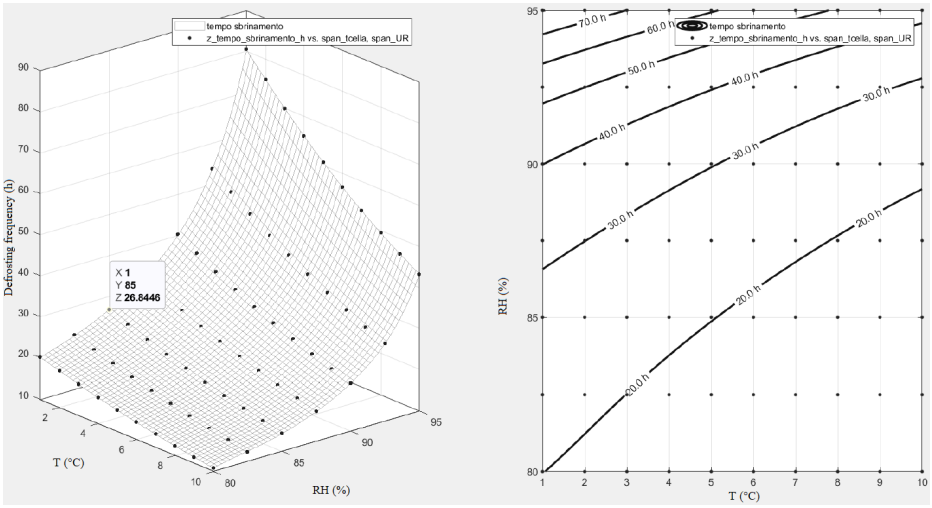

Figure 63 – Defrosting frequency

Finally, Figure 64 shows the calculated difference in water vapor pressure between the product surface and the surrounding air for the considered operating conditions. This pressure difference represents the driving force for transpiration and directly correlates with the predicted mass loss. The results confirm that even small changes in room humidity can substantially modify the vapor pressure deficit and, consequently, the rate of water loss from the stored product.

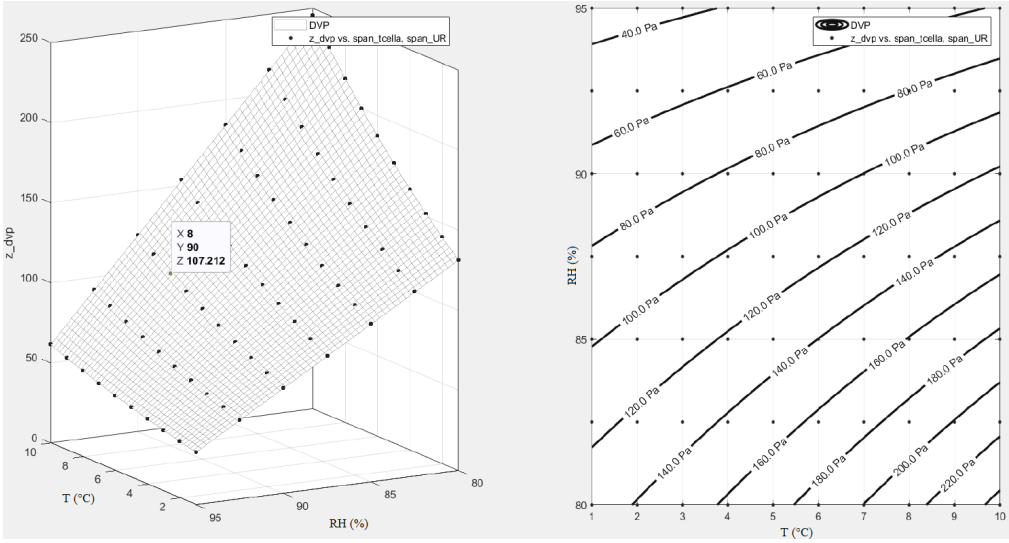

Figure 64 - Difference in water vapor pressure between the product surface and the cold room environment

Overall, the simulation outcomes indicate that maintaining high relative humidity levels in the cold room is essential to minimize weight loss, while at the same time the interaction with defrost control must be considered, since more humid conditions favor frost formation and may require more frequent defrost cycles.

4.5. Energy Saving Assessment Through Inverter Control

The introduction of inverters in refrigeration systems represents one of the most effective solutions for reducing energy consumption and optimizing performance. The continuous regulation of compressor and fan speeds allows the absorbed power to adapt to the actual thermal load, avoiding the inefficiencies typical of fixed-speed operation.

This chapter presents a technical–economic assessment of the impact of adopting inverters in a refrigeration system installed in a cold room for fruit and vegetable storage, including the compressor, condenser fans, and evaporator fans. The objective is to quantify energy savings, CO_2 emission reductions, and the economic return on investment (ROI).

Estimation of Current Energy Consumption

Considering an average operating time of 18 hours per day, the total daily energy consumption amounts to 457 kWh, corresponding to approximately 140,250 kWh per year for a system without inverters.

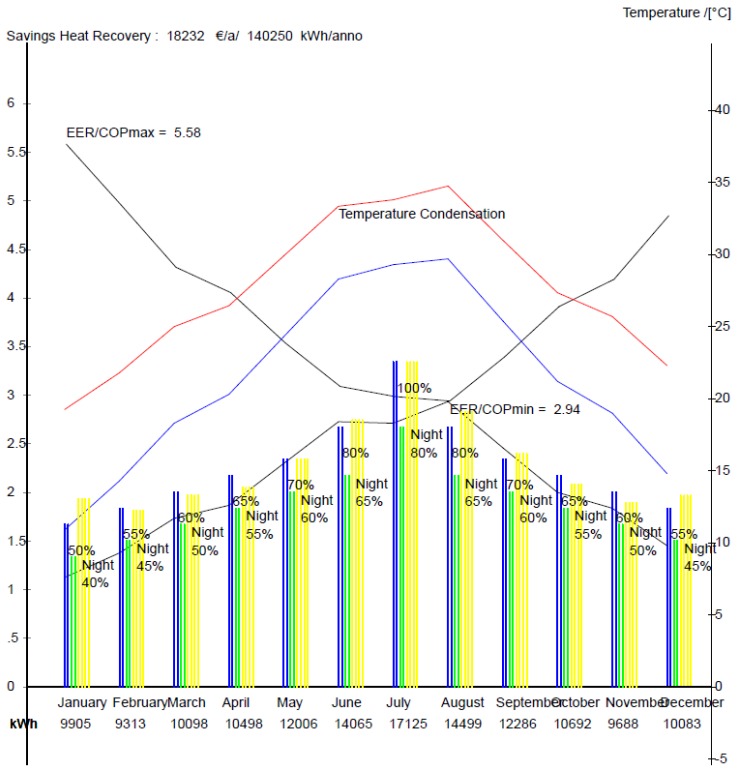

Figure 65 - Total annual energy consumption (kWh/year) – Configuration without inverter

The equipment in operation includes:

- one compressor equipped with an inverter,
- one condenser with two inverter-driven fans,
- one evaporator with four inverter-driven fans,

for a total cooling capacity of 50 kW and a total electrical power input of approximately 25 kW.

Energy Comparison Scenarios

The assessments were carried out considering the following four different configurations:

Configuration	Total energy consumption [kWh/year]	Emissions CO_2 [t/year]	Energy costEnergy cost [€/anno]
Without inverter	140,250	77.137	18,232.00 €
Inverter: compressor	120,922	66.507	15,719.00 €
Inverter: compressor + condenser	107,832	59.307	14,018.00 €
Inverter: compressore + condenser + evaporator	92,730	51.001	12,054.00 €

Table 6 – Electrical Energy Consumption and Operating Costs for Different Configurations

Savings Analysis

The gradual adoption of inverters leads to increasing energy savings and a consequent reduction in operating costs.

- In particular: with the inverter applied only to the compressor, a reduction in consumption of 13.7% is achieved compared to the baseline condition.

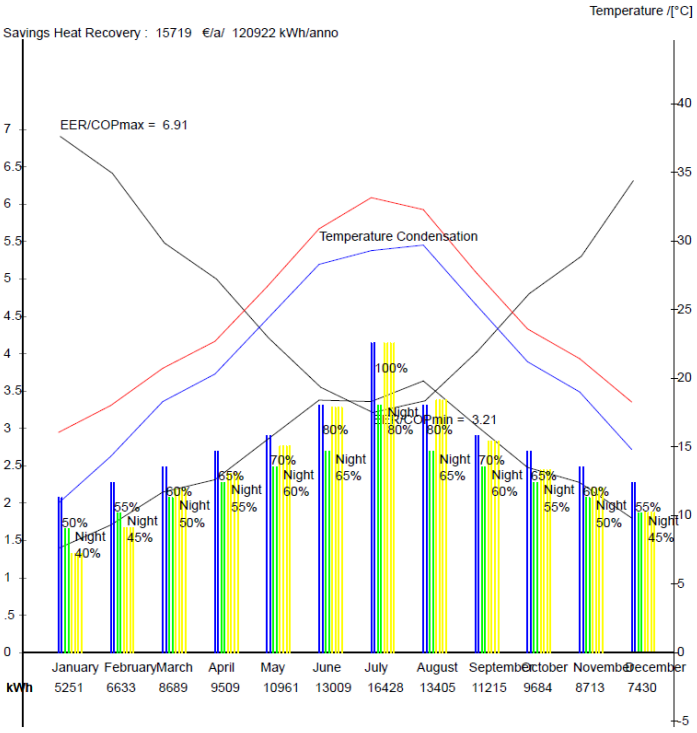

Figure 66 - Total annual energy consumption (kWh/year) – Configuration with inverter on compressor

- by extending the control to the condenser as well, the energy saving increases to approximately 23%;

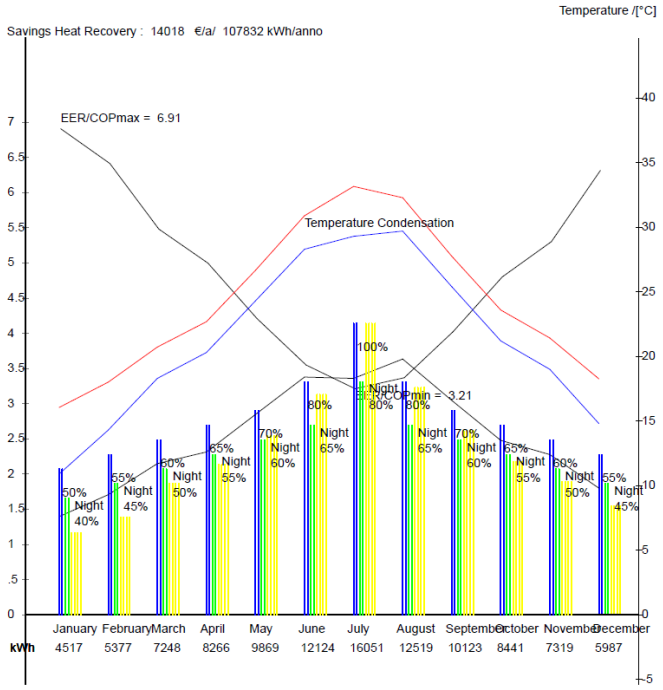

Figure 67 - Total annual energy consumption (kWh/year) – Configuration with inverter on compressor and condenser

- implementing the inverter also on the evaporator fans results in a total energy saving of 34%, with consumption decreasing from 140,250 to 92,730 kWh/year.

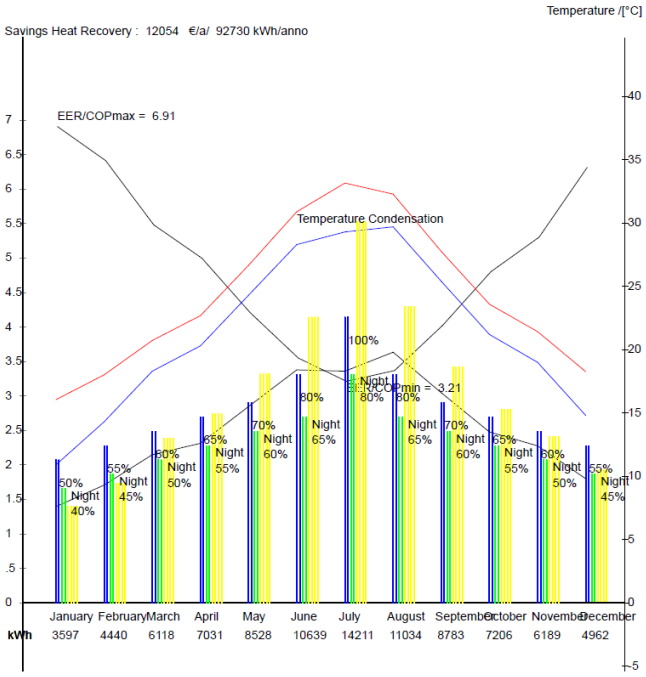

Figure 68 - Total annual energy consumption (kWh/year) – Configuration with inverter on compressor, condenser, and evaporator

At the same time, CO_2 emissions are reduced by approximately 26 tons per year, and the annual energy cost decreases from € 18,232 to € 12,054, resulting in an estimated economic saving of 34%.

Economic Return of the Investment (ROI)

Considering an investment of €8,000 for system upgrading and assuming the same implicit electricity tariff (≈0.13 €/kWh), the annual economic savings are as follows:

- € 2,513 with the inverter applied only to the compressor (–13.78%),
- € 4,214 with inverters on both the compressor and condenser (–23.11%)
- € 6,178 when inverters are also extended to the evaporator fans (–33.89%).

The corresponding payback times are 3.18 years, 1.90 years, and 1.29 years, respectively. It follows that the configuration with inverters on the compressor, condenser, and evaporator is the most advantageous, allowing cost recovery in approximately 16 months while providing the maximum reduction in operating costs.

5. Conclusions

The long-term storage of fruit and vegetable products presents several critical aspects that can significantly affect their shelf life. Once detached from the plant, fruits and vegetables become much more sensitive to physiological degradation processes, particularly transpiration and respiration, which lead to a progressive loss of water from plant tissues with no possibility of replenishment. External environmental factors can further exacerbate this tendency: the temperature and relative humidity levels in the storage environment are closely linked to the amount of water lost daily by the product. Fluctuations in these parameters cause variations in relative humidity, directly influencing the daily weight loss of stored commodities. These variations are largely dependent on the type of refrigeration system used and on the design and operating characteristics of the installed air coolers. Moreover, the air temperature control system within the storage room also plays a key role, as it must ensure sufficient precision and responsiveness. The number, placement, and response time of temperature sensors are crucial factors in maintaining uniform and stable thermal conditions.

The research work presented in this thesis focused on the optimization of refrigeration systems used in the fruit and vegetable storage sector, with particular attention to cold-room applications. The study aimed to improve both energy efficiency and product preservation quality, addressing the relationship between the refrigeration system, the storage environment, and the physiological behavior of the stored commodities.

To achieve these objectives, the research adopted a twofold approach, considering both direct and indirect strategies for controlling the ambient humidity and, consequently, the weight loss of the products due to transpiration.

1. Direct control of the storage environment

The first step of this study involved industrial-scale experimental tests carried out in a real cold storage facility, where both temperature and humidity levels were continuously monitored and controlled in the presence of actual fruit loads. Several operating scenarios were analyzed by varying the evaporation temperature, in order to assess its influence on the air temperature, relative humidity, and product dehydration rate within the cold room. The results showed that the design and sizing choices adopted for the prototype enable the system to maintain a relative humidity level between 91% and 93% under steady-state conditions (closed-cell operation, with no product movement). When these steady conditions are disturbed—for example, due to door openings or the introduction of warmer products—the humidity level temporarily decreases, creating conditions that promote higher moisture loss from the stored produce. Nevertheless, the adopted direct expansion refrigeration

configuration proves to be both energetically efficient and economically advantageous: it allows stable operation and effective humidity control at a cost approximately 30% lower than that of an indirect refrigeration system capable of maintaining a relative humidity of about 95%. Higher humidity levels (>95%) could only be achieved through the use of additional mist humidification systems.

Overall, the analysis confirms that, with a temperature difference (ΔT) of about 5 K between the air and the evaporator surface, it is possible to achieve a relative humidity of around 92%, which represents an optimal balance between product preservation, energy efficiency, and system simplicity.

2. Optimization of the refrigeration system design and operation

The second step focused on defining the optimal design and operational parameters of the refrigeration system used in cold rooms. By continuously monitoring key performance parameters—such as suction and discharge pressures, refrigerant temperatures, compressor power consumption, and heat exchange efficiency, it was possible to observe the real-time behavior of the system and assess its operational stability.

This real-time data analysis provided valuable insights into the system's response to varying loads and environmental conditions, enabling the identification of early signs of inefficiency or malfunction. Such monitoring makes it possible to predict maintenance needs and implement preventive technical interventions before system performance deteriorates or failures occur—conditions that could otherwise compromise both the refrigeration process and the quality of the stored fruit.

3. Innovative defrost methods in comparison to traditional

Building on these findings, a new intelligent defrost initiation strategy was developed, enabling the system to detect and respond to frost accumulation in a more efficient and adaptive manner. The performance of this approach was compared with traditional defrost methods, such as fixed-time control.

The results demonstrated that the proposed method can reduce the number of defrost cycles by up to 70%, significantly decreasing the overall defrosting time and associated energy consumption, while maintaining optimal heat transfer efficiency, system reliability, and product preservation quality.

4. Development of a MATLAB simulation model

To complement the experimental work, a MATLAB-based simulation model was developed to estimate product weight loss due to transpiration under various storage conditions.

The model considers different fruit types, ambient temperature and humidity levels, and storage durations, allowing prediction of daily moisture loss and its impact on overall product quality. This tool provides a practical way to simulate different operating scenarios and supports the design of improved storage management strategies.

5. Energy efficiency assessment and inverter analysis

In the final phase of the research, a detailed energy analysis of the refrigeration system was carried out. The entire system was continuously monitored through a dedicated data acquisition platform, allowing precise evaluation of energy consumption trends, component performance, and operational stability.

A comparative study was performed between configurations with and without inverters applied to the compressor, condenser fans, and evaporator fans. The results demonstrated a significant reduction in energy consumption—up to 34%—and a corresponding decrease in CO_2 emissions and operating costs when inverter control was implemented across all components.

This continuous monitoring approach not only validated the energy-saving potential of inverter technology but also provided valuable insight into where and how to intervene in the system to further enhance its overall efficiency and reliability.

Overall, the results of this study demonstrate that a systematic approach to refrigeration system optimization can lead to substantial improvements in both energy efficiency and product preservation quality. By combining experimental analysis, real-time system monitoring, and simulation modeling, it was possible to identify the key parameters influencing the thermo-hygrometric balance of the storage environment and the performance of the refrigeration system. The introduction of intelligent defrost control and inverter-driven components proved particularly effective, enabling significant reductions in energy consumption, defrost frequency, and operational costs, while ensuring stable conditions for fruit and vegetable conservation.

The findings confirm that integrating data-driven control strategies and advanced monitoring tools represents a promising direction for the next generation of cold storage facilities, capable of adapting dynamically to varying loads and environmental conditions.

Furthermore, the results obtained through numerous experimental campaigns confirmed the reliability and repeatability of the intelligent defrost system based on fan power consumption

monitoring. This approach proved robust across different operating conditions, offering a practical and non-invasive method for detecting frost accumulation.

Future developments will focus on extending the application of this method to different types of fans—such as three-phase asynchronous and brushless DC motors—in order to verify its adaptability and performance consistency.

Additional work will also explore the integration of this control logic with predictive algorithms and real-time energy management platforms.

Given the encouraging results achieved, the possibility of patenting the proposed defrost control system is currently under evaluation, as it represents an innovative and cost-effective solution for improving the operational efficiency of commercial refrigeration systems.

References

Abdulla, M. O. A., Deniz, E., Karagöz, M., & Gürüf, G. (2021). An experimental study on a novel defrosting method for cold room. *Applied Thermal Engineering*, *188*. https://doi.org/10.1016/j.applthermaleng.2021.116573

Allard, J., & Heinzen, R. (1988). Adaptive Defrost. In *IEEE TRANSACTIONS ON INDUSTRY APPLICATIONS* (Vol. 24).

ASHRAE Handbook: Fundamentals. (2012).

Ashrae Handbook Refrigeration. (2018).

Chen, H., Thomas, L., & Besant, R. W. (n.d.). *Fan supplied heat exchanger fin performance under frosting conditions*. www.elsevier.com/locate/ijrefrig

da Silva, D. L., & Hermes, C. J. L. (2018a). Optimal defrost cycle for air coolers revisited: A study of fan-supplied tube-fin evaporators. *International Journal of Refrigeration*, *89*, 142–148. https://doi.org/10.1016/j.ijrefrig.2018.02.009

da Silva, D. L., & Hermes, C. J. L. (2018b). Optimal defrost cycle for air coolers revisited: A study of fan-supplied tube-fin evaporators. *International Journal of Refrigeration*, *89*, 142–148. https://doi.org/10.1016/j.ijrefrig.2018.02.009

Dichi, D. B., & Bekele, D. (n.d.). *Review on Factors Affecting Postharvest Quality of Fruits Review Article*. *5*. https://www.researchgate.net/publication/362715930

Drossos, P. V., Fortis, S. P., Anastasiadi, A. T., Pavlou, E. G., Tsantes, A. G., Spyratos, G. A., Papageorgiou, E. G., Nomikou, E. G., Stamoulis, K. E., Dryllis, G., Tzounakas, V. L., Politou, M., Valsami, S., & Kriebardis, A. G. (2025). Cold vs. Room Temperature: A Comparative Analysis of Platelet Functionality in Cold Storage. *Biomedicines*, *13*(2). https://doi.org/10.3390/biomedicines13020310

Fricke, B. A., & Sharma, V. (2011). *Demand Defrost Strategies in Supermarket Refrigeration Systems*.

Gouda, M. H. B., & Duarte-Sierra, A. (2024). An Overview of Low-Cost Approaches for the Postharvest Storage of Fruits and Vegetables for Smallholders, Retailers, and Consumers. In *Horticulturae* (Vol. 10, Issue 8). Multidisciplinary Digital Publishing Institute (MDPI). https://doi.org/10.3390/horticulturae10080803

Inanlu, M. J., Gurumukhi, Y., Kabirzadeh, P., Anand, R., Khodakarami, S., Viswanathan, V., Stillwell, A., & Miljkovic, N. (2024). Capacitive sensing of frost growth dynamics on aluminum surfaces with different wettabilities. *International Journal of Heat and Mass Transfer*, *225*. https://doi.org/10.1016/j.ijheatmasstransfer.2024.125377

Iturralde-García, R. D., Cinco-Moroyoqui, F. J., Martínez-Cruz, O., Ruiz-Cruz, S., Wong-Corral, F. J., Borboa-Flores, J., Cornejo-Ramírez, Y. I., Bernal-Mercado, A. T., & Del-Toro-Sánchez, C. L. (2022). Emerging Technologies for Prolonging Fresh-Cut Fruits' Quality and Safety during Storage. In *Horticulturae* (Vol. 8, Issue 8). MDPI. https://doi.org/10.3390/horticulturae8080731

James Thompson, F.G. Mitchell, & R.F. Kasmire. (2002). *Cooling horticultural commodities*.

Janet Bachmann, & Richard Earles. (2000). Postharvest_Handling_of_Fruits_and_Veget. *ATTRA, 2000*.

Jeongkeun Kim, Jieun Hwang, & Keumnam Cho. (2013). Effect of Local Frost Characteristics on Thermal Performance of Fin Tube Heat Exchanger Under Frosting Condition. *ASME 2013*.

Kim, M. H., & Lee, K. S. (2015a). Determination method of defrosting start-time based on temperature measurements. *Applied Energy*, *146*, 263–269. https://doi.org/10.1016/j.apenergy.2015.02.071

Kim, M. H., & Lee, K. S. (2015b). Determination method of defrosting start-time based on temperature measurements. *Applied Energy*, *146*, 263–269. https://doi.org/10.1016/j.apenergy.2015.02.071

Lee, S. K., & Kader, A. A. (2000). Preharvest and postharvest factors influencing vitamin C content of horticultural crops. In *Postharvest Biology and Technology* (Vol. 20). www.elsevier.com/locate/postharvbio

Lufu, R., Ambaw, A., & Opara, U. L. (2020). Water loss of fresh fruit: Influencing pre-harvest, harvest and postharvest factors. In *Scientia Horticulturae* (Vol. 272). Elsevier B.V. https://doi.org/10.1016/j.scienta.2020.109519

Mago, P. J., & Sherif, S. A. (2005). Frost formation and heat transfer on a cold surface in ice fog. *International Journal of Refrigeration*, *28*(4), 538–546. https://doi.org/10.1016/j.ijrefrig.2004.10.004

Malik, A. N., Khan, S. A., & Lazoglu, I. (2021). A novel demand-actuated defrost approach based on the real-time thickness of frost for the energy conservation of a refrigerator. *International Journal of Refrigeration*, *131*, 168–177. https://doi.org/10.1016/j.ijrefrig.2021.07.032

Mohammed Amer, & Chi-Chuan Wang. (2017). *Review of defrosting methods*.

Na, B., & Webb, R. L. (2004). New model for frost growth rate. *International Journal of Heat and Mass Transfer*, *47*(5), 925–936. https://doi.org/10.1016/j.ijheatmasstransfer.2003.09.001

Nawaz, K., Elatar, A., & Fricke, B. (2018). *A Critical Literature Review of Defrost Technologies for Heat Pumps and Refrigeration Systems*. http://www.osti.gov/scitech/

O'Neal D.L. (1984). *Measurement of Frost Growth and Density in a Parallel Plate Geometry" ASHRAE Transactions; Vol 90, pt.2*.

P. Rapin, & P. Jacquard. (2000). *Tecnologia dei materiali frigoriferi*.

Paull, R. E. (1999). Effect of temperature and relative humidity on fresh commodity quality. In *Postharvest Biology and Technology* (Vol. 15).

Pegallapati, A. S., & Ramgopal, M. (2021). Effect of heat transfer area distribution on frosting performance of refrigerator evaporator. *International Journal of Heat and Mass Transfer*, *175*. https://doi.org/10.1016/j.ijheatmasstransfer.2021.121317

R. Le. Gall, & J.M. Grillot. (1997). *Modelling of frost growth and densification*.

Schneider, H. W. (n.d.). *EQUATION OF THE GROWTH RATE OF FROST FORMING ON COOLED SURFACES*.

Shen, X., Zhang, M., Devahastin, S., & Guo, Z. (2019). Effects of pressurized argon and nitrogen treatments in combination with modified atmosphere on quality characteristics of fresh-cut potatoes. *Postharvest Biology and Technology*, *149*, 159–165. https://doi.org/10.1016/j.postharvbio.2018.11.023

Shen, Y., & Wang, X. (2019). Real-time frost porosity detection using capacitance sensing approach. *International Journal of Heat and Mass Transfer*, *134*, 1171–1179. https://doi.org/10.1016/j.ijheatmasstransfer.2019.02.060

Song, M., & Dang, C. (2018). Review on the measurement and calculation of frost characteristics. In *International Journal of Heat and Mass Transfer* (Vol. 124, pp. 586–614). Elsevier Ltd. https://doi.org/10.1016/j.ijheatmasstransfer.2018.03.094

Sujau, M., Merts, I., & Cleland, D. J. (n.d.). *Relative Humidity Control in Refrigerated Facilities*.

Thulasimani, K. (2002). *Design of cold storage for fruits and vegetables*. https://doi.org/10.13140/RG.2.2.14335.82082

Tso, C. P., Cheng, Y. C., & Lai, A. C. K. (2006). An improved model for predicting performance of finned tube heat exchanger under frosting condition, with frost thickness variation along fin. *Applied Thermal Engineering*, *26*(1), 111–120. https://doi.org/10.1016/j.applthermaleng.2005.04.009

Velderrain-Rodríguez, G. R., Quirós-Sauceda, A. E., González Aguilar, G. A., Siddiqui, M. W., & Ayala Zavala, J. F. (2015). Technologies in fresh-cut fruit and vegetables. In *Food Engineering Series* (pp. 79–103). Springer. https://doi.org/10.1007/978-3-319-10677-9_5

Walther Pohlmann. (1996). *Pohlmann Taschenbuch der Kältetechnik*.

Wilbert F. Stoecker. (2004). *Industrial Refrigeration Handbook*. www.digitalengineeringlibrary.com

Wu, X. M., & Webb, R. L. (n.d.). *Investigation of the possibility of frost release from a cold surface*. www.elsevier.nl/locate/etfs

X.C. Guo, & T.S. Zhao. (1989). *EA Parametric Study Of An Indirect Evaporative Air Cooler*.

Yoon, Y., Jeong, H., & Lee, K. S. (2018). Adaptive defrost methods for improving defrosting efficiency of household refrigerator. *Energy Conversion and Management*, *157*, 511–516. https://doi.org/10.1016/j.enconman.2017.12.039